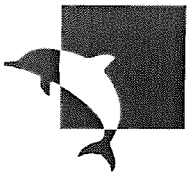

University of Southampton
Faculty of Engineering and Applied Science
Department of Electronics and Computer Science

A High-Performance, Efficient, and Reliable Receiver for Bluetooth Signals

by

Charles TIBENDERANA

A doctoral thesis submitted in partial fulfilment
of the requirements for the award of
Doctor of Philosophy

December 2005

Dedicated to my parents,
for all they have done for us.

UNIVERSITY OF SOUTHAMPTON

ABSTRACT

FACULTY OF ENGINEERING AND APPLIED SCIENCE
SCHOOL OF ELECTRONICS AND COMPUTER SCIENCE

Doctor of Philosophy

A High-Performance, Efficient, and Reliable Receiver for Bluetooth Signals

By Charles Tibenderana

The key defining feature of a software defined radio is the flexibility to reconfigure itself to different modes, frequency bands, or wireless standards. This is achieved by, for example, running software modules on a general purpose digital signal processor. The complexity of a common hardware platform shared by Bluetooth and a relatively costly wireless standard like Wi-Fi, must have the capacity to handle the more demanding system. In such scenarios, there will be extra resources available when Bluetooth is running and Wi-Fi is in an idle state. This thesis contains suggestions on the most effective way to use this surplus capability to improve the reception of Bluetooth signals.

Our approach involves selecting the most appropriate receiver capable of very low bit error ratio, but ensuring that it is realised in a very efficient manner; and providing algorithms to compensate for multipath effects, and carrier and modulation index offsets, which would otherwise degrade performance. Together these features contribute towards a Bluetooth receiver that has a high-performance, yet is efficient and reliable.

High-performance Receiver

In order to choose a suitable receiver, we first consider the use of high-performance receiver algorithms such as the Viterbi and the matched filter bank (MFB) receiver, both of which exhibit several dB gain over alternative schemes. However, the MFB receiver is more favourable because of the stringent accuracy requirements of the Viterbi receiver on parameters such as carrier frequency and modulation index, both of which have considerable tolerances in Bluetooth systems.

Efficient Receiver

However, the MFB receiver requires several matched filters of considerable length, and is

therefore prohibitive to most applications in terms of computational cost. Hence, through the formulation of a novel recursive realisation of the MFB, which employs a much smaller filter bank but processes the results over several stages, we decrease its complexity by two orders of magnitude without any sacrifice in performance, and thereby make the MFB receiver a more practical option.

Reliable Receiver

Efforts were made to combat irregularities with the received signal such as multipath propagation, carrier frequency and modulation index offsets, which would otherwise undermine the effectiveness of the efficient MFB receiver, and which can be expected in Bluetooth networks.

To deal with dispersive channels we require an algorithm that is resilient to carrier frequency offsets that may exist, and would not yet have been corrected for. Additionally, because of the short bursty nature of Bluetooth transmissions, and the requirement for equalisation to take place before parameter synchronisation algorithms further along the signal processing chain can converge, it is desirable that the equalisation algorithm should converge relatively quickly. Hence, for this purpose we adopt the normalised sliding window constant modulus algorithm (NSWCMA). However, to cater for the correlation between samples of a Bluetooth signal that could make the procedure unstable, we apply and compare a new high-pass signal covariance matrix regularisation, with a diagonal loading scheme.

For parameter synchronisation, a new algorithm for carrier frequency offset correction that is based on stochastic gradient techniques, and appropriate for Bluetooth, is developed. We also show the intermediate filter outputs inherent in the efficient realisation of the MFB may be used to detect carrier frequency and modulation index offsets, which can then be corrected for by recomputing the coefficients of a relatively small intermediate filter bank.

The results of this work could make it possible to achieve the maximum bit error ratio specified for Bluetooth at a much lower signal to noise ratio than is typical, in harsh conditions, and at a much lower associated cost in complexity than would be expected. It would therefore make it possible to increase the range of a Bluetooth link, and reduce the number of requests for packets to be retransmitted, thus increasing throughput.

Acknowledgements

I am very grateful to Dr Stephan Weiss for his friendly personality that has enabled me to interact freely and learn a lot from him about signal processing and telecommunications, I could not have wished for a better PhD supervisor. Many thanks also to Dr Jeff Reeve and Dr John Carter, for the valuable advice they offered towards making this thesis a better one.

My gratitude goes out to Prof. Lajos Hanzo, Dr. Bee-Leong Yeap, Dr Soon X Ng, Denise Harvey, Mahmoud Hadef, Choo Leng Koh, Chunguang Liu, Chi Hieu Ta, Kai-Wen Lien, and Mohammed Zia Hayat. These are just some of the members of the communications research group that have greatly enriched my experience here.

I really appreciate the efforts of inspiring people like Dr Francis Tusubira, Dr Vincent Kasangaki, Mr Sam Busulwa, Mr Sekubuge and Mr Buinza, who have served as my teachers and mentors in the past, and who are responsible for steering me towards this point.

I will always be indebted to my family. My parents, Prof. Peter K. Tibenderana and Mrs Prisca K. G. Tibenderana, they have been the strong pillars that have offered me a stable environment and a clear mind, without which I could not have pursued an education to this level. My elder brother Dr James Kananura Tibenderana, on whose personal computer I wrote my first code and sent my first email, I have always been able to learn from his experiences. My lovely sisters Emily Kemigisha Tibenderana and Josepha Tumuhairwe Tibenderana, they have always been a source of motivation.

I have been truly blessed to cross paths with all these wonderful people, and for that I thank God, from whom all good things come.

List of Publications

1. **Charles Tibenderana and Stephan Weiss**, "Simplified Matched Filter Bank Receiver for Multilevel GFSK," Submitted to *IEEE Transactions on Circuits and Systems I.*

2. **Charles Tibenderana and Stephan Weiss**, "Efficient and Robust Detection of GFSK Signals Under Dispersive Channel, Modulation Index and Carrier Frequency Offset Conditions," *Special Issue on DSP Enabled Radio, EURASIP Journal on Applied Signal Processing*, Accepted for Publication.

3. **Charles Tibenderana and Stephan Weiss**, "Investigation of Offset Recovery Algorithms for High Performance Bluetooth Receivers," in *Proc. IEE Colloquium on DSP Enabled Radio*, UK, September 2005, Accepted for Publication.

4. **Charles Tibenderana and Stephan Weiss**, "Rapid Equalisation for a High Integrity Bluetooth Receiver," *IEEE Workshop on Statistical Signal Processing*, Bordeaux, France, July 2005.

5. **Charles Tibenderana and Stephan Weiss**, "Fast Multi-level GFSK Matched Filter Receiver," *IMA Conference on Mathematics in Signal Processing*, Cirencester, Essex, UK, December 2004, pp. 191-194.

6. **Charles Tibenderana and Stephan Weiss**, "A Low-Cost Scalable Matched Filter Bank Receiver for GFSK Signals with Carrier Frequency and Modulation Index Offset Compensation," *Asilomar Conference on Signals, Systems, and Computers*, California, USA, November 2004, pp. 682-686.

7. **Charles Tibenderana and Stephan Weiss**, "Blind Equalisation and Carrier Offset Compensation for Bluetooth Signals," in *Proc. 12th European Signal Processing Conference*, Vienna, Austria, September, 2004, pp. 909-912.

8. **Charles Tibenderana and Stephan Weiss**, "Low-Complexity High-Performance GFSK Receiver With Carrier Frequency Offset Correction," in *Proc. IEEE International Conference on Acoustics, Speech, and Signal Processing*, Montreal, Canada, May 2004, vol. IV, pp. 933-936.

9. **Charles Tibenderana and Stephan Weiss**, "A Low-Complexity High-Performance Bluetooth Receiver," in *Proc. IEE Colloquium on DSP Enabled Radio*, Robert W. Stewart and Daniel Garcia-Alis, Eds., Livingston, Scotland, UK, September 2003, pp. 426-435.

10. **Charles Tibenderana, Terence E. Dogson, Stephan Weiss, and Derek Babb**, "Towards Software Defined Radio (SDR) Bluetooth and IEEE 802.11b Modem Integration," in *9th Wireless World Research Forum Meeting*, Zurich, Germany, July 2003.

11. **Charles Tibenderana and Stephan Weiss**, "SDR Enablers and Obstacles: Technology Study on Waveforms", School of Electronics and Computer Science, University of Southampton, Southampton, UK, Report for the UK Office of Communications (OFCOM), March 2005.

12. **Stephan Weiss and Charles Tibenderana**, "Antenna Processing in a Software Defined Radio", School of Electronics and Computer Science, University of Southampton, Southampton, UK, Report for the UK Office of Communications (OFCOM), January 2005.

13. **Charles Tibenderana and Terence E. Dogson**, "Integrated Modulators and Demodulators," *UK Patent Application 0219740.8*, Samsung Electronics Research Institute, Stains, UK, August 2002.

Contents

Chapter 1

Introduction

In this introductory chapter the research motivation is outlined with respect to the current trends in transceiver design and the opportunities they present. Subsequently, novel contributions of this thesis are highlighted. The organisation of this thesis is contained in the final section of this chapter.

1.1 Research Motivation

In a software defined radio (SDR), receive digitisation is performed at some stage downstream from the antenna, typically after wideband filtering, low noise amplification, and down conversion to a lower frequency — with the reverse process occurring for the transmit digitisation. The flexibility offered by digital signal processing and the reconfigurable functional blocks that define the characteristics of the transceiver, are the key features of an SDR [1, 2]. Hence, the bulk of the signal processing tasks on an SDR are accomplished by running software algorithms on general purpose hardware.

Multiple wireless communication standards can be executed on an SDR by downloading software modules related to a specific wireless interface onto a general purpose digital signal processor (DSP) [3]. If common software modules can be defined for a number of modes, then a system of parameterisation can be employed [4, 5], whereby only a list of standard specific parameters need to be downloaded. Hence, the internal functionalities of a software defined radio are passed to it from "outside" via software or parameter download. DSPs have a "hard" limit to the number of mathematical operations they can perform each second and the amount of memory storage available; these features contribute towards

the computational capacity of the DSP. Since different systems vary in computational requirements, an SDR is bound to shift from operating under heavy to low computational load, and vice versa, as it switches from a highly complex standard to a much cheaper one. Hence, when the simpler system is operational, the excess capacity can be utilised to improve performance. Researchers elsewhere are also carrying out work based on this principle [6, 7, 8].

A wide range of wireless interfaces are defined to satisfy a variety of applications, bit rates and channel conditions. For example IEEE 802.16 [9], IEEE 802.16a [10], and HiperMAN [11] are devoted to wireless metropolitan area networks (WMAN), IEEE 802.11 [12], IEEE 802.11a [13], IEEE 802.11b [14], IEEE 802.11g [15] and HiperLAN 2 [16] are meant for wireless local area networks (WLAN), while Bluetooth [17, 18], IEEE 802.15.3 [19] and IEEE 802.15.4 [20] are employed in wireless personal area networks (WPAN). Bluetooth and IEEE 802.11b (otherwise known as wireless fidelity or Wi-Fi) are good candidate standards for integration in a software defined radio, and there are already several cases of their combination in a single radio [21, 22, 23, 24, 25, 26]. Tab. 1.1 highlights some properties of the Bluetooth and Wi-Fi wireless interfaces.

A number of reasons favour the amalgamation of Bluetooth and Wi-Fi. First of all, Bluetooth is the world's leading technology for WPAN, while Wi-Fi is the most popular WLAN system today. Hundreds of millions of Bluetooth or Wi-Fi enabled units are in use all over the world today [27], hence, a transceiver capable of both systems will have access to this large resource since it can adapt to the technology available on its desired communication partner.

Additionally, Bluetooth and Wi-Fi both operate in the 2.4 GHz industrial, scientific and medical (ISM) radio frequency band, which is defined as 2446.5-2483.5 MHz in France, 2445.0-2475.0 MHz in Spain, 2471.0-2497.0 MHz in Japan, and 2400.0-2483.5 MHz in most remaining countries. Their collocation in terms of spectrum presents an opportunity for an

Standard	Application	Modulation	Bit Rate (Mbps)	Spectrum	Channel BW (MHz)
Bluetooth (IEEE 802.15.1)	WPAN	GFSK	1	2.4 GHz Band	1
Wi-Fi	WLAN	DBPSK/CCK	5.5	2.4 GHz Band	22
		DQPSK/CCK	11		

Table 1.1: Summary of Bluetooth and Wi-Fi wireless interfaces.

Aspect	Bluetooth	Wi-Fi
Max. bit rate (Mbps)	1	11
Range (m)	10	100
Power (dBm)	0 (Type 3)	20
Spread spectrum	FHSS	DSSS
Application	Wireless cable replacement	Wireless cable extension
Usage location	Anywhere at least 2 Bluetooth devices exist	Within range of WLAN infrastructure

Table 1.2: Selected differences between Bluetooth and Wi-Fi systems in their primary configuration.

efficient merger in an SDR. To put this in context it must be noted that the high carrier frequencies involved in most wireless systems today, and the limited speeds of modern analogue to digital converters (ADC), digital to analogue converters (DAC), and general purpose processors imply that digitisation and software processing is mostly relevant at baseband or low intermediate frequencies (IF) [2]. Therefore, front-end processing is likely to be performed in hardware, and since hardware realisation is largely dependent on the frequency of the expected signal [28], waveforms at widely variant frequencies will require different hardware. So an SDR can benefit from a common front-end shared by Bluetooth and Wi-Fi systems.

Generally speaking, Bluetooth and Wi-Fi both facilitate the transfer of information bits from an electronic device to another. However, these systems have differences (summarised in Tab. 1.2) that will favour one system over the other in any communication scenario [29, 17, 14]. For example, low transmit power and short range make Bluetooth more feasible when a number of devices close together need to be connected, and vice versa if the units are widely distributed. Unlike Bluetooth, Wi-Fi is wasteful at relatively low average bit rates, but is capable of the high data rates necessary for efficient file transfer. Additionally, Wi-Fi sends voice as compressed files, making it unsuitable for audio applications like the cordless phone [29], this is not the case with Bluetooth [29, 17, 14]. As a practical illustration we can imagine that a Bluetooth and Wi-Fi enabled multimedia device will employ Bluetooth to connect to a wireless headphone, but will require Wi-Fi to download large audio and video files.

Owing to major differences in the baseband functionalities in Bluetooth and Wi-Fi, a multi-standard SDR will need to download separate software relevant to the desired operational mode onto a general purpose DSP, and purge unwanted functions. Furthermore,

since DSPs have a fixed and finite limit to the number of mathematical operations they can perform each second, its capacity must be determined by the most complex functions it implements. For example, Wi-Fi employs a more demanding direct sequence spread spectrum (DSSS) technique compared to the simpler frequency hopping spread spectrum (FHSS) used in Bluetooth [30]. Furthermore, the bit rate of Wi-Fi is 11 times that in Bluetooth, and since doubling bit rate generally implies quadrupling the complexity [31], it is apparent that Wi-Fi is much more complex than Bluetooth, and that a common hardware platform will have excess capacity when running Bluetooth.

Hence, the extra resource available when Bluetooth is operational can be utilised to increase efficacy, and in order to do so we consider various areas where there is room for improvement:

Detection

Gaussian frequency shift keying (GFSK) is a bandwidth preserving modulation technique that is used in Bluetooth [17]. In our quest to improve reception of Bluetooth signals we first consider the best performing receivers for GFSK modulated signals in order to select a suitable one to optimise for Bluetooth. Such schemes are based on multi-bit detection and have more than 6 dB gain with respect to simpler methods [32].

For example, maximum likelihood detection of a sequence of GFSK modulated bits can be achieved with a Viterbi receiver, which correlates the received signal over a symbol period with all authentic transmit possibilities, before deploying the Viterbi algorithm to penalise illegitimate state transitions [33]. However, the use of a Viterbi receiver is limited to coherent detection of signals with a rational modulation index (h), thereby ensuring a finite number of states [33]. In addition according to [34], the Viterbi receiver is very vulnerable to inaccuracies in h, and has been shown to be robust to only very small variations of $|\Delta h| \leq 0.01$. Even if it was possible to estimate the transmitter modulation index accurately, it would be difficult to compensate for this at the receiver because the receiver architecture, including the number of states, would have to be changed [35]. The Viterbi receiver therefore seems unsuitable for Bluetooth, where an initial offset in modulation index of $\Delta h \leq 0.07$ is allowed, and where there is no guarantee that h will be rational [17].

Alternatively we consider a matched filter bank (MFB) receiver, which has been used for reception of continuous phase frequency shift keying (CPFSK)[1] modulated signals in

[1]GFSK is a subset of CPFSK.

[36, 37, 38]. This receiver achieves a near optimal estimate of the maximum likelihood of a single symbol using a system of filters that are matched to legitimate waveforms over an observation interval of several symbol periods [35]. The filter with the largest output determines the received waveform, and in non-coherent mode, the symbol at the center of the modulating symbol-sequence responsible for producing the received waveform is chosen as the received symbol. The MFB receiver is more suitable for Bluetooth than the Viterbi receiver because of its relative insensitivity to errors in modulation index and its ability to accommodate irrational values of h, but its complexity is prohibitive. However, computational power of state of the art DSPs increase rapidly according to Moore's law [39], and in this thesis we propose a more efficient realisation of the MFB receiver that will ensure it is a viable option for most applications, if not today then in the near future.

Equalisation

Multipath signal propagation can cause significant degradation to Bluetooth signals. For instance, large sized rooms in which Bluetooth transceivers would be expected to operate have been shown to exhibit dispersive channels with root mean square (RMS) delay spreads in excess of $\sigma_\tau = 300$ ns [40, 41]. Fig. 1.1 demonstrates that this will cause considerable performance loss, and so an equaliser is required. This problem will be further aggravated if pleas to increase the operational range and speed are heeded [42].

Since there is a potential for carrier frequency offsets in Bluetooth networks, phase sensitive equalisation techniques are not a reliable option. Moreover Bluetooth transmissions comprise of short data bursts, and carrier frequency correction algorithms will require an equalised signal to operate on, therefore the equaliser should converge quickly to give sufficient time to other signal processing blocks to complete their tasks, ideally within the time it takes to receive the mutually known 72-bit access code, and thus prevent information loss. This problem is compounded because Bluetooth signals are coloured, and therefore most equaliser procedures will be slower in such conditions [43]. As a solution we enhance the normalised sliding window constant modulus algorithm for use with Bluetooth.

Carrier Frequency and Modulation Index Offsets

In a bid to keep the cost of production of Bluetooth transceivers low, the Bluetooth specification for carrier frequency and modulation index are quite lax, whereby offsets of 75 KHz and 0.07 respectively are permitted [17]. Other researchers have demonstrated that carrier fre-

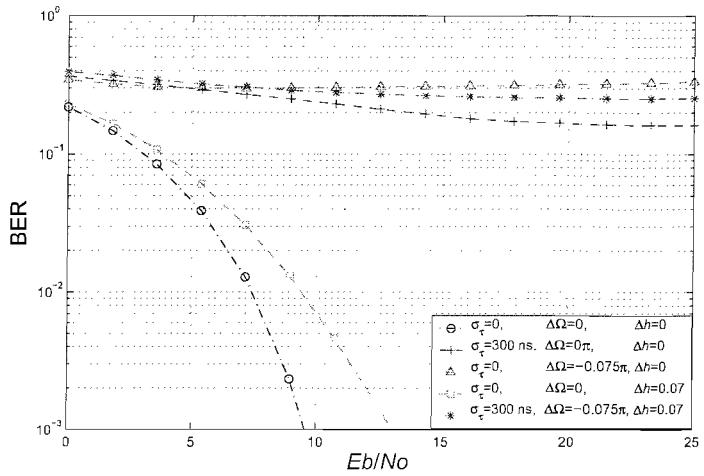

Figure 1.1: BER performance for Bluetooth signal reception using an MFB receiver with a 9-bit observation interval, $N = 2$, $K_{BT} = 0.5$ and $h = 0.35$.

quency errors of this magnitude can hamper reception by single-bit detection algorithms [44]. This is even more severe for multi-bit receivers because the errors propagate and accumulate over a longer observation interval. This is exemplarily shown for a 9-bit long MFB receiver in Fig. 1.1, where 75 kHz carrier frequency offset (normalised to $\Delta\Omega = \frac{2\pi 75}{N \cdot 1000}$) causes the system to collapse, while a modulation index of 0.07 results in a 3.5 dB loss. Therefore in order to ensure data integrity, we will develop carrier frequency and modulation index offset correction algorithms suitable for Bluetooth.

Hence, the focus of this thesis shall be to make proposals on how to utilise the extra resource to improve the performance of the system when running Bluetooth, so as to facilitate high integrity transmission even under adverse conditions detailed in the previous paragraphs.

1.2 Original Contributions

- **Lower Complexity Matched Filter Bank Receiver for GFSK Modulated Signals [45, 46, 47, 48, 49]**

  The complexity of a matched filter bank receiver for GFSK modulated signals was reduced by approximately 80% for an observation interval of 9 symbol periods, without sacrificing performance. This was achieved through a careful study of the nature of

GFSK signals that enabled us to design a recursive algorithm that would eliminate redundancy in providing the matched filter outputs. Using this method, filtering is done only over a single symbol period, with the results being propagated and processed appropriately over the desired observation interval. We demonstrate that the algorithm is applicable in binary and multilevel systems.

- **Equalisation of GFSK Signals using the Normalised Sliding Window Constant Modulus Algorithm [50, 48, 51]**

  The normalised sliding window constant modulus algorithm (NSWCMA) is an equalisation procedure that is resilient to carrier frequency offsets, and its convergence speed can be improved by increasing the window size. However, when applied to coloured signals like those used in Bluetooth, instability may arise due to inversion of the received signal covariance matrix. To retain the desirable convergence speed of the NSWCMA, while maintaining its stability during equalisation of Bluetooth signals, we develop a novel regularisation technique using a high-pass signal covariance matrix, and demonstrate that it enables quicker convergence than the existing method of employing a diagonal matrix.

- **Stochastic Gradient Carrier Frequency Offset Correction Algorithm [46, 50, 48, 52]**

  A very simple stochastic gradient algorithm was developed for correction of carrier frequency offsets that may exist in a Bluetooth system. It was developed by first multiplying the received signal with a modulating phasor so as to form a modified signal. The modified signal was then used in a constant modulus cost function, and stochastic gradient techniques were applied to derive formulae for the adaptation of the modulating phasor.

- **Intermediate Filter Output Carrier Frequency and Modulation Index Offset Correction Algorithms [53, 48, 52]**

  We also show that when a carrier frequency or modulation index offset exists, there is a difference in the signal phase trajectories computed by the transmitter and assumed by the receiver that can give insight into the size of the offsets. We demonstrate that this mismatch is easily identifiable from the outputs of the intermediate filters of the simplified matched filter bank receiver and the estimated received bit. Hence, synchronisation can be accomplished by a stepwise adjustment of the receiver's carrier frequency and modulation index, and periodically recomputing the coefficients of the

relatively small intermediate filter bank.

1.3 Outline of Thesis

After this introduction, subsequent chapters in this thesis are organised as follows:

Chapter 2 begins by highlighting the convention used to represent signals and systems in this thesis. This is followed by a detailed development of our GFSK signal model, and an explanation of the Saleh-Valenzuela indoor multipath propagation model. Quantisations for dispersive channels and additive white Gaussian noise are then defined, mainly to gain insight into the magnitude of the task facing adaptive signal processing algorithms implemented in future chapters, but also to facilitate accurate reproduction of our simulations.

Chapter 3 contains a review of some conventional low-performance receivers like the FM and phase-shift discriminators, as well as high-performance ones such as the Viterbi receiver and the use of a matched filter bank (MFB). These classical receivers are then compared with a view to make a case for the adoption of the MFB receiver, provided its complexity can be reduced. Subsequently, a novel low-complexity realisation of the matched filter bank receiver for GFSK signals is derived for binary GFSK, and extended to multilevel GFSK. It is shown that the efficient MFB represents the best performance-complexity trade-off when compared to the Viterbi or the standard MFB implementation. The chapter concludes with simulations and discussions that highlight the potential benefits of the low-complexity algorithm.

Chapter 4 addresses equalisation, firstly with a brief discussion of the equalisation problem, and an introduction of Wirtinger calculus, which is used throughout the chapter. This paves the way for the formulation and discussion of: (i) the minimum mean square error equaliser solution, which is our performance benchmark; (ii) the least mean square algorithm, which is arguably the most popular adaptive algorithm used today, but which unfortunately is susceptible to carrier frequency offsets; (iii) the constant modulus algorithm (CMA), which has the desirable property of resilience to carrier frequency offsets; and (iv) the normalised sliding window constant modulus algorithm (NSWCMA), which combines the benefits of the CMA with a potential for greater convergence speeds. Regularisation of the NSWCMA is then discussed as a

way to ensure the algorithm remains stable even when applied to coloured signals like Bluetooth. Thereafter simulations results are used to point out various aspects relevant to equalisation of Bluetooth signals.

Chapter 5 focuses on the problem of synchronisation of the transmitter and receiver carrier frequency and modulation index. A new stochastic gradient procedure to correct frequency errors is derived. While novel algorithms that are specific to the low-complexity MFB receiver, and can be used to correct carrier frequency and modulation index offsets are also formulated. The synchronisation procedures are assessed via simulations.

Chapter 6 concludes the thesis with a brief background to the research, before recounting its main achievements. Potential areas for improvement and future research are then highlighted.

Chapter 2

Signal and Channel Model

This chapter contains a detailed description of the signal flow through the transmitter depicted in Fig. 2.1. It begins with a mention of the conventions used to represent signals and systems in this report in Sec. 2.1, and then delves into the development of a GFSK modulated signal in Sec. 2.2, where parameters adopted typify a Bluetooth system [17]. A description of the multipath propagation channel model used is presented in Sec. 2.3 before defining our quantitative measure for additive white Gaussian noise in Sec. 2.4. Conclusions are drawn in Sec. 2.5.

2.1 Convention for Representing Signals and Systems

The convention used throughout this thesis is to describe a signal according to its digital quadrature form. This is sometimes referred to as an "analytic" signal representation, and implies that each signal is defined by its complex baseband samples. For example, ordinarily a sinusoidal signal with amplitude A, initial phase θ_0, and angular frequency ω,

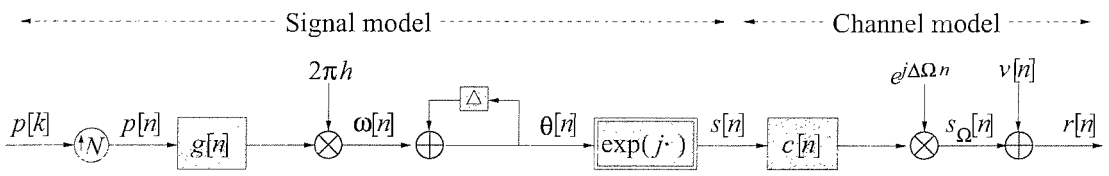

Figure 2.1: Transmission system model.

that is modulated by a carrier with an angular frequency Ω, is expressed as [54]

$$s(t) = A\cos(\Omega t + \omega t + \theta_o) \qquad -\infty < t < \infty \quad ,$$

where t is the continuous time variable. However, $s(t)$ can be represented by its discrete baseband samples given by

$$s[n] = Ae^{j(\hat{\omega}n+\theta_0)} \qquad n \in \{0, \pm 1, \pm 2, \cdots, \pm\infty\} \quad , \tag{2.1}$$

without any loss of information [55]. In (2.1), n is a sample index, and $\hat{\omega} = \omega T_s$ $(= \frac{\omega}{f_s})$ is the normalised angular frequency of the information signal, where T_s is a sampling period (and f_s is the sampling frequency) that satisfies the Nyquist criterion [56]. Since little future reference will be made to the information signal's unnormalised angular frequency, for simplicity, unless stated otherwise, in future we shall omit the " $\hat{}$ ", and label the normalised angular frequency as ω. The quadrature signal sequence $s[n]$, permits signal processing at the least possible computational cost. Practical methods to obtain $s[n]$ from $s(t)$ include [57]

1. complex downconversion followed by low-pass filtering,
2. quadrature bandpass sampling, and
3. use of analogue or digital phase splitting (Hilbert transform).

Systems will also take on their corresponding digital baseband format, with channel and filter coefficients comprising of complex numbers [55].

2.2 Signal Model

GFSK generally modulates a multilevel symbol stream $p[k]$, which here is assumed to be binary, $p[k] \in \{\pm 1\}$ with symbol index k. This symbol sequence is expanded by a factor of N and passed through a Gaussian filter with a bandwidth-time product of K_{BT} and impulse response $g[n]$. Coefficients of the Gaussian filter are given by [58]

$$g[n] = \frac{1}{4N}\left[\mathrm{erf}\left(\pi K_{BT}\sqrt{\frac{2}{\ln 2}}\left(\frac{n}{N}+\frac{1}{2}\right)\right) - \mathrm{erf}\left(\pi K_{BT}\sqrt{\frac{2}{\ln 2}}\left(\frac{n}{N}-\frac{1}{2}\right)\right)\right], \tag{2.2}$$

where n is the sample index and $\mathrm{erf}(\cdot)$ is the error function. Smaller values of K_{BT} result in a larger support length for $g[n]$, which is depicted in Fig. 2.2. The Bluetooth standard [17]

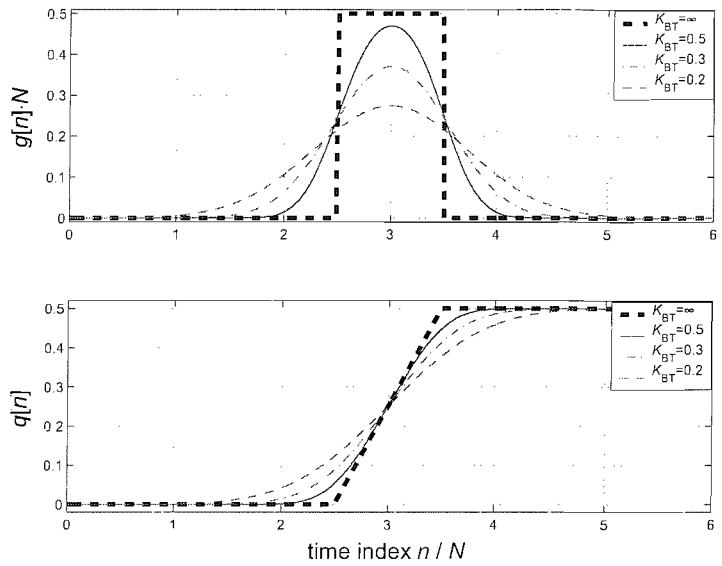

Figure 2.2: Gaussian filter impulse response $g[n]$ (top), and its cumulative sum $q[n]$ (bottom).

specifies K_{BT}=0.5, and Fig. 2.2 demonstrates that the resulting Gaussian filter has a support length that is sufficiently well approximated by $L = 3$ symbol periods, which causes each symbol to be blurred over $L-1$ adjacent symbols. The output of the Gaussian filter is then scaled by $2\pi h$ to obtain the angular frequency signal plotted in Fig. 2.3, and given by

$$\omega[n] = 2\pi h \sum_{k=-\infty}^{\infty} p[k]g[n - kN] \quad . \tag{2.3}$$

Hence, the phase of the transmitted signal can be derived as [54]

$$\theta[n] = \sum_{\nu=-\infty}^{n} \omega[\nu] \quad , \tag{2.4}$$

so that the transmitted signal is given by

$$s[n] = e^{j\theta[n]} = \exp\{j \sum_{\nu=-\infty}^{n} \omega[\nu]\} = \prod_{\nu=-\infty}^{n} e^{j\omega[\nu]} \quad . \tag{2.5}$$

Thus, while $g[n]$ acts as a frequency smoothing function, its cumulative sum

$$q[n] = \sum_{\nu=-\infty}^{n} g[\nu] \quad , \tag{2.6}$$

depicted in Fig. 2.2, is a phase smoothing function.

From (2.3), (2.4), (2.2), and the portrayal of $q[n]$ in Fig. 2.2, which shows that for $n \to -\infty$, $q[n] = 0$, and at $n \to \infty$, $q[n] = \frac{1}{2}$, we can conclude that the maximum phase

change imposed on the transmitted signal by a modulating symbol $p[k] \in \{\pm 1\}$ is $\pm\pi h$. This is clarified in Fig. 2.3, which shows the phase tree evolution over the first 5 symbol periods. The power spectral density plots in Fig. 2.4 elucidate that smoother phase transitions make $s[n]$ more bandwidth efficient.

According to the system model in Fig. 2.1, $s[n]$ is dispersed by (convolved with) a stationary channel impulse response (CIR) $c[n]$. Sec. 2.3 contains details on how $c[n]$ is derived. To simulate a carrier frequency mismatch between the transmitter and receiver, the channel output at time instant n is multiplied by $e^{j\Delta\Omega n}$, with $\Delta\Omega$ symbolising the difference in normalised angular carrier frequency of the two devices. In order to derive the normalising factor we suppose that the carrier frequencies of the transmitter and receiver are f_c and $\hat{f}_c$ respectively, where $f_c = \hat{f}_c + \Delta f_c$, so that Δf_c is the carrier frequency offset of the transmitter relative to the receiver in Hz. Then the phase of the carrier wave is

$$\theta_c(t) = 2\pi(\hat{f}_c + \Delta f_c)t \quad ,$$

while the phase of the corresponding discrete time signal is [54]

$$\begin{aligned} \theta_c[n] &= 2\pi(\hat{f}_c + \Delta f_c)nT_s \\ &= 2\pi(\hat{f}_c + \Delta f_c)\frac{n}{f_s} \\ &= 2\pi(\hat{f}_c + \Delta f_c)\frac{n}{N \cdot R} \quad , \end{aligned} \tag{2.7}$$

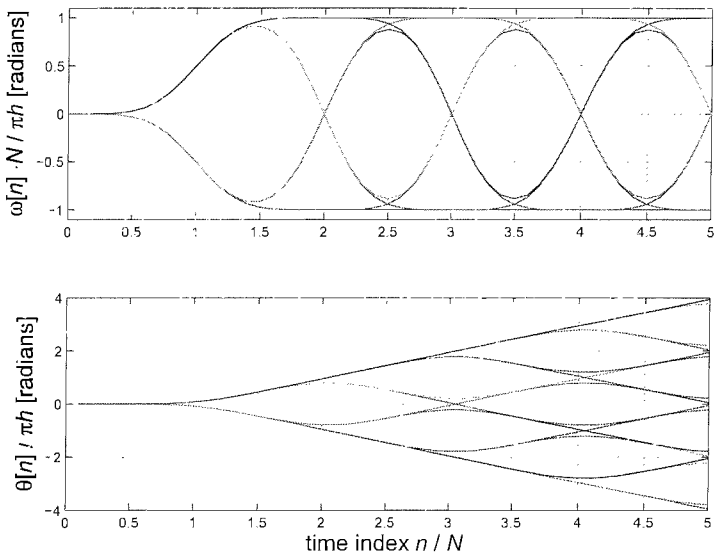

Figure 2.3: Instantaneous frequency (top) and phase (bottom) trees for a binary GFSK modulated signal, with $K_{BT} = 0.5$ ($L = 3$).

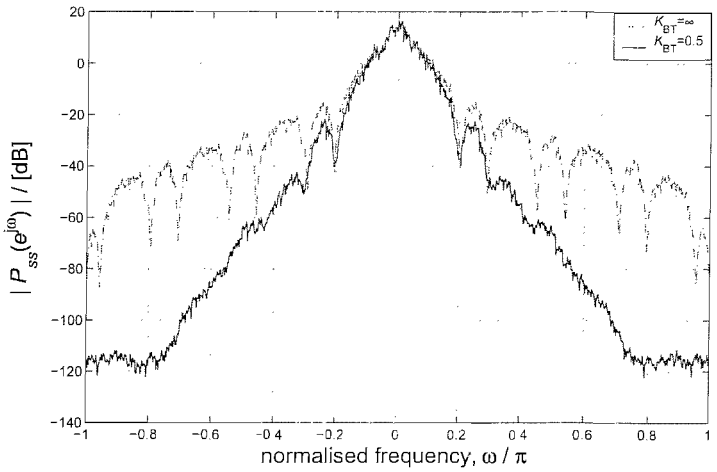

Figure 2.4: Power spectral density of the transmitted signal $s[n]$ with $N = 8$ and $h = 0.35$.

where R and N denote the symbol rate and the number of samples per symbol respectively. As indicated earlier, a baseband signal model implies a zero carrier frequency [55], and therefore, at the receiver, the residual phase due to the carrier signal after enforcing $\hat{f}_c = 0$ is derived from (2.7), and is given by

$$\theta_c[n] = \frac{2\pi(\Delta f_c)}{N \cdot R} n \quad . \tag{2.8}$$

Consequently, the normalised angular carrier frequency offset is obtained by assuming T_s is very small and differentiating (2.8) with respect to n [54], so that

$$\begin{aligned} \Delta\Omega &= \frac{\partial}{\partial n}\left\{\frac{2\pi(\Delta f_c)}{N \cdot R} n\right\} \\ &= \frac{2\pi(\Delta f_c)}{N \cdot R} \end{aligned}$$

Hence, Δf_c is normalised by $N \cdot R$. As an example, considering that the maximum carrier frequency offset permitted in Bluetooth is $\Delta f_c = 75$ kHz, and its bit rate is $R = 1$ Mbps [17], the maximum normalised angular carrier frequency offset is $\Delta\Omega = \frac{2\pi 75}{N \cdot 1000}$. It must be noted that in the model depicted in Fig. 2.1, even though $e^{j\Delta\Omega n}$ is applied before adding the AWGN $v[n]$, this only simplifies the mathematical analysis in future chapters, and has no effect on the accuracy of the results because AWGN is white, and is therefore not statistically affected by a translation in the frequency domain. The received signal can therefore be expressed as

$$r[n] = \left(\sum_{\nu=0}^{L_c-1} c[\nu]\ s[n-\nu]\right) e^{j\Delta\Omega n} + v[n] \quad , \tag{2.9}$$

with L_c being the length of the CIR. Suitable models for the CIR will be discussed in Sec. 2.3, while appropriate measures to quantify $v[n]$ appear in Sec. 2.4.

2.3 Multipath Propagation Channel Model

Signals emitted by a transmitter are reflected and scattered by obstacles, and experience refraction as they travel through the propagation medium. The resulting rays may arrive at the receiver along with the ray that travelled via the direct path, thereby forming a composite signal that is "seen" by the receiver. Since each ray follows a different path to the receiver, and may experience varying levels of attenuation, they will each have a different propagation delay and amplitude. This phenomenon is referred to as multipath propagation [59, 60], and causes distortion of the received signal. Multipath propagation is certain to happen in most commercial wireless transmissions, however, the severity of a channel is related to the relative delay and amplitudes of the component rays arriving at the receiver, and the bandwidth of the transmitted signals.

2.3.1 Parameters of Multipath Channels

Parameters commonly used to quantify the severity of multipath channels and assess system performance will be defined below, and the measure adopted in this thesis is pointed out.

2.3.1.1 Time Dispersion Parameters

Channels can be characterised and compared on the basis of time dispersive parameters that include the mean excess delay ($\bar{\tau}$), and root mean square (RMS) delay spread (σ_τ) [60]. The mean excess delay is the first moment of the power delay profile, and is defined by

$$\bar{\tau} = \frac{\sum_\nu \alpha_\nu^2 (t_\nu - t_0)}{\sum_\nu \alpha_\nu^2} = \frac{\sum_\nu \alpha_\nu^2 \tau_\nu}{\sum_\nu \alpha_\nu^2} \quad ,$$

where α_ν and t_ν are the amplitude and arrival time of the $(\nu+1)$th ray, with α_0 and t_0 corresponding to the first ray to arrive at the receiver antenna. The RMS delay spread, which is the second central moment of the power delay profile, is given by

$$\sigma_\tau = \sqrt{\bar{\tau^2} - (\bar{\tau})^2} \quad ,$$

where

$$\bar{\tau^2} = \frac{\sum_\nu \alpha_\nu^2 (t_\nu - t_0)^2}{\sum_\nu \alpha_\nu^2} = \frac{\sum_\nu \alpha_\nu^2 \tau_\nu^2}{\sum_\nu \alpha_\nu^2} \quad .$$

The RMS delay spread is a defining feature of the degradation caused by channel induced intersymbol interference (ISI) [61], and will be the main quantitative measure employed in

this work. RMS values of indoor channels have been found to reach 1470 ns for frequencies of the order of 2 GHz [62], and this is relevant to Bluetooth because it operates in the 2.4 GHz ISM band [17]. However, studies specifically targeted at the 2.4 GHz band for indoor channels suggest an RMS of 300 ns to be more accurate [63, 64], and so we shall adopt a channel with this level of severity for our simulations. A more comprehensive list of RMS values for different environments and frequencies is available in [41, 60].

2.3.1.2 Coherence Bandwidth

Knowledge of the channel RMS delay spread allows us to estimate the channel coherence bandwidth, which is given by [65]

$$B_c \approx \frac{1}{5\sigma_\tau} \quad ,$$

and is a statistical measure of the range of frequencies over which the frequency correlation function is above 0.5 [60]. Signal frequency components separated by less than B_c Hz, experience almost equal gain and linear phase shift as they pass through the channel. This implies that the channel can only be considered "flat" over a bandwidth of B_c, because if the bandwidth of the transmitted signal exceeds B_c, then significant dispersion will occur, and an equaliser is required to restore the signal. Since Bluetooth signals are 1 MHz in bandwidth [17], they will be considerably distorted by channels whose RMS delay spreads surpass 200 ns.

2.3.1.3 Doppler Spread and Coherence Time

Apart from a signal propagation channel being dispersive, if there is relative motion between the transmitter, receiver, and surrounding obstacles, then the channel may also be time varying. The Doppler spread and coherence time provide a means to evaluate this phenomenon. Doppler spread (B_D) is a measure of spectral broadening due to the rate of change of the channel [60]. To illustrate, considering a scenario in which the receiver travels directly towards the transmitter with a velocity u for Δt seconds. The phase change of the carrier wave incident at the receiver antenna over this period is a function of the fraction of the carrier wavelength (λ_c) travelled by the receiver [59], or

$$\Delta\theta_c = -2\pi\frac{u \cdot \Delta t}{\lambda_c} \quad ,$$

where the negative sign emanates from the relative direction of travel. As a result, the signal will experience a frequency shift, which is obtained by computing the phase change

for an infinitesimal interval Δt [59, 60], that is

$$\begin{aligned} B_D &= -\frac{1}{2\pi}\frac{\Delta\theta_c}{\Delta t} \qquad \Delta t \to 0 \quad , \\ &= \frac{u}{\lambda_c} \quad , \\ &= \frac{u \cdot f_c}{c} \quad , \end{aligned} \tag{2.10}$$

with $c = 3 \times 10^8$ ms^{-1} and f_c representing the velocity of light and carrier frequency respectively. Consequently, coherence time can be derived from B_D by [58]

$$T_c \approx \frac{2}{B_D} \quad .$$

It is a statistical measure of the time duration over which the CIR is essentially invariant.

If the baseband bandwidth (B) of a transmitted signal surpasses B_D, then time variation of the channel can be neglected [60], for Bluetooth where $B = 1$ MHz and $f_c \approx 2.4$ GHz, this requires $u > 125,000$ ms^{-1} for B_D to exceed B. However, the short distance between nodes of a Bluetooth network make this case highly unlikely, and hence we shall assume stationary channel conditions.

2.3.2 Mathematical Description of a Discrete Channel

During the reception of a signal, multiple rays arrive at the receiver antenna from the transmitter after being reflected, refracted, and scattered by transmission medium and surrounding obstacles. This means that at a specific time instant, the perceived incoming signal is the summation of incoming rays at that time. Hence, the effects of multipath propagation can be modelled by a linear time-varying filter [41, 66, 67, 68]. However, for cases in which the rate of change of the linear time-varying filter is negligible with respect to the data rate, the channel response can be assumed to be constant [69, 70, 71], and by discretizing the stationary channel response into equispaced time-delay bins [72, 73], it reduces to a channel impulse response

$$c[n] = \sum_{\nu=0}^{L_c-1} \alpha_\nu e^{j\beta_\nu}\, \delta[n-\nu] \quad ,$$

where α_ν, and β_ν are the amplitude and phase sequences of the resolved rays, while n and L_c represent the sample index and the total number of resolved rays respectively.

2.3.3 Saleh-Valenzuela Indoor Propagation Model

In most practical situations it is not possible to predict the exact CIR in which a wireless system will have to operate. Therefore, to facilitate proper design of communication systems, mathematical models have been developed to explain statistical observations in various physical environments, alternatively, some specimen channel impulse responses have been obtained via field measurements. Examples of channel models in use today include Rice university's SPIB channel model [74, 75], the $\Delta - K$ channel model [76], Clarke's flat fading model [77], Jakes simulator [78], and the Saleh-Valenzuela model [79]. Each model listed above can be categorised as being suitable for stationary/time-varying or indoor/outdoor environments. In this thesis we adopt the Saleh-Valenzuela model, which is very popular for simulation of stationary, indoor multipath signal propagation, and which has already been recognised as very suitable for the simulation of WPAN systems [80].

2.3.3.1 Saleh-Valenzuela Channel Model

The Saleh-Valenzuela (S-V) indoor multipath propagation channel model [79] is based on the physical realisation that rays arrive at the receiver antenna in clusters, with each cluster comprising of multiple rays. S-V asserts that clusters arrive according to a Poisson arrival process [81, 82] with an average arrival rate of Λ clusters per second, and the rays within each cluster also follow a Poisson process, but with a much higher average arrival rate of λ rays per second. If the arrival time for the first ray of the $(l+1)$th cluster (cluster arrival time) is denoted T_l, and the arrival time of $(k+1)$th ray of the $(l+1)$th cluster is designated τ_{kl}, so that the first cluster arrives at $T_0 = 0$ and the first ray in the $(l+1)$th cluster arrives at $\tau_{0l} = 0$. Then T_l and τ_{kl} are described by the independent interarrival exponential probability density functions

$$\mathcal{P}(T_l|T_{l-1}) = \Lambda \exp\{-\Lambda(T_l - T_{l-1})\} \qquad l > 0 \quad ,$$

and

$$\mathcal{P}(\tau_{kl}|\tau_{(k-1)l}) = \lambda \exp\{-\lambda(\tau_{kl} - \tau_{(k-1)l})\} \qquad k > 0 \quad .$$

The S-V model also assumes that rays arriving at the receiver antenna will have average power gains $\bar{\alpha}_{kl}^2$, which decay according to

$$\bar{\alpha}_{kl}^2 = \bar{\alpha}_{00}^2 e^{-T_l/\Gamma} e^{-\tau_{kl}/\gamma} \quad ,$$

where $\bar{\alpha}_{00}^2$ is the average power gain of the first ray of the first cluster, while Γ and γ are power decay time constants for the first ray of each cluster, and the rays within a cluster respectively. The power gains are selected from a Rayleigh distribution

$$\mathcal{P}(\alpha_{kl}) = \frac{2\alpha_{kl}}{\bar{\alpha}_{kl}^2} e^{-\frac{\alpha_{kl}^2}{\bar{\alpha}_{kl}^2}} \quad , \quad \alpha_{kl} > 0 \quad ,$$

and the angles β_{kl} are assumed to be uniformly distributed between $(0, 2\pi)$. Fig. 2.5 clarifies the cluster and ray power decay concepts. Hence, the continuous time S-V CIR can be represented as

$$c(t) = \sum_{l=0}^{\infty} \sum_{k=0}^{\infty} \alpha_{kl} e^{j\beta_{kl}} \delta(t - T_l - \tau_{kl}) \quad , \tag{2.11}$$

where $\delta(t)$ is the Dirac function. It follows that if we assume time bins of T_s seconds, then (2.11) can be discretised by the process [72]

$$c[n] = \int_{nT_s}^{(n+1)T_s} c(t)dt \quad .$$

The S-V model was developed from measurements taken between vertically polarised omni-directional antennas located in a two-story building with floor space measuring 14 m by 115 m in dimension. Under these conditions it was discovered that $1/\Lambda \in (200, 300$ ns), $1/\lambda \in (5.10$ ns), $\Gamma = 60$ ns, and $\gamma = 20$ ns should apply for the generated CIR to fit practical measurements. However, in Figs. 2.6 and 2.7 we have scaled these parameters to $1/\Lambda = 150$ ns, $1/\lambda = 10$ ns, $\Gamma = 240$ ns and $\gamma = 40$ ns in order to obtain an average RMS of 300 ns, which would typify a large sized room [60]. The channel impulse response and corresponding frequency response plotted in Fig. 2.6 describe one ensemble probe of the S-V model simulator obtained at a sampling rate of 200 MHz, which is the same resolution used in [79]. It is resolved at 2 MHz in Fig. 2.7, which is twice the Bluetooth symbol rate.

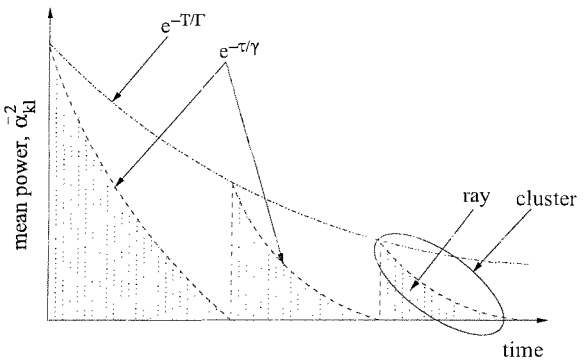

Figure 2.5: Stylised exponential decaying cluster and ray average powers of the S-V channel model [79].

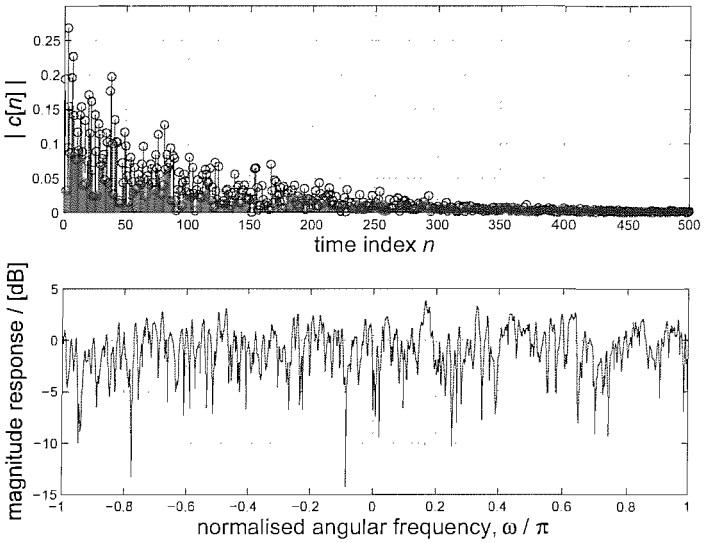

Figure 2.6: An example of a S-V channel impulse response (top) and its frequency response (bottom), with $1/\Lambda = 150$ ns, $1/\lambda = 10$ ns, $\Gamma = 240$ ns, $\gamma = 40$ ns, $\sigma_\tau = 270$ ns, and 200 MHz sample rate.

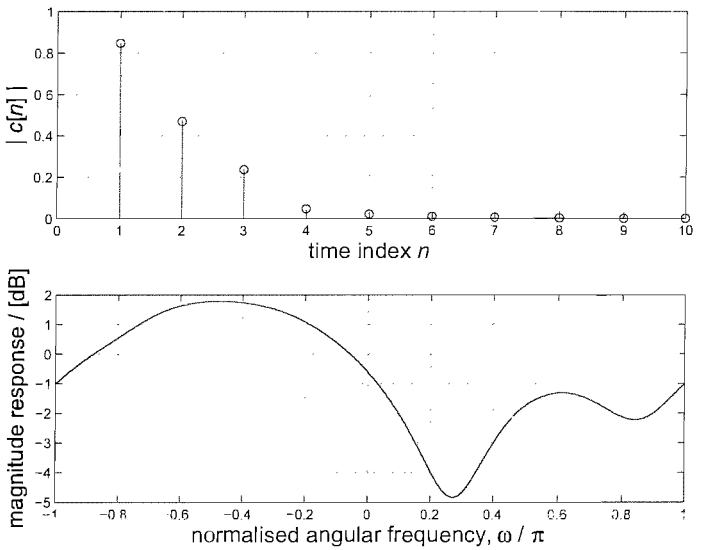

Figure 2.7: An example of a S-V channel impulse response (top) and its frequency response (bottom), with $1/\Lambda = 150$ ns, $1/\lambda = 10$ ns, $\Gamma = 240$ ns, $\gamma = 40$ ns, $\sigma_\tau = 300$ ns, and 2 MHz sampling rate.

2.4 Additive White Gaussian Noise

Additive white Gaussian noise (AWGN) is a fundamental limiting factor in communication systems, and must be considered in receiver design. It could be a result of a number of phenomena that include atmospheric noise, RF interference, and thermal energy that causes random Brownian motion of electrons within the receiver circuit elements. AWGN is characterised by a Gaussian probability density function (PDF), portrayed in Fig. 2.8, and given by

$$\mathcal{P}(v) = \frac{1}{\sqrt{2\pi}\sigma_v} e^{-\frac{(v-\bar{v})^2}{2\sigma_v^2}}$$

where v symbolises the amplitude of the noise samples with a variance of $\sigma_v^2 = 1$ and a mean of $\bar{v} = 0$ [83].

Popular measures for the noise level relative to that of the desired signal include signal to noise ratio (SNR), given by

$$\text{SNR} = \frac{\sigma_s^2}{\sigma_v^2} \quad , \tag{2.12}$$

where σ_s^2 and σ_v^2 are the variance of the information $s[n]$ and noise $v[n]$ signals respectively. In (2.12) it is assumed that the channel $c[n]$ depicted in Fig. 2.1 is an ideal channel, otherwise the σ_s^2 must be replaced with the variance of the channel output. An alternate quantification for the amount of noise in a received signal is the bit energy to noise power density ratio (E_b/N_o), which is derived from SNR in Appendix A, and is given by the expression [84, 85]

$$E_b/N_0 = \text{SNR} \cdot \frac{N}{N_b} \quad , \tag{2.13}$$

where N and N_b denote the spreading factor and number of bits per symbol respectively.

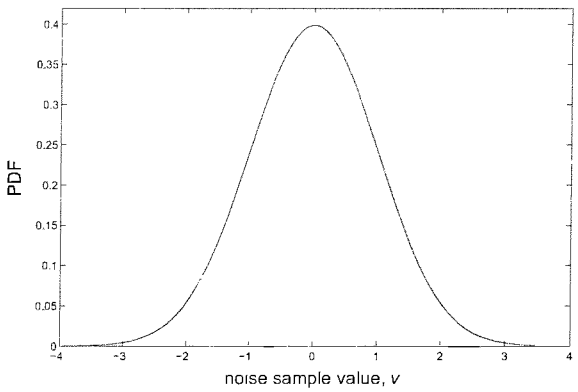

Figure 2.8: Gaussian probability density function with $\bar{v} = 0$ and $\sigma_v^2 = 1$.

Noting that as Bluetooth is a binary signalling system (2.13) can be simplified to

$$E_b/N_0 = \text{SNR} \cdot N \quad . \tag{2.14}$$

It is important to note from (2.14) that for complex binary signals with no oversampling applied, E_b/N_0 and SNR are equivalent. However, generally speaking E_b/No is a more convenient quantity for system calculations and performance comparisons because results are independent of N and N_b [85], it will therefore be used for bit error ratio (BER) performance evaluations in this thesis.

However, despite the fact that simulation methods for Gaussian processes are well covered in the literature, and include the Box Muller algorithm [59, 82], appropriate scaling of a Gaussian noise sequence to reflect a desired SNR or E_b/N_0 is not well documented, and is sometimes a source for confusion. To ensure clarity, our "noise scaling" is as follows: From (2.12) the desired standard deviation for AWGN is

$$\sigma_v = \frac{\sigma_s}{\sqrt{\text{SNR}}} \quad ,$$

where SNR is known and σ_s can be measured. Hence, given an arbitrary Gaussian sequence $v[n]$ with variance σ_v^2, we derive the AWGN sequence via

$$\begin{aligned} v[n] &= \frac{v[n]}{\sigma_v} \cdot \sigma_v \quad , \\ &= \frac{v[n]}{\sigma_v} \cdot \frac{\sigma_s}{\sqrt{\text{SNR}}} \quad , \end{aligned} \tag{2.15}$$

and everything on the right hand side is either known, or can be measured.

Similarly, given a desired E_b/N_0, the relationship in (2.13) combined with the result in (2.15), enables

$$v[n] = \frac{v[n]}{\sigma_v} \cdot \frac{\sigma_s}{\sqrt{E_b/N_0}} \cdot \sqrt{\frac{N}{N_b}} \quad .$$

The noise sequence $v[n]$ is then added to the information signal as illustrated in Fig. 2.1.

2.5 Conclusion

This chapter sets the stage for the rest of the thesis by highlighting conventions used to represent signals and systems. A detailed GFSK signal development was presented with emphasis on parametrisation for Bluetooth. The Saleh-Valenzuela channel model, which will

be used to simulate dispersive channel conditions in the following chapters was discussed, and important quantifications for channel dispersiveness were stressed. AWGN scaling to obtain desired E_b/N_0 and SNR, as applied in our simulations, was also described. The next chapter will focus on receivers for GFSK modulated signals.

Chapter 3

Receivers for GFSK Modulated Signals

In Chapter 2 it was revealed that the modulation technique specified for Bluetooth is binary Gaussian frequency shift keying [17]. From the description of GFSK in Chapter 2 we can conclude that binary GFSK modulation involves the frequency modulation (FM) of a Gaussian filtered bipolar pulse sequence. It is therefore not surprising that FM demodulation techniques like FM discrimination and phase-shift discrimination are commonly used for the reception of GFSK modulated signals [86]. These algorithms fall into the class of single symbol demodulation methods because they make decisions based on observation of only one symbol period. They are therefore simple, but perform quite modestly [32]. More robust receivers for continuous phase modulated (CPM) signals[1] are based on multi-symbol observation intervals, and include the Viterbi receiver and the matched filter bank (MFB) receiver [35]. Such high-performing algorithms exhibit more than 6 dB gain over single symbol detectors [6].

This chapter contains a brief review of the FM discriminator in Sec. 3.1, the phase-shift discriminator in Sec. 3.2, the Viterbi receiver in Sec. 3.3, and the conventional matched filter bank receiver in Sec. 3.4. Our new efficient realisation of the MFB receiver for binary GFSK signals is presented in Sec. 3.6 [45, 46, 48], and is extended to multi-level GFSK in Sec. 3.7 [47, 49]. Coverage of the classic receivers in Secs. 3.1 to 3.4 is mainly a review to gain insight into their computational requirements, and therefore a reader purely interested in our novel contribution may proceed to Sec.3.6.

[1]CPM is a broad group of signals that encompasses GFSK.

3.1 FM Discriminator

The goal of an ideal FM discriminator is to translate a frequency shift in the received signal into an amplitude change in its output that is proportional to the size of the frequency deviation, and it is for this reason that an FM discriminator is said to perform FM-AM conversion [87, 88, 86, 89, 32]. This is achieved through the two stage process portrayed in Fig. 3.1 as a differentiation of the incoming signal, followed by a low pass filter that serves as an envelope detector. Some form of detection mechanism is then utilised to decide on the received symbol.

For example, if we suppose that the received analog GFSK modulated signal after down-conversion is given by

$$\hat{s}(t) = \cos\left(\int_{-\infty}^{t} \omega(\tau)\, d\tau \right) \quad , \tag{3.1}$$

then the output of the differentiator is

$$V_{\text{diff}}(t) = -\omega(t) \cdot \sin\left(\int_{-\infty}^{t} \omega(\tau)\, d\tau \right) \quad ,$$

which is the result of differentiating (3.1) with respect to t. Thereafter $V_{\text{diff}}(t)$ is fed to an envelope detector, which is a circuit that produces an output voltage $V_{\text{env}}(t)$ that is proportional to envelope of its input. That is to say,

$$V_{\text{env}}(t) \propto \omega(t) \quad . \tag{3.2}$$

However, in the digital domain approximate differentiation can be performed by the operation

$$V_{\text{diff}}[n] = \hat{s}[n] - \hat{s}[n-1] \quad , \tag{3.3}$$

while the function of the envelope detector can be performed with a low pass filter (LPF).

According to Fig. 3.1, a decision on the received symbol $\hat{p}[k]$ is based on the output of the LPF. The detector block in Fig. 3.1 is implemented by an integrate-and-dump algorithm [32],

Figure 3.1: FM discriminator.

whereby the sum of the detectors input samples during a symbol interval is compared with a predetermined threshold to decide the received symbol. It is intuitive from (3.2) that for binary GFSK the detector reference should be 0, and the detection procedure is similar to

$$\hat{p}[k] = \text{sign}\left\{ \sum_{\nu=kN-N+1}^{kN} V_{\text{env}}[\nu] \right\} \quad . \tag{3.4}$$

The FM discriminator described above has an observation interval of one symbol period, and hence if effectively programmed (3.3), (3.4) and the LPF will each require N complex valued multiply accumulates each symbol period. Hence, the complexity of this receiver accrues to $12N$ real valued multiply accumulates (MACs) per symbol (per bit for binary GFSK), because a complex operation is equivalent to 4 real valued ones[2]. The error performance of this receiver is rather poor in comparison to multi-symbol receivers, and it only achieves the maximum error ratio permitted in Bluetooth of BER=10^{-3} when $E_b/N_0 \geq 16.8$ dB [32].

3.2 Phase-Shift Discriminator

A phase-shift discriminator effectively unravels the FM modulated signal $\omega(t)$, from the received GFSK modulated signal $\hat{s}[n]$, through a series of processes depicted in Fig. 3.2 [86, 89, 32]. It operates on a baseband signal, which is assumed here to be ideal, and thus given by

$$\hat{s}[n] = \exp\left(j \sum_{\nu=-\infty}^{n} \hat{\omega}[\nu]\right) \quad .$$

The received baseband signal $\hat{s}[n]$ is first passed through an operator $\angle(\cdot)$ to extract its phase

$$\hat{\theta}[n] = \angle(\ \hat{s}[n]\ ) = \sum_{\nu=-\infty}^{n} \hat{\omega}[\nu] \quad , \tag{3.5}$$

which is then subjected an approximate differentiation shown as the middle block of Fig. 3.2, and mathematically equivalent to

$$\hat{\omega}[n] = \hat{\theta}[n] - \hat{\theta}[n-1] \quad . \tag{3.6}$$

[2]A complex MAC can be calculated by 3 multiplies and an increased number of additions [82], but this is not considered here.

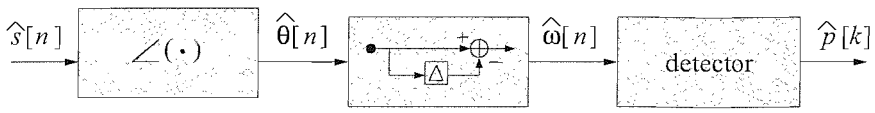

Figure 3.2: Phase-shift discriminator.

It is interesting to note that the output of each block of the phase-shift discriminator, and given in (3.5) and (3.6), would ideally be sequences encountered in the modulation process described in Sec. 2.2, and so phase-shift discrimination can be seen as the reverse of the FM modulation process.

The approximate differentiator output $\hat{\omega}[n]$ is utilised by a detector to select a received symbol $\hat{p}[k]$. Analogous to the FM discriminator integrate-and-dump, decision feed-forward, and decision feed-back may be employed at this stage [32]. However, if integrate-and-dump is employed, then for binary GFSK

$$\hat{p}[k] = \text{sign}\left\{ \sum_{\nu=kN-N+1}^{kN} \hat{\omega}[\nu] \right\} \quad . \tag{3.7}$$

The phase-shift discriminator described above has an almost equal BER performance to the FM discriminator in Sec. 3.1, requiring 16.6 dB for BER=10^{-3} [32]. And computational effort of approximately $8N$ MACs per symbol (per bit for binary GFSK) is expended on (3.6) and (3.7) per symbol period.

3.3 Viterbi Receiver

The optimum way to receive GFSK signals in AWGN — subject to restrictions discussed later — is by using a Viterbi receiver, which is discussed in [33, 35, 66, 58]. A Viterbi receiver computes the maximum likelihood [90] that a legitimate transmit waveform $s_i[n]$ was sent, given that a signal $\hat{s}[n]$ was received, whereby the subscript i differentiates one authentic waveform from the rest. This is achieved by minimising the function

$$\sum_{\nu=-\infty}^{\infty} |\hat{s}[\nu] - s_i[\nu]|^2 = \sum_{\nu=-\infty}^{\infty} \hat{s}[\nu]\hat{s}^*[\nu] + \sum_{\nu=-\infty}^{\infty} s_i[\nu]s_i^*[\nu] - 2\Re\left\{ \sum_{\nu=-\infty}^{\infty} \hat{s}[\nu]s_i^*[\nu] \right\} \quad \forall\, i \quad ,$$

or equivalently, by maximising the correlation

$$Z_i = \Re\left\{ \sum_{\nu=-\infty}^{\infty} \hat{s}[\nu]s_i^*[\nu] \right\} \quad \forall\, i \quad . \tag{3.8}$$

The modulating bit stream responsible for producing $s_i[n]$ that maximises (3.8), is chosen as the received data sequence.

However, performing the calculation in (3.8) is not practical even for short data bursts because of the exponential rise in complexity caused by the increased number and length of waveforms $s_i[n]$. For this reason, the Viterbi receiver comprises of a matched filter bank, followed by a Viterbi algorithm to search a trellis for the path that maximises Z_i in (3.8). This arrangement is portrayed in Fig. 3.3. Path metrics utilised by Viterbi are computed recursively once each symbol period by [33, 35, 66, 58]

$$\begin{aligned} Z_i[k] &= \sum_{\nu=-\infty}^{(k-1)N} \hat{s}[\nu]s_i^*[\nu] + \sum_{\nu=(k-1)N+1}^{kN} \hat{s}[\nu]s_i^*[\nu] \\ &= Z_i[k-1] + z_i[k] \quad , \end{aligned} \tag{3.9}$$

where $Z_i[k]$ and $z_i[k]$ are a path and incremental metrics for the ith path and at kth symbol period respectively. It is worth noting that the first term on the right hand side of (3.9) is available from the previous symbol period, while the second term can be computed using a filter bank matched to all legitimate waveforms transmitted across one symbol period. Careful analysis of (3.9) will reveal that the number of path metrics $Z_i[k]$, is unbounded unless the modulation index h is rational [33, 35, 66, 58]. The following trellis development illustrates this, and sheds light on how detection is achieved.

In order to simplify the discussion we adopt a formulation used in [35], and redefine the phase of the transmitted signal in (2.4) using (2.3) and (2.6) as

$$\begin{aligned} \theta[n] &= 2\pi h \sum_{\nu=-\infty}^{k} p[\nu]q[n-\nu N] && (k-1)N+1 \leq n \leq kN \quad , \\ &= \pi h \sum_{\nu=-\infty}^{k-L} p[\nu] + 2\pi h \sum_{\nu=k-L+1}^{k} p[\nu]q[n-\nu N] && (k-1)N+1 \leq n \leq kN \quad , \\ &= \phi_k + \phi[n] && (k-1)N+1 \leq n \leq kN \quad , \end{aligned} \tag{3.10}$$

so that ϕ_k is referred to as the *phase state*. Note that if h is a rational number given by $\frac{2m}{l}$, where m and l are integers, then l phase states exist, and they are given by $\{0, \frac{2\pi}{l}, \frac{2\cdot 2\pi}{l}, \ldots, \frac{(l-1)\cdot 2\pi}{l}\}$. Additionally, M^{L-1} *correlative states* are defined by the modulating symbol sequence $\{p_{k-1}, p_{k-2}, \ldots, p_{k-L+1}\}$, where M and L refer to the number of modulation levels, and optimal support length (in symbol periods) of the Gaussian filter

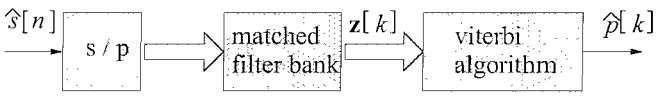

Figure 3.3: A Viterbi receiver comprising of a matched filter bank in series with a Viterbi algorithm to select the optimum path metric.

respectively. Phase and correlative states combine to form $l \cdot M^{L-1}$ states in the trellis of the form $\{\phi_k, p_{k-1}, p_{k-2}, \ldots, p_{k-L+1}\}$.

Example.

Considering a case typical of Bluetooth, where $h = \frac{1}{3}$, $M = 2$, and $L = 3$, the phase states are $\{0, \frac{\pi}{3}, \frac{2\cdot\pi}{3}, \pi, \frac{4\cdot\pi}{3}, \frac{5\cdot\pi}{3}\}$, while the correlative states are $\{\{-1,-1\}, \{-1,+1\}, \{+1,-1\}, \{+1,+1\}\}$, thus resulting in a total of 24 (6 × 4) states depicted in the trellis diagram in Fig. 3.4. In the trellis diagram of Fig. 3.4, $p_k = 1$ and $p_k = -1$ are symbolised with a dashed and solid line respectively. The next phase state in the trellis is determined by incrementing the current one by $p_{k-2} \cdot \frac{\pi}{3}$, while the next correlative state depends on p_k. An initial state of $\{0, -1, -1\}$ is often chosen [58, 35].

If initial phases are neglected, in this case there are 8 (M^L with $L = 3$ and $M = 2$) distinct and credible waveforms per symbol period, while 6 phase states exist. Therefore a total of 48 (8 × 6) authentic waveforms that are possible within each symbol period [33], and receipt of either of these signals implies a transition from a specific state on the trellis to another. Hence, each arrow connecting states of the trellis in Fig. 3.4 is associated with a 1-

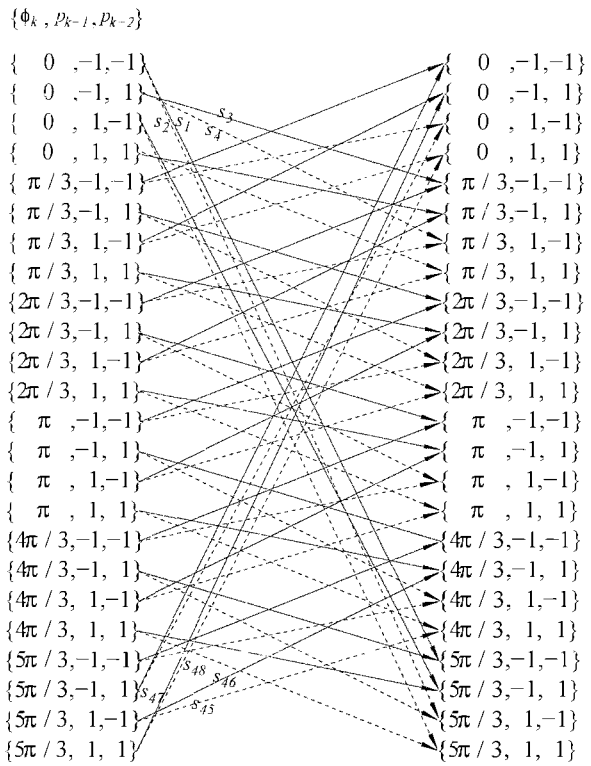

Figure 3.4: Trellis diagram for binary GFSK with $h = \frac{1}{3}$ and $L = 3$.

symbol long prototype signal $s_i[n]$, where $i \in \{1, 2, \ldots, 48\}$, and a matched filter is required for each one of these signals in order to determine which one is received per symbol period. In other words

$$\text{number of filters} = l{\cdot}M^L \quad ,$$

where $l.M^{L-1}$ is equal to the number of states, and M is indicative of the number of authentic transitions from or to each state.

Having discussed the nature of the trellis, and explained recursive computation of path metrics, selection of the optimum path via the Viterbi algorithm is well known and is covered extensively in [91, 92, 93]. Here it suffices to say that the maximum BER allowed in Bluetooth systems is 10^{-3} [17], and the Viterbi receiver accomplishes this with E_b/N_0 of 11 dB and 9.8 dB when h is $\frac{1}{3}$ [34, 6] and 0.35 [94] respectively. However, it has been established that the Viterbi receiver is susceptible to modulation index offsets in excess of 0.01 [34], and so a new trellis must be designed when $\Delta h \geq 0.01$. This is not convenient in Bluetooth networks because a precise value for h is not specified, but rather a range of $h \in (0.28, 0.35)$ [17]. Carrier frequency offsets of the magnitude permitted in Bluetooth are also likely to affect the trellis. These problems make the Viterbi receiver unsuitable for Bluetooth [34]. Nevertheless, assuming perfect synchronisation of all parameters, $4l{\cdot}M^L(N+1)$ real valued MACs are required per symbol (per bit for binary GFSK) to calculate the path metrics $Z_i[k]$ in (3.9).

3.4 Matched Filter Bank Receiver

A matched filter bank (MFB) receiver is based on filters matching legitimate waveforms of finite length, and effectively evaluates

$$Z_i[k] = \sum_{\nu=0}^{KN-1} \hat{s}[\nu - kN] s_i^*[\nu] \quad , \tag{3.11}$$

where K is an integer representing the observation interval in symbol periods [36, 37, 38, 35, 66]. Notice that (3.11) is similar to (3.8) except for a difference in limits. The MFB receiver has been used for reception of continuous phase frequency shift keying (CPFSK)[3] modulated signals, and differs from the Viterbi receiver in the sense that it achieves near optimal maximum likelihood detection of a single symbol, does not require a rational modulation

[3] A group of signal types of which GFSK is a subset.

index, and is relatively insensitive to errors in the modulation index because of its limited time span [36, 37, 38, 35, 66].

For the interval $(k-K)N+1 \leq n \leq kN$, due to the support length of the Gaussian filter, 2^{K+L-1} possible received signals exist if we neglect the initial phase shift, and a matched filter is provided for each one of these sequences. The filter with the largest output determines the received signal, and the symbol at the center of the modulating symbol sequence responsible for the received waveform is chosen as the detected symbol[4]. A slicer then converts the estimated symbol $\hat{p}[k]$ to a received bit $\hat{b}[k]$. The resulting scheme is depicted in Fig. 3.5, where $s_{i,j}[n]$ are possible transmitted sequences with $i \in \{\pm 1\}$ indicating the value of the middle symbol in the modulating symbol sequence, and $j = 0(1)2^{K+L-2}-1$ indexing the possible combinations of the remaining $K+L-2$ symbols that influence the waveform, and a detector selects the largest magnitude value, determining the output $\hat{p}[k]$ as

$$\hat{p}[k] = \arg\max_i \left\{ \max_j \left| \sum_{n=0}^{KN-1} \hat{s}[kN-n] \cdot s_{i,j}^*[-n] \right| \right\} \quad , \tag{3.12}$$

where $s_{i,j}^*[-n]$ are the 2^{K+L-1} matched filter responses. Note that the detector imposes a delay such that ideally $\hat{p}[k] = p[k - \frac{K+1}{2}]$.

The performance of this receiver improves with an increase in the observation interval K. For example, provided $L = 3$ and $h = 0.35$, when $K = 7$ or $K = 9$, the MFB receiver has been shown to attain the maximum permitted Bluetooth BER of 10^{-3} at an E_b/N_0 of 10.2 or 9.8 dB respectively [45, 46, 48, 49]. Beyond $K = 9$ the gain appears trivial.

However, despite its performance merits, for $M = 2$ modulation levels, the computational complexity accrues to

$$C_{\text{standard}} = 2\ NK2^{K+L-1} \tag{3.13}$$

real valued multiply accumulates (MACs) per bit, or

$$\tilde{C}_{\text{standard}} = 2\ NK2^{K} \tag{3.14}$$

MACs, if a small performance degradation is acceptable, and 2^{L-1} marginal modulating symbols are neglected, thereby using a subset of $s_{i,j}[n]$ with 2^K unique central modulating symbols. The costs in (3.13) and (3.14) consider the fact that the possible sequences $s_{i,j}[n]$ consist of complex conjugate pairs, and that a complex valued operation accounts for 4 real

[4]Assuming non-coherent mode, where K must be odd [36].

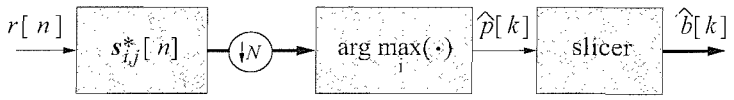

Figure 3.5: Standard matched filter bank receiver for CPFSK signals.

valued one. Nevertheless, the complexity in (3.13) is prohibitively large for implementation. Therefore, in the Sec. 3.6 we seek a low complexity implementation of this receiver, but first a qualitative comparison of the classic GFSK receivers is presented in Sec. 3.5.

3.5 Comparative Summary of Classic GFSK Receivers

While introducing this thesis in Sec.1.1, we indicated that our aim was to take advantage of the additional computational capacity available to Bluetooth when it shares a common hardware platform with a more complex WLAN, in order to improve BER of Bluetooth links. In such an effort there are several potential areas for improvement, but probably chief amongst them is the selection of an appropriate receiver, that will provide good performance under perfect conditions and do fairly well when common signal adversities exist.

The discussions in this chapter so far have focused on classic receivers, which may be categorised as those with a single-symbol observation interval or $K = 1$, and those which require a longer period. Longer observation intervals imply more processing, hence in Tab. 3.1, while the FM and phase-shift discriminators consume only 24 and 16 MACs per symbol, the Viterbi and MFB receivers require 3840 and 73728 MACs respectively. However, work by other researchers suggests that single-symbol detection algorithms like the FM discriminator and the phase-shift discriminator need more than 16 dB E_b/N_0 to achieve a BER of 10^{-3} [32], which is the minimum acceptable performance for Bluetooth [17]. This is in contrast to multi-symbol receivers such as the Viterbi and MFB receivers, that require a mere 9.8 dB for the same feat [94, 45, 46, 48, 49].

Columns 2 and 3 of Tab. 3.1 summarise the results from the last paragraph, and suggest that the Viterbi receiver is the best performance-complexity compromise when extra resource is available. However, Bluetooth has a lax specification on carrier frequency offsets, and a range of acceptable modulation indices [17]. A mismatch in either of these parameters will cause errors that will accumulate over the full length of the observation interval. Even though single-symbol receivers are affected by these offsets [44, 95], a larger K entails less resilience [46, 50, 53, 48]. It is therefore not surprising that the Viterbi receiver, with theo-

retical $K \to \infty$, is too sensitive to unsynchronised parameters, and is therefore unsuitable for cheap and imprecise standards like Bluetooth [34]. Even if the transmitter parameters are discernible at the receiver, offset compensation is difficult because it involves a complete redesign of the Viterbi receiver, including the number of states [35].

According to column 4 of Tab. 3.1, the MFB receiver is less susceptible to frequency and modulation index errors than Viterbi [46, 50, 53, 48], therefore in the following section an efficient realisation of the MFB receiver is derived, which retains error performance and resilience of its conventional implementation, but employs a number of MACS more comparable to those required for the Viterbi receiver.

RECEIVER	E_b/N_0 for BER=10^{-3} (dB)	COMPLEXITY (MACs)	RESILIENCE TO PARAMETER MISMATCH
FM discriminator	16.8	24	High
Phase-shift discriminator	16.6	16	High
Viterbi receiver ($h = 0.35$)	9.8	3840	Very low
MFB receiver ($K = 9$, h=0.35)	9.8	73728	Medium

Table 3.1: An exemplar comparison of classic GFSK receivers [32, 94, 45, 46, 48, 49], with $N = 2$.

3.6 Low Complexity MFB Receiver for Binary GFSK

In our presentation of a lower complexity implementation of the MFB receiver for GFSK signals [45, 46, 48, 49], we will first inspect the matched filter responses in Sec. 3.6.1, and thereafter develop a recursive scheme for their representation in Sec. 3.6.2, leading to an analysis of its complexity in Sec. 3.8. This section shall consider only binary GFSK, where $p[k] \in \pm 1$, and each symbol encodes 1 bit of information. An extension for M-ary GFSK (M-GFSK) follows in Sec. 3.7.

3.6.1 Received Signals

For simplicity we assume in the following that the channel distortion and carrier frequency offset have been eliminated by preceding signal processing blocks. Therefore let us assume that K symbol (or bit) periods of the received signal $\hat{s}[n]$ are held in a tap delay line (TDL)

vector $\hat{\mathbf{s}}_k$, synchronised with the kth symbol to be the most recent datum.

$$\hat{\mathbf{s}}_k = \begin{bmatrix} \grave{s}_k \\ \grave{s}_{k-1} \\ \vdots \\ \grave{s}_{k-K+1} \end{bmatrix} = \mathbf{s}_k + \mathbf{v}_k = \underbrace{\begin{bmatrix} \tilde{s}_k \\ \tilde{s}_{k-1} \\ \vdots \\ \tilde{s}_{k-K+1} \end{bmatrix}}_{\mathbf{s}_k} + \mathbf{v}_k \tag{3.15}$$

where $\mathbf{v}_k \in \mathbb{C}^{NK}$ holds the noise samples. The vector $\tilde{\mathbf{s}}_k$ is defined as

$$\tilde{\mathbf{s}}_k = [s[kN] \;\; s[kN-1] \;\; \ldots \;\; s[(k-1)N+1]]^{\mathrm{T}} \quad ,$$

and $\grave{\mathbf{s}}_k$ is defined analogously. According to (2.5), $\tilde{\mathbf{s}}_k$, holding N samples within a symbol period, can be expanded as

$$\tilde{\mathbf{s}}_k = \underbrace{\begin{bmatrix} \prod_{\nu=(k-1)N+1}^{kN} e^{j\omega[\nu]} \\ \prod_{\nu=(k-1)N+1}^{kN-1} e^{j\omega[\nu]} \\ \vdots \\ e^{j\omega[(k-1)N+1]} \end{bmatrix}}_{\mathbf{u}_k} \cdot \prod_{\nu=-\infty}^{(k-1)N} e^{j\omega[\nu]} \tag{3.16}$$

whereby for the samples in $\mathbf{u}_k$ the instantaneous frequency is only accumulated from the start of the kth symbol period. Inserting (3.16) into $\mathbf{s}_k$ from (3.15) yields

$$\mathbf{s}_k = \begin{bmatrix} \mathbf{u}_k & \cdot e^{j(\theta_{k-K+1}+\cdots+\theta_{k-2}+\theta_{k-1})} \\ \mathbf{u}_{k-1} & \cdot e^{j(\theta_{k-K+1}+\cdots+\theta_{k-2})} \\ \vdots & \\ \mathbf{u}_{k-K+2} & \cdot e^{j\theta_{k-K+1}} \\ \mathbf{u}_{k-K+1} & \cdot 1 \end{bmatrix} \cdot e^{j\theta_0}$$

with

$$\theta_k = \sum_{\nu=(k-1)N+1}^{kN} \omega[\nu] \qquad \text{and} \quad \theta_0 = \sum_{\nu=-\infty}^{(k-K)N} \omega[\nu] \quad .$$

Firstly, note that each vector $\mathbf{u}_k$ can take on the shape of 2^L different waveforms, whereby L was the support length of the Gaussian window in symbol periods. Secondly, observe that a phase correction term $e^{j\theta_k}$ contains the instantaneous frequency values accumulated over the kth symbol period, which is held in the top element of $\mathbf{u}_k$ in (3.16) and is applied to all subsequent symbol periods. The initial phase of $s[n]$ entering the TDL is θ_0.

3.6.2 Recursive Matched Filter Formulation

The matched filter responses $s^*_{i,j}[-n]$ are designed from the transmitted signal $s[n]$ in (2.5). Utilising the previous observation that $\mathbf{u}_k$ only takes on 2^L basic waveforms independent of k, we will construct a matched receiver in steps.

Case $K = 1$. Consider a matched filter for $K = 1$ covering the kth symbol period. The 2^L matched filter outputs are given by

$$\mathbf{y}_k^{(1)} = \mathbf{W}^{(1)} \grave{\mathbf{s}}_k$$

with $\mathbf{W}^{(1)} \in \mathbb{C}^{2^L \times N}$ containing the possible complex conjugated waveforms in its rows. The superscript $^{(1)}$ indicates that only a single symbol period $K = 1$ is observed. The first column of $\mathbf{W}^{(1)}$, denoted by $\mathbf{w}$, holds the 2^L possible values for $e^{-j\theta_k}$. We assume that the first row of $\mathbf{W}^{(1)}$ is the matched filter for the symbol at the center of a L symbol sequence, all of value -1, binary coded decimally down so that the last row of $\mathbf{W}^{(1)}$ matches the symbol at the middle of a sequence of L symbols of value +1. Hence, rows of $\mathbf{W}^{(1)}$ are formed from the central N samples obtained via GFSK modulation[5] of L bits of value 0, binary coded decimally down to the last row with L bits of value 1.

Case $K = 2$. Expanding to $K = 2$, we can denote

$$\mathbf{y}_k^{(2)} = \mathbf{W}^{(2)} \begin{bmatrix} \grave{\mathbf{s}}_k \\ \grave{\mathbf{s}}_{k-1} \end{bmatrix} \tag{3.17}$$

with $\mathbf{W}^{(2)} \in \mathbb{C}^{2^{L+1} \times 2N}$ consisting of all possible 2^{L+1} complex conjugated and time reversed versions of the transmitted signals in its rows. Therefore note that in constructing the 2^{L+1} matched filter responses in $\mathbf{W}^{(2)}$, only one extra modulating symbol needs to be considered compared to the responses in $\mathbf{W}^{(1)}$.

Example. For $L = 3$, the rows in $\mathbf{W}^{(1)}$ should contain the central N samples of the responses to the bit sequences $\{0,0,0\}$ to $\{1,1,1\}$, while $\mathbf{W}^{(2)}$ would cater for an additional bit, hence covering the middle $2N$ samples of responses to the combinations $\{0,0,0,0\}$ to $\{1,1,1,1\}$. So for each possible sequence contained in $\mathbf{W}^{(1)}$, two new possibilities arise in $\mathbf{W}^{(2)}$, and so on for higher values of K. This formulation is portrayed in Fig. 3.6, and to clarify, Fig. 3.7 features the instantaneous frequency and phase of the response to combinations $\{0,0,0,0\}$ to $\{1,1,1,1\}$, with the response to the combination $\{0,0,0,1\}$

[5]Includes encoding of a bit stream into a symbol stream and FM modulation of the symbol stream.

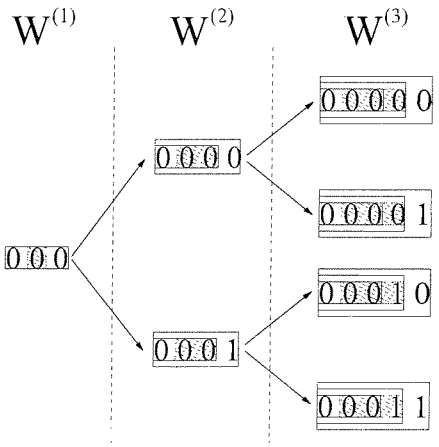

Figure 3.6: Tree of modulating bit sequences for filter responses derived from the first row of $\mathbf{W}^{(1)}$, with $L = 3$ and $M = 2$.

plotted in bold. Thus, 2^L outputs of filter bank $\mathbf{W}^{(1)}$ from the previous symbol period can be used with its current results to compute the 2^{L+1} outputs of $\mathbf{W}^{(2)}$, enabling us to write

$$\begin{aligned} \mathbf{y}_k^{(2)} &= \mathbf{D}^{(2)}\,\mathbf{A}^{(2)}\,\mathbf{W}^{(1)}\,\grave{\mathbf{s}}_k \;+\; \mathbf{M}^{(2)}\,\mathbf{W}^{(1)}\,\grave{\mathbf{s}}_{k-1} \\ &= \mathbf{D}^{(2)}\,\mathbf{A}^{(2)}\,\mathbf{y}_k^{(1)} \;+\; \mathbf{M}^{(2)}\,\mathbf{y}_{k-1}^{(1)} \end{aligned} \tag{3.18}$$

whereby $\mathbf{y}_{k-1}^{(1)}$ are the single-symbol matched filter outputs for the $(k-1)$st symbol period. The matrix $\mathbf{A}^{(2)}$,

$$\mathbf{A}^{(2)} = \text{blockdiag}\left\{ \begin{bmatrix} 1 \\ 1 \end{bmatrix} \right\} \in \mathbb{Z}^{2^{L+1} \times 2^L} \quad ,$$

produces an extra copy of the outputs of the intermediate filter bank $\mathbf{W}^{(1)}$ during the kth symbol period, in other words an extra copy of each element of $\mathbf{y}_k^{(1)}$, while

$$\mathbf{D}^{(2)} = \begin{bmatrix} \text{diag}\{\mathbf{w}\} & \mathbf{0} \\ \mathbf{0} & \text{diag}\{\mathbf{w}\} \end{bmatrix} \in \mathbb{C}^{2^{L+1} \times 2^{L+1}}$$

applies the 2^L possible phase correction terms due to the previous symbol period $e^{-j\theta_{k-1}}$, and the matrix

$$\mathbf{M}^{(2)} = \begin{bmatrix} \mathbf{I}_{2^L} \\ \mathbf{I}_{2^L} \end{bmatrix} \in \mathbb{Z}^{2^{L+1} \times 2^L} \quad ,$$

whereby $\mathbf{I}_{2^L}$ is a $2^L \times 2^L$ identity matrix, performs an almost similar function as $\mathbf{A}^{(2)}$ by producing an extra copy of the outputs of the intermediate filter bank $\mathbf{W}^{(1)}$ during the $(k-1)$th symbol period, that is to say an extra copy of each element of $\mathbf{y}_{k-1}^{(1)}$, and arranging them in a fashion that facilitates expansion (addition) by the extra symbol considered for $K = 2$, compared to an observation interval of just $K = 1$.

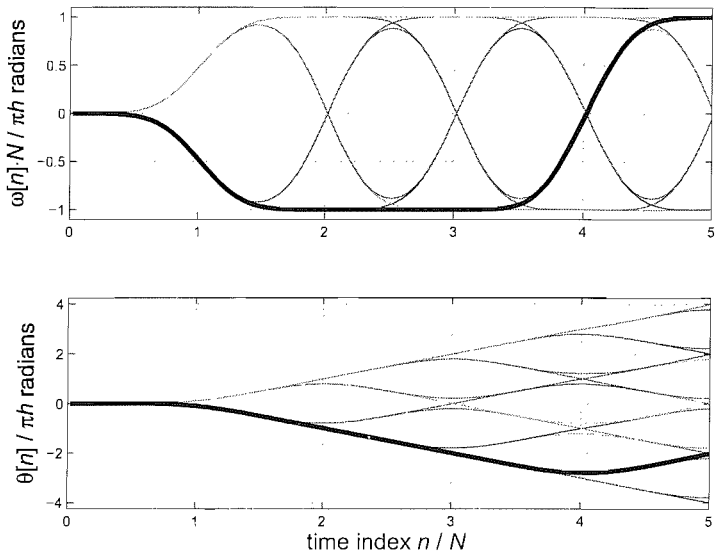

Figure 3.7: Binary GFSK signal frequency (top) and phase (bottom) trajectories.

From the expansion of (3.18) in Fig. 3.8, it is clear that $\mathbf{M}^{(2)}$ and $\mathbf{A}^{(2)}$ serve merely as permutation matrices for vectors $\mathbf{y}_{k-1}$ and $\mathbf{y}_k$ respectively. While $\mathbf{D}^{(2)}$ imposes a phase shift on the elements of $\mathbf{y}_k$ due to the corresponding elements of $\mathbf{y}_{k-1}$. The example highlighted in Fig. 3.8 can be stated in words as follows: The output of the 11th 2-symbol long filter at the kth symbol period $y_k^{(2)}[11]$ is derived by adding the output of the 3rd 1-symbol long filter — 3rd row of $\mathbf{W}^{(1)}$ — during the $(k-1)$th symbol period $y_{k-1}^{(1)}[3]$, to the product of the output of the 6th 1-symbol long filter — 6th row of $\mathbf{W}^{(1)}$ — during the kth symbol period $y_k^{(1)}[6]$ and the third element of $\mathbf{w}$ — whose angle reflects the phase gained across the 3rd intermediate filter, or 3rd row of $\mathbf{W}^{(1)}$. Notice that no 2-symbol long filter was employed to compute $y_k^{(2)}[11]$.

Case K arbitrary. Generalising from the previous cases, we formulate recursively for $\mathbf{y}_k^{(K)} \in \mathbb{C}^{2^{K+L-1}}$

$$\mathbf{y}_k^{(K)} = \mathbf{D}^{(K)}\, \mathbf{A}^{(K)}\, \mathbf{y}_k^{(K-1)} \;+\; \mathbf{M}^{(K)}\, \mathbf{y}_{k-K+1}^{(1)}\,, \tag{3.19}$$

where

$$\mathbf{M}^{(K)} \;=\; \begin{bmatrix} \mathbf{M}^{(K-1)} \\ \mathbf{M}^{(K-1)} \end{bmatrix} \in \mathbb{Z}^{2^{L+K-1}\times 2^L}\,, \qquad \text{with} \quad \mathbf{M}^{(1)} = \mathbf{I}_{2^L} \tag{3.20}$$

$$\mathbf{A}^{(K)} = \begin{bmatrix} \mathbf{A}^{(K-1)} & \mathbf{0} \\ \mathbf{0} & \mathbf{A}^{(K-1)} \end{bmatrix} \in \mathbb{Z}^{2^{L+K-1} \times 2^{L+K-2}}, \quad \text{with} \tag{3.21}$$

$$\mathbf{A}^{(1)} = \text{blockdiag}\left\{ \begin{bmatrix} 1 \\ 1 \end{bmatrix} \right\} \in \mathbb{Z}^{2^L \times 2^{L-1}},$$

$$\mathbf{D}^{(K)} = \begin{bmatrix} \mathbf{D}^{(K-1)} & \mathbf{0} \\ \mathbf{0} & \mathbf{D}^{(K-1)} \end{bmatrix} \in \mathbb{Z}^{2^{L+K-1} \times 2^{L+K-1}}, \text{ with } \mathbf{D}^{(1)} = \text{diag}\{\mathbf{w}\}. \tag{3.22}$$

This form of the matched filter bank receiver is depicted by the flow graph in Fig. 3.9. A detector similar to (3.12), selecting the index of the largest element would operate on $\mathbf{y}_k^{(K)}$ to determine the correct output symbol $\hat{p}[k]$.

$$\begin{bmatrix} y_k^{(2)}[1] \\ y_k^{(2)}[2] \\ y_k^{(2)}[3] \\ y_k^{(2)}[4] \\ y_k^{(2)}[5] \\ y_k^{(2)}[6] \\ y_k^{(2)}[7] \\ y_k^{(2)}[8] \\ y_k^{(2)}[9] \\ y_k^{(2)}[10] \\ y_k^{(2)}[11] \\ y_k^{(2)}[12] \\ y_k^{(2)}[13] \\ y_k^{(2)}[14] \\ y_k^{(2)}[15] \\ y_k^{(2)}[16] \end{bmatrix} = \begin{bmatrix} w[1] \cdot y_k^{(1)}[1] \\ w[2] \cdot y_k^{(1)}[1] \\ w[3] \cdot y_k^{(1)}[2] \\ w[4] \cdot y_k^{(1)}[2] \\ w[5] \cdot y_k^{(1)}[3] \\ w[6] \cdot y_k^{(1)}[3] \\ w[7] \cdot y_k^{(1)}[4] \\ w[8] \cdot y_k^{(1)}[4] \\ w[1] \cdot y_k^{(1)}[5] \\ w[2] \cdot y_k^{(1)}[5] \\ w[3] \cdot y_k^{(1)}[6] \\ w[4] \cdot y_k^{(1)}[6] \\ w[5] \cdot y_k^{(1)}[7] \\ w[6] \cdot y_k^{(1)}[7] \\ w[7] \cdot y_k^{(1)}[8] \\ w[8] \cdot y_k^{(1)}[8] \end{bmatrix} + \begin{bmatrix} y_{k-1}^{(1)}[1] \\ y_{k-1}^{(1)}[2] \\ y_{k-1}^{(1)}[3] \\ y_{k-1}^{(1)}[4] \\ y_{k-1}^{(1)}[5] \\ y_{k-1}^{(1)}[6] \\ y_{k-1}^{(1)}[7] \\ y_{k-1}^{(1)}[8] \\ y_{k-1}^{(1)}[1] \\ y_{k-1}^{(1)}[2] \\ y_{k-1}^{(1)}[3] \\ y_{k-1}^{(1)}[4] \\ y_{k-1}^{(1)}[5] \\ y_{k-1}^{(1)}[6] \\ y_{k-1}^{(1)}[7] \\ y_{k-1}^{(1)}[8] \end{bmatrix}$$

$$\mathbf{y}_k^{(2)} = \mathbf{D}^{(2)} \cdot \mathbf{A}^{(2)} \mathbf{y}_k^{(1)} + \mathbf{M}^{(2)} \mathbf{y}_{k-1}^{(1)}$$

Figure 3.8: Expansion of Equation (3.18) for $\mathbf{y}_k^{(2)}$.

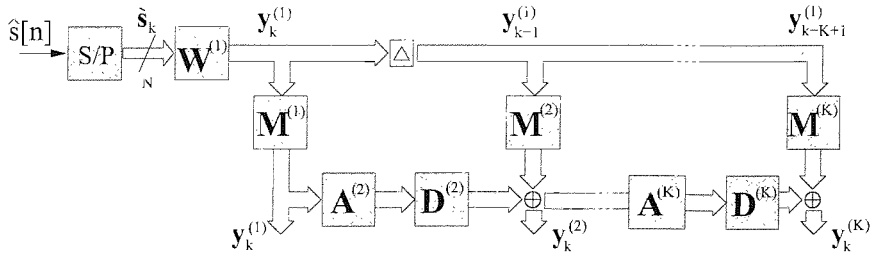

Figure 3.9: Lower-complexity implementation of a matched filter bank receiver. The received GFSK signal $\hat{s}[n]$ is passed through a serial/parallel converter and an intermediate filter bank $\mathbf{W}^{(1)}$ with a single symbol duration. Processed over K stages, the matched filter bank outputs are contained in $\mathbf{y}_k^{(K)}$.

3.7 Low Complexity MFB Receiver for Multi-level GFSK

The explanation of the operation of the low-complexity MFB receiver for the simple case of binary GFSK in Sec. 3.6, will form a basis for extending the discussion to M-ary GFSK (M-GFSK) in the following. However, since subsequent chapters are primarily concerned with binary GFSK, if use of the low-cost receiver for M-GFSK signals is not of interest, the reader may proceed to Sec. 3.8 for a analysis of the computational cost associated with the efficient realisation of the MFB.

For clarity, the discussions of M-GFSK will parallel those in Sec. 3.6, with the matched filter responses in Sec. 3.7.2, the recursive scheme for their representation is given in Sec. 3.7.3, and the complexity evaluation in Sec. 3.8. In order to maintain conciseness only deviations from the earlier explanations will be emphasised here, for detailed coverage of multilevel processing refer to the papers [47, 49]. However, before we start with a short signal development in Sec. 3.7.1, we point out that analogous to Sec. 3.4, a standard M-GFSK MFB receiver will require M^{K+L-1} filters of length KN, and thereby result in a complexity of

$$C_{\text{standard}} = (2\,NKM^{K+L-1})/N_b \tag{3.23}$$

real valued MACs per bit, with N_b equal to the number of bits per symbol, or

$$\tilde{C}_{\text{standard}} = (2\,NKM^{K})/N_b \tag{3.24}$$

MACs, if M^{L-1} marginal modulating symbols are neglected, and only a subset of $s_{i,j}[n]$ with M^K unique central modulating symbols are utilised.

3.7.1 Signal Model

M-GFSK modulation requires that groups of N_b data bits are mapped onto multilevel symbols, $p[k] \in \{\pm 1, \pm 3, \pm 5, \ldots, \pm(M-1)\}$. Each symbol can have one of M amplitude levels, symmetrically distributed above and below zero, such that $M = 2^{N_b}$, whereby the mapping from bit to symbol stream is accomplished via Gray coding [58, 59]. The rest of the signal development is similar to that in Sec. 2.3, with the symbol stream expanded by a factor of N and passed through a Gaussian filter with impulse response $g[n]$, to yield the instantaneous frequency signal in (2.3), and subsequently the transmitted signal is evaluated according to (2.5). The Gaussian filter introduces intersymbol interference, with each symbol smeared into $(L-1)/2$ adjacent symbols on each side. Consequently, there are M^L authentic instantaneous frequency waveforms $\omega[n]$ per symbol period, which form an eye portrayed in Fig. 3.10. The exponential growth in legitimate signals with symbol period (M^k) is more obvious from the phase tree in Fig. 3.10. Hence, in this case the MFB receiver will have to cater for M^{K+L-1} possibilities, such that i in (3.12) can take on 1 of M options and $j = 0(1)M^{K+L-2}-1$. The slicer in Fig. 3.5 must now perform Gray decoding to convert $\hat{p}[k]$ to a vector of N_b received bits $\hat{\mathbf{b}}[k]$.

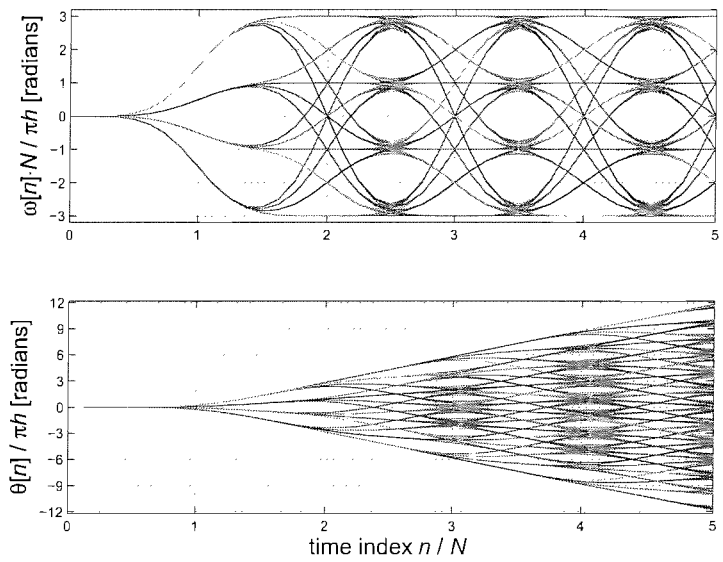

Figure 3.10: Instantaneous frequency (top) and phase (bottom) trees for a GFSK modulated signal, with $M = 4$, and $K_{BT} = 0.5$ ($L = 3$).

3.7.2 Received Signals

Filter responses are determined analogous to Sec. 3.6.1, except for a change in the dimensions of matrices due to M^L possibilities for $\mathbf{u}_k$.

3.7.3 Recursive Matched Filter Formulation

The development of the recursive matched filter responses is similar to Sec. 3.6.2, except for the fact that $\mathbf{W}^{(1)} \in \mathbb{C}^{M^L \times N}$, with its first column $\mathbf{w}$, holding M^L authentic values for $e^{-j\theta_k}$. Analogous to the system for binary GFSK, the first and last rows of $\mathbf{W}^{(K)}$ contain the filter coefficients that match the KN samples in the middle of the sequence that results from M-GFSK modulating a sequence of $(K+L-1)N_b$ 0s and 1s respectively. Hence, rows of $\mathbf{W}^{(1)}$ are formed from the central N samples obtained via M-GFSK modulation of LN_b bits of value 0, binary coded decimally down to the last row with LN_b bits of value 1.

Even though the recursive algorithm in (3.19) does not change, the matrices $\mathbf{A}$, $\mathbf{D}$ and $\mathbf{M}$ need to be adjusted to reflect the increased size of $\mathbf{W}^{(1)}$. Hence,

$$\mathbf{M}^{(K)} = \left[\mathbf{M}^{(K-1)} \quad \dots \quad \mathbf{M}^{(K-1)}\right]^T \in \mathbb{Z}^{M^{L+K-1} \times M^L}, \tag{3.25}$$

with $\mathbf{M}^{(1)} = \mathbf{I}_{M^L}$,

$$\mathbf{A}^{(K)} = \begin{bmatrix} \mathbf{A}^{(K-1)} & & \mathbf{0} \\ & \ddots & \\ \mathbf{0} & & \mathbf{A}^{(K-1)} \end{bmatrix} \in \mathbb{Z}^{M^{L+K-1} \times M^{L+K-2}}, \tag{3.26}$$

with

$$\mathbf{A}^{(1)} = \text{blockdiag}\left\{\left[\underbrace{1 \quad \dots \quad 1}_{M}\right]^{\mathrm{T}}\right\} \in \mathbb{Z}^{M^L \times M^{L-1}},$$

and

$$\mathbf{D}^{(K)} = \begin{bmatrix} \mathbf{D}^{(K-1)} & & \mathbf{0} \\ & \ddots & \\ \mathbf{0} & & \mathbf{D}^{(K-1)} \end{bmatrix} \in \mathbb{Z}^{M^{L+K-1} \times M^{L+K-1}}, \tag{3.27}$$

with $\mathbf{D}^{(1)}$= diag$\{\mathbf{w}\}$. It is interesting to note that recursive matched filter formulation is independent of the coding system used to map bits to symbols, and is scalable to different M by a simple system of parameterisation, these are attractive features for a SDR.

3.8 Computational Complexity

Inspecting the operations in Fig. 3.9, per symbol period, M^L matched filter operations of length N have to be performed by $\mathbf{W}^{(1)}$. The matrices $\mathbf{M}^{(k)}$ and $\mathbf{A}^{(k)}$ only performing indexing, so that the only arithmetic operations required are multiplications with the diagonal elements of the phase correction matrices $\mathbf{D}^{(K)}$, yielding a total of

$$C_{\text{efficient}} = \left(4M^L N + 4\sum_{k=1}^{K-1} M^{L+k}\right)\frac{1}{N_b} \tag{3.28}$$

MACs per bit.

If marginal symbols are disregarded analogously to (3.14), then desired outputs $\tilde{\mathbf{y}}_k^{(K)} = \mathbf{S}^{(K)}\mathbf{y}_k^{(K)}$ can be extracted. As an example for $L = 3$ and $M = 2$, the extraction matrix $\mathbf{S}^{(K)}$ takes the form

$$\mathbf{S}^{(K)} = \left[\begin{array}{cc} \mathbf{G}^{(K)} & 0_{M^K \times M^{K+L-2}} \end{array}\right] \in \mathbb{Z}^{M^K \times M^{K+L-1}}$$

with

$$\mathbf{G}^{(K)} = \text{blockdiag}\{[1 \underbrace{0 \ \ldots \ 0}_{M-1}]\} \in \mathbb{Z}^{M^K \times M^{K+L-2}}$$

The extraction matrices can be appropriately absorbed into (3.20)–(3.22), yielding a reduced complexity of

$$\tilde{C}_{\text{efficient}} = \left(4M^L N + \frac{4}{M^{L-1}}\sum_{k=1}^{K-1} M^{L+k}\right)\frac{1}{N_b}$$

MACs per bit.

The computational cost for the standard and lower complexity MFB receiver in terms of real valued MACs expressed in (3.23) and (3.28) respectively, are evaluated in Figs. 3.11 and 3.12 for increasing observation interval K, oversampling factor N, and number of levels M. The figures portray an exponential rise in the computational savings for the low-complexity realisation with increase in K and M, and a linear gain for with increase in N. This gain is exemplified by approximately 80% reduction when $K = 9$, $N = 2$, $M = 2$ and $L = 3$, while even greater gains are possible for longer observation intervals K and modulation levels M.

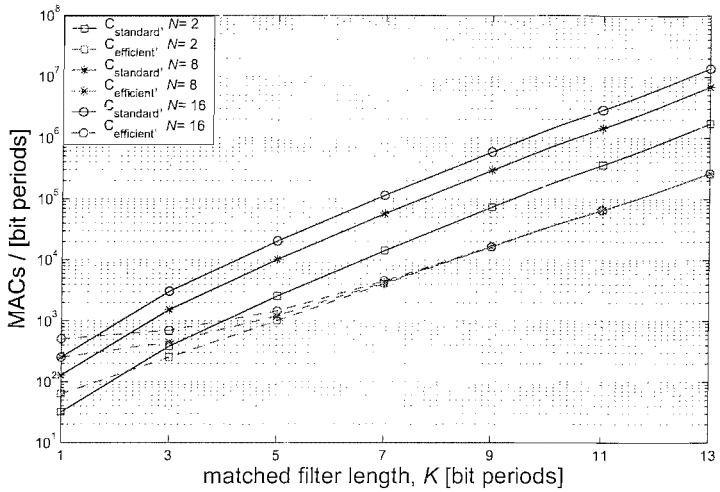

Figure 3.11: Complexity comparison: standard (solid lines) vs. efficient (dashed lines) MFB receiver for GFSK signals, with $M = 2$, and K_{BT}=0.5 ($L = 3$).

3.9 Comparative Summary of GFSK Receivers

Following the complexity analysis of the novel efficient MFB receiver for GFSK modulated signals in Sec. 3.8, we revise the presentation of Sec. 3.5, and compare classic receivers with the efficient MFB receiver in Tab. 3.2. It is perceivable from Tab. 3.2 that unlike the standard implementation of the MFB receiver, the efficient is more comparable with the Viterbi receiver in terms of complexity, while also maintaining the desirable BER typical of the standard MFB receiver. Additionally, superior resilience to unsynchronised parameters favours the use of the new algorithm in high-performance scenarios, instead of Viterbi.

RECEIVER	E_b/N_0 for BER=10^{-3} (dB)	COMPLEXITY (MACs)	RESILIENCE TO PARAMETER MISMATCH
FM discriminator	16.8	24	High
Phase-shift discriminator	16.6	16	High
Viterbi receiver (h = 0.35)	9.8	3840	Very Low
MFB receiver (K = 9, h=0.35)	9.8	73728	Medium
Eff. MFB receiver (K = 9, h=0.35)	9.8	16384	Medium

Table 3.2: An exemplar comparison of GFSK receivers [32, 94, 45, 46, 48, 49], with $N = 2$.

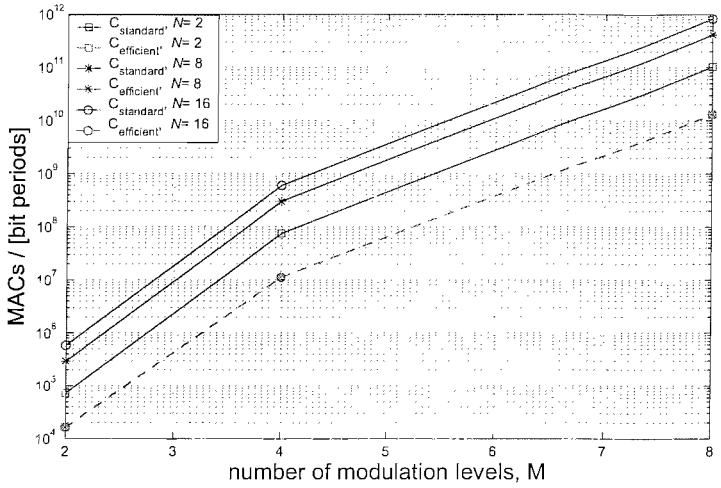

Figure 3.12: Complexity comparison: standard (solid lines) vs. efficient (dashed lines) MFB receiver for GFSK signals, with $K = 9$, and K_{BT}=0.5 ($L = 3$).

3.10 Simulations and Results

This section contains an evaluation of the lower complexity MFB receiver implementation. In our simulations the signal was developed according to Sec. 2.2, with a parameter set of $K_{BT} = 0.5$, $L = 3$, $N = 2$, and $h = 0.35$, so as to simulate a Bluetooth signal [17]. Where $M > 2$, Gray coding specified in [12] was used to map data bits onto M-ary bipolar symbols. In order to maintain similar bandwidth for different number of modulation levels, the modulation index was normalised with the magnitude of the greatest symbol, so that $h = 0.35$ for $M = 2$, $h = 0.35/3$ for $M = 4$, and $h = 0.35/7$ for $M = 8$. Fig. 3.13 confirms that similar spectral characteristics were achieved for different M.

3.10.1 Bit Error Ratio

From the derivation in Sec. 3.6 it is evident that the efficient algorithm is equivalent to the standard MFB receiver for GFSK signals. The efficient algorithm simply eliminates redundancy involved in providing the matched filter outputs, and therefore does not sacrifice performance. However, the BER of the two implementations was confirmed to be equivalent via simulation, and is displayed in Fig. 3.14. Results indicate better reception for longer observation intervals, up to $K \approx 9$, beyond which increasing K does not appear to yield significant improvements. The MFB receiver's high performance is exemplified by the fact that it attains BER=10^{-3}, which is the maximum permitted in Bluetooth networks [17],

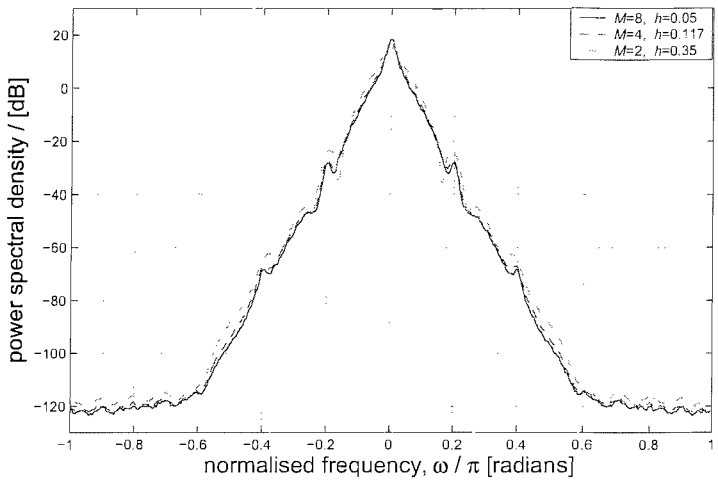

Figure 3.13: Power spectral density for M-GFSK signals with $M \in \{2, 4, 8\}$, K_{BT}=0.5 and $N = 10$.

at 9.8 dB E_b/N_0 with $K = 9$ and $M = 2$. This is impressive considering that the Viterbi receiver performs similarly [94], and relatively simple receivers require in excess of 15 dB for the same feat [32], while some practitioners even assume that 21 dB is needed [96].

The reduction in distance between adjacent symbols with increase in M manifests in poorer BER. Results depicted in Fig. 3.15 indicate that for $K = 5$, an increase of 6.86 dB and 12.88 dB E_b/N_0 is necessary to attain a BER of 10^{-3} when the number of modulation levels is raised from $M = 2$ to $M = 4$ and $M = 8$ respectively. However, selecting $M = 4$ or $M = 8$, will facilitate the doubling or quadrupling of the data rate without increasing bandwidth occupancy, and this might be an attractive proposition in future revisions of the Bluetooth specification [42, 97]. It is interesting to note from Fig. 3.16 that with $K_{BT} = 0.5$, the position of the detected symbol κ, in the sequence of K modulating symbols, does not significantly affect the BER, provided the first and last symbols are not selected, that is provided $\kappa \in \{2, 3, \ldots, (K-1)\}$.

3.11 Summary and Concluding Remarks

GFSK is the modulation scheme specified for Bluetooth [17]. Various types of receivers exist for GFSK signals. These include single-symbol receivers like the FM discriminator and the phase-shift discriminator, which have modest performance, and multi-symbol receivers like the Viterbi and MFB receivers. Multi-symbol receivers offer at least 6 dB gain over single-symbol detectors [6]. Since wireless standards vary in their computational requirements, a

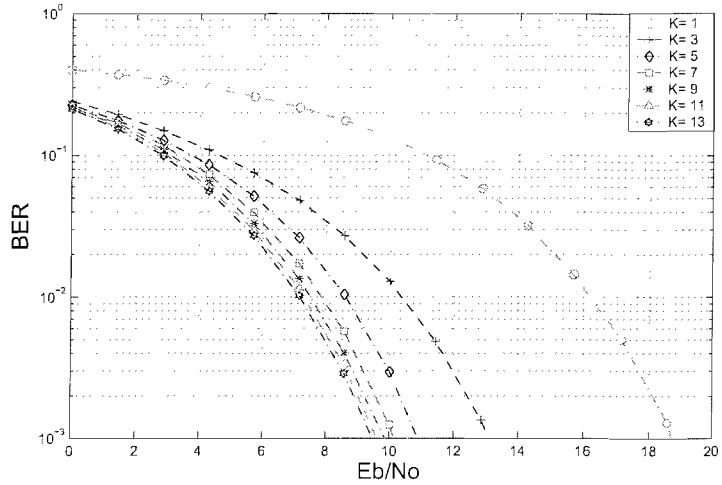

Figure 3.14: BER performance of the standard and low-complexity MFB receiver for GFSK signals, with parameters K_{BT}=0.5, h=0.35.

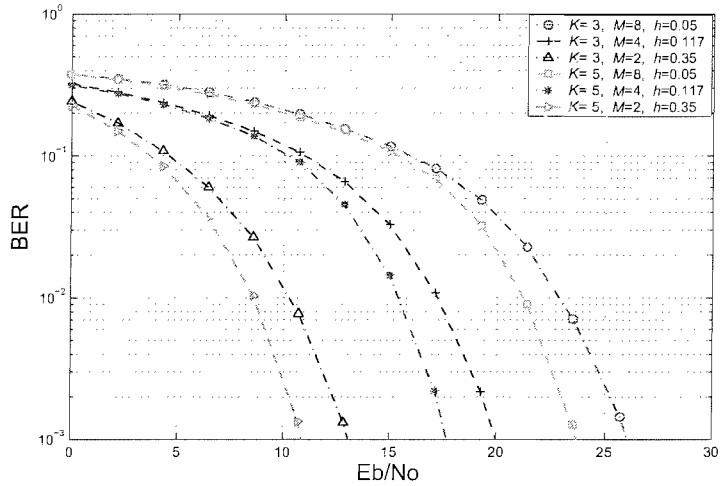

Figure 3.15: BER performance of the MFB receiver for M-GFSK signals with $K \in \{3,5\}$, $M \in \{2,4,8\}$, and K_{BT}=0.5 ($L = 3$).

multi-standard SDR implementing Bluetooth and a relatively complex WLAN system on a common hardware platform will have excess recourses when running Bluetooth. This extra capacity could be used to improve Bluetooth reception by employing high performance algorithms such as the Viterbi or the MFB receiver. Indeed there have already been efforts to simplify the Viterbi algorithm for this purpose [6]. However, a large range of acceptable modulation indices [17], and the inability of the Viterbi receiver to deal with unsynchronised h, makes it unsuitable for reception of Bluetooth signals. For example, while the Bluetooth standard permits modulation indices $h \in (0.28, 0.35)$, the Viterbi algorithm requires h to be a rational number. In addition, it has been demonstrated that the Viterbi receiver is

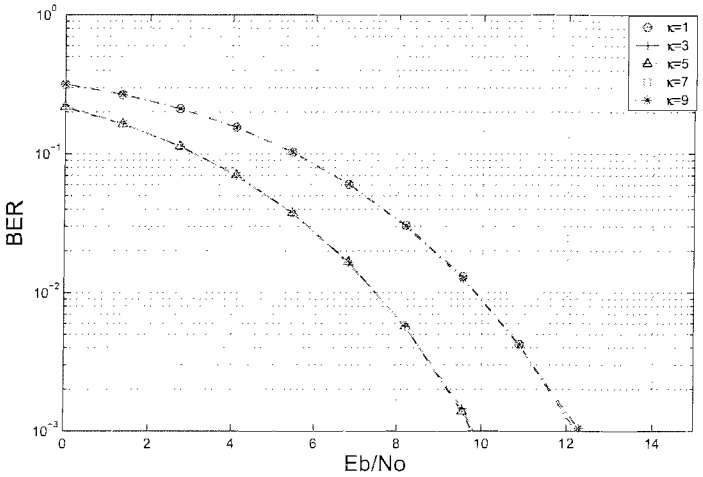

Figure 3.16: BER performance of the MFB receiver for GFSK signals, with different position of the detected symbol κ, and with parameters K_{BT}=0.5, h=0.35 and $K = 9$.

only robust to modulation index offsets of $|\Delta h| \leq 0.01$ [34], while offsets of $|\Delta h| \leq 0.07$ are clearly possible with Bluetooth. The effort of redesigning the Viterbi algorithm for different modulation indices also appears too costly [35], thus hindering the use of the sort of adaptive algorithms developed in Chapter 5 to adjust h.

The MFB receiver is akin to the Viterbi receiver because its matched filter outputs are analogous to the Viterbi path metrics, except for the limited time span represented by the filter outputs. A shorter observation interval makes the MFB physically realisable even with an irrational modulation index, and minimises effects of unsynchronised parameters. Theoretically, Viterbi optimises the maximum likelihood that a specific sequence of symbols was received [35], while each symbol period the MFB determines the received symbol with the highest probability [35]. Even though the symbol at the center of the observation interval, that is $\kappa = (K + 1)/2$, is chosen, Fig. 3.16 suggests that all but the 1st and the Kth symbols do equally well when $K_{BT} = 0.5$. This presents an opportunity for further reductions in complexity that has not been considered in this thesis, because more than one symbol can be detected on a single iteration.

However, the error ratio improves with an increase in observation interval. The size of K required for best performance is influenced by the support length L of the Gaussian filter. BER results in Fig. 3.11, with $K \geq 9$, mirror those achieved for the Viterbi receiver in [94], and suggest that the consequence of optimising the likelihood of each symbol being received accurately, is to maximise the probability of detecting the correct sequence.

Despite the potential benefits of the MFB receiver highlighted above, the high complexity of the filter bank for the large values of K necessary to ensure best performance is prohibitive. Through our recursive algorithm that eliminates redundancy involved in providing the matched filter outputs, which was developed in Sec. 3.6, we have made steps towards offering the MFB receiver as a plausible option for the reception of GFSK signals. The efficient algorithm is equivalent to the standard one in terms of performance, as it achieves the maximum permitted BER in Bluetooth of 10^{-3} at 9.8 dB E_b/N_0 when $K = 9$, 6 dB less than common single-symbol detectors [32], and identical to the Viterbi receiver [94]. The algorithm is also easily adaptable for different observation intervals, modulation levels, and oversampling factors by a simple system of parametrisation.

For derivation of the low-complexity MFB receiver in Sec. 3.6, an AWGN channel was assumed. The following chapters aim at mitigating real world problems such as hostile dispersive channels, as well as carrier frequency and modulation index offsets, which are likely in low cost wireless networks like Bluetooth. In particular, multipath signal propagation typical of large enclosed areas in which Bluetooth transceivers may operate could cause considerable degradation. Carrier frequency offsets permitted by the Bluetooth standard propagate from one symbol period to the next and amplify the problem if long observation intervals are employed. Also, despite comparative unsusceptibility to modulation index errors compared to the Viterbi algorithm, the MFB receiver does suffer some degradation due to offsets in h.

Hence, the next target shall be to devise techniques to rectify these problems on a digital transceiver. We aim for algorithms that do not require use of a training signal, partly because such signals may experience multiple signal impairments, hence an algorithm aimed at synchronising one signal parameter, may be undermined by the presence of other signal adversities meant to be resolved further along the signal processing chain. Therefore the following chapter will focus on channel equalisation, while Chapter 5 addresses carrier frequency and modulation index offset correction.

Chapter 4

Equalisation

As signals travel from the transmitter to a remote receiver they are reflected, refracted and scattered by objects in the transmission medium, resulting in time-shifted and attenuated versions of the same signal being superimposed at the receive antenna and thus forming a distorted composite signal at the receiver input [60]. In large enclosed areas like open plan office spaces, in which Bluetooth transceivers would be expected to operate, delayed components take longer to arrive and may not be sufficiently attenuated, and therefore degrade performance. This problem will become prevalent if pleas to increase the operation range are heeded [42]. Where there is relative motion of the transceiver pair or the obstructing objects, then the way in which signal components combine linearly changes with time and the channel is said to be time varying. However, we shall assume that any change in channel conditions is negligible compared to the data rate of 1 Mbps [17], such that we can presume a stationary channel.

An equaliser is any device designed to mitigate the effects of the distortion introduced by the channel. Several taxonomies exist for equalisers, including operational modes, structures, optimisation criteria and adaptive algorithms [73]. The training mode requires use of a transmitted training sequence, which the receiver "knows" and employs to compensate for the channel. Some researchers and practitioners use Bluetooth's 72 bit access code for this purpose [98, 99]. However, without any compensation such equalisers will perceive a carrier frequency offset as a rapidly changing channel, and may not be able to converge. Blind equalisation using a constant modulus criterion is therefore a more robust operational mode. Similarly, carrier frequency offsets will undermine the use of decision feedback equalisation on the instantaneous frequency of the received signal [97, 42].

The constant modulus algorithm is covered in Sec. 4.5 and can be used to update the equaliser portrayed in Fig. 4.1 if the switch is in position 2. It forms the basis of the normalised sliding window constant modulus algorithm in Sec. 4.6, which is the equalising procedure that we enhance for Bluetooth signals. Reasons for this decision will become apparent in future sections. However, we first characterise the equalisation problem in Sec. 4.1, and highlight necessary mathematical tools for our discussions in Sec. 4.2. A brief review of the minimum mean square error solution, which is a useful performance benchmark for equalisation algorithms, is derived in Sec. 4.3, while the most popular equalisation method used today, known as the least mean square algorithm, is addressed in Sec. 4.4 and could be an option to adapt the equaliser depicted in Fig. 4.1 if the switch is at position 1.

4.1 General Equalisation Problem

As stated in Sec. 2.3, the received sequence $r[n]$ comprises of a superposition of multipath components of the transmitted signal $s[n]$. And this superposition can be modelled by a channel impulse response $c[n]$ of finite length L_c, so that the channel output is given by the convolution $c[n] * s[n]$, and the received signal $r[n]$ is obtained after subsequent application of additive white Gaussian noise $v[n]$ and a carrier frequency offset $\Delta\Omega$. The received signal was expressed in (2.9), and is reproduced here for easy reference as

$$r[n] = \left(\sum_{\nu=0}^{L_c-1} c[\nu]\ s[n-\nu] \right) e^{j\Delta\Omega n} + v[n] \quad .$$

In this work, the equaliser either seeks to maximise a relationship (or correlation) between the equaliser output $\tilde{r}[n]$ and a desired signal $s[n-d]$, where d is an integral delay constant, or to enforce a predetermined condition on $\tilde{r}[n]$. A finite impulse response (FIR)

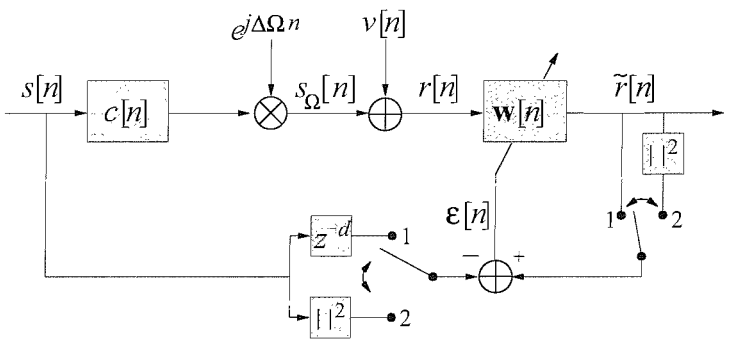

Figure 4.1: Flow graph of equalisation.

filter will be employed to process $r[n]$, firstly because unlike infinite impulse response (IIR) filters, they are inherently stable [55]. Hence, the equaliser output is given by

$$\tilde{r}[n] = \sum_{\nu=0}^{L_{\mathrm{w}}-1} \mathrm{w}_n[\nu]\, r[n-\nu]$$

where $\mathrm{w}_n[\nu]$ is the time varying impulse response of the equaliser, L_{w} is its length, and the ideal output $\tilde{r}[n]$ depends on the cost function chosen to set the equaliser coefficients.

4.2 Wirtinger Calculus

This section is a brief diversion into Wirtinger calculus [100, 101], a mathematical tool of prime importance to numerical analysis in the following sections. The explanation here emulates that in [102].

Let $f(\mathrm{w})$ be a function of a complex valued variable $\mathrm{w} = \mathrm{w}_r + j\mathrm{w}_i \in \mathbb{C}$, whereby w_r and w_i are the real and imaginary parts of w respectively, and $j = \sqrt{-1}$. From Wirtinger calculus [100, 101]

$$\frac{\partial f(\mathrm{w})}{\partial \mathrm{w}} = \frac{1}{2}\left(\frac{\partial f(\mathrm{w})}{\partial \mathrm{w}_r} - j\frac{\partial f(\mathrm{w})}{\partial \mathrm{w}_i}\right) \tag{4.1}$$

$$\frac{\partial f(\mathrm{w})}{\partial \mathrm{w}^*} = \frac{1}{2}\left(\frac{\partial f(\mathrm{w})}{\partial \mathrm{w}_r} + j\frac{\partial f(\mathrm{w})}{\partial \mathrm{w}_i}\right) \quad . \tag{4.2}$$

It is evident from (4.1) and (4.2) that [103]

$$\frac{\partial \mathrm{w}}{\partial \mathrm{w}} = 1 \quad , \frac{\partial \mathrm{w}}{\partial \mathrm{w}^*} = 0 \quad . \tag{4.3}$$

Therefore if multiple parameters are involved, in a filter coefficient vector[1]

$$\mathbf{w} = [\mathrm{w}_0^*, \mathrm{w}_1^*, \ldots, \mathrm{w}_{L_{\mathrm{w}}-1}^*]^T \tag{4.4}$$

for instance, then effective notation necessitates the definition of a vectorial gradient operator

$$\frac{\partial}{\partial \mathbf{w}^*} = \begin{bmatrix} \frac{\partial}{\partial \mathrm{w}_0} \\ \frac{\partial}{\partial \mathrm{w}_1} \\ \vdots \\ \frac{\partial}{\partial \mathrm{w}_{L_{\mathrm{w}}-1}} \end{bmatrix} \quad , \tag{4.5}$$

[1] No ambiguity should arise from denoting an equaliser coefficient vector with $\mathbf{w}$ in this chapter, and symbolising the first column in the matched filter bank $\mathbf{W}$ with the same in Chapter 3.

and together (4.3), (4.4) and (4.5) imply that

$$\frac{\partial \mathbf{w}^T}{\partial \mathbf{w}^*} = \begin{bmatrix} \frac{\partial \mathrm{w}_0^*}{\partial \mathrm{w}_0} & \frac{\partial \mathrm{w}_1^*}{\partial \mathrm{w}_0} & \cdots & \frac{\partial \mathrm{w}_{L_\mathrm{w}-1}^*}{\partial \mathrm{w}_0} \\ \frac{\partial \mathrm{w}_0^*}{\partial \mathrm{w}_1} & \frac{\partial \mathrm{w}_1^*}{\partial \mathrm{w}_1} & \cdots & \frac{\partial \mathrm{w}_{L_\mathrm{w}-1}^*}{\partial \mathrm{w}_1} \\ \vdots & \vdots & \ddots & \vdots \\ \frac{\partial \mathrm{w}_0^*}{\partial \mathrm{w}_{L_\mathrm{w}-1}} & \frac{\partial \mathrm{w}_1^*}{\partial \mathrm{w}_{L_\mathrm{w}-1}} & \cdots & \frac{\partial \mathrm{w}_{L_\mathrm{w}-1}^*}{\partial \mathrm{w}_{L_\mathrm{w}-1}} \end{bmatrix} = \mathbf{0} \in \mathbb{R}^{L_\mathrm{w} \times L_\mathrm{w}} \quad , \tag{4.6}$$

and

$$\frac{\partial \mathbf{w}^H}{\partial \mathbf{w}^*} = \begin{bmatrix} \frac{\partial \mathrm{w}_0}{\partial \mathrm{w}_0} & \frac{\partial \mathrm{w}_1}{\partial \mathrm{w}_0} & \cdots & \frac{\partial \mathrm{w}_{L_\mathrm{w}-1}}{\partial \mathrm{w}_0} \\ \frac{\partial \mathrm{w}_0}{\partial \mathrm{w}_1} & \frac{\partial \mathrm{w}_1}{\partial \mathrm{w}_1} & \cdots & \frac{\partial \mathrm{w}_{L_\mathrm{w}-1}}{\partial \mathrm{w}_1} \\ \vdots & \vdots & \ddots & \vdots \\ \frac{\partial \mathrm{w}_0}{\partial \mathrm{w}_{L_\mathrm{w}-1}} & \frac{\partial \mathrm{w}_1}{\partial \mathrm{w}_{L_\mathrm{w}-1}} & \cdots & \frac{\partial \mathrm{w}_{L_\mathrm{w}-1}}{\partial \mathrm{w}_{L_\mathrm{w}-1}} \end{bmatrix} = \mathbf{I}_{L_\mathrm{w}} \in \mathbb{R}^{L_\mathrm{w} \times L_\mathrm{w}} \quad . \tag{4.7}$$

4.3 Theoretical Minimum Mean Square Error Solution

Before delving into equaliser algorithms a popular solution for equalisation procedures, commonly referred to as the minimum mean square error (MMSE) solution, shall be considered here. As the name suggests, the MMSE equaliser solution comprises of coefficients that will minimise the mean square error (MSE) of the equaliser output with respect to the ideal received signal, and it is a useful benchmark on which the performance of equaliser algorithms can be compared, and will be compared in this thesis. To facilitate the discussion, part of Fig. 4.1 showing the channel and equaliser input and output signals, but neglecting the carrier frequency offset, is reproduced in Fig. 4.2, and from this figure the mean square error is given by

$$\xi_{\mathrm{MSE}} = \mathcal{E}\left\{|\epsilon[n]|^2\right\} = \mathcal{E}\left\{|\tilde{r}[n] - s[n-d]|^2\right\} \quad , \tag{4.8}$$

where $\mathcal{E}\{\cdot\}$ is the expectation operator and d is a suitable delay constant. Hence, according to Fig. 4.2 the MMSE solution ξ_{MMSE} is achieved if $\mathbf{w}[n] = \mathbf{w}$ is maintained as the MMSE equaliser coefficient vector $\mathbf{w}_{\mathrm{opt}}$. The equaliser coefficient vector that ensures the MMSE

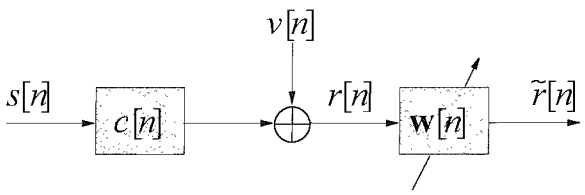

Figure 4.2: Channel and equaliser setup.

is attained, is employed in this work for comparison purposes, and so a more elaborate derivation of it than that provided in [104, 105, 51] is presented in the following.

Firstly, if L_{w} and L_c are the length of the equaliser and CIR respectively, then we can express the channel and time varying equaliser coefficients in vector notation as

$$\mathbf{c} = [\, c_0, c_1, \cdots, c_{L_c-1} \,]^H$$

and

$$\mathbf{w}[n] = \mathbf{w}_n = [\, \mathrm{w}_0[n], \mathrm{w}_1[n], \cdots, \mathrm{w}_{L_{\mathrm{w}}-1}[n] \,]^H$$

respectively. However, assuming constant coefficients, $\mathbf{w}_n$ is simplified to

$$\mathbf{w} = [\, \mathrm{w}_0, \mathrm{w}_1, \cdots, \mathrm{w}_{L_{\mathrm{w}}-1} \,]^H \quad .$$

The vectors of the transmitted signal samples and the noise sequence which contribute to the nth equaliser output are defined as

$$\mathbf{s}[n] = \mathbf{s}_n = [\, \mathrm{s}_0[n], \mathrm{s}_1[n], \cdots, \mathrm{s}_{L_{\mathrm{w}}+L_c-1}[n] \,]^T$$

and

$$\mathbf{v}[n] = \mathbf{v}_n = [\, \mathrm{v}_0[n], \mathrm{v}_1[n], \cdots, \mathrm{v}_{L_{\mathrm{w}}-1}[n] \,]^T$$

respectively[2]. In this case it helps to refer to Fig. 4.2 and view the channel and equaliser as a composite system with input vector $\mathbf{s}[n]$. This in turn allows the definition of the channel-equaliser input signal and AWGN covariance matrices as

$$\mathbf{R}_{ss} = \mathcal{E}\{\mathbf{s}[n]\mathbf{s}[n]^H\} \qquad \in \mathbb{C}^{(L_{\mathrm{w}}+L_c)\times(L_{\mathrm{w}}+L_c)}$$

and

$$\mathbf{R}_{vv} = \mathcal{E}\{\mathbf{v}[n]\mathbf{v}[n]^H\} \qquad \in \mathbb{C}^{L_{\mathrm{w}}\times L_{\mathrm{w}}}$$

respectively. Additionally, the channel convolutional matrix is given by

$$\mathbf{C} = \begin{bmatrix} \mathbf{c}^H & & \mathbf{0} \\ & \ddots & \\ \mathbf{0} & & \mathbf{c}^H \end{bmatrix} \qquad \in \mathbb{C}^{L_{\mathrm{w}}\times(L_{\mathrm{w}}+L_c)} \quad .$$

Now if we define a pinning vector as

$$\mathbf{d}_d = [\, 0\,,\, \cdots\,,\, 0\,,\, 1\,,\, 0\,,\, \cdots\,,\, 0 \,]^T \in \mathbb{R}^{(L_{\mathrm{w}}+Lc)\times 1} \quad ,$$

[2]Note that in Fig. 4.2 $\tilde{r}[n] = s[n] * (c[n] * \mathrm{w}[n]) + v[n] * \mathrm{w}[n]$.

whereby d is the index of the non-zero element[3]. and assume that $s[n]$ and $v[n]$ are statistically independent random processes, then the following formulation arises from (4.8)

$$\begin{aligned}
\xi_{\text{MSE}} &= \mathcal{E}\{|\tilde{r}[n] - \mathbf{d}_d^H \mathbf{s}_n|^2\} \\
&= \mathcal{E}\{(\mathbf{w}^H(\mathbf{C}\mathbf{s}_n + \mathbf{v}_n) - \mathbf{d}_d^H \mathbf{s}_n)(\mathbf{w}^H(\mathbf{C}\mathbf{s}_n + \mathbf{v}_n) - \mathbf{d}_d^H \mathbf{s}_n)^H\} \\
&= \mathcal{E}\{(\mathbf{w}^H(\mathbf{C}\mathbf{s}_n + \mathbf{v}_n) - \mathbf{d}_d^H \mathbf{s}_n)((\mathbf{C}\mathbf{s}_n + \mathbf{v}_n)^H \mathbf{w} - \mathbf{s}_n^H \mathbf{d}_d)\} \\
&= \mathcal{E}\{\mathbf{w}^H(\mathbf{C}\mathbf{s}_n + \mathbf{v}_n)(\mathbf{s}_n^H \mathbf{C}^H + \mathbf{v}_n^H)\mathbf{w}\} - \mathcal{E}\{\mathbf{w}^H(\mathbf{C}\mathbf{s}_n + \mathbf{v}_n)\mathbf{s}_n^H \mathbf{d}_d\} - \\
&\quad \mathcal{E}\{\mathbf{d}_d^H \mathbf{s}_n(\mathbf{s}_n^H \mathbf{C}^H + \mathbf{v}_n^H)\mathbf{w}\} + \mathcal{E}\{\mathbf{d}_d^H \mathbf{s}_n \mathbf{s}_n^H \mathbf{d}_d\} \\
&= \mathbf{w}^H \mathbf{C}\mathbf{R}_{ss}\mathbf{C}^H \mathbf{w} + \mathbf{w}^H \mathbf{C}\mathcal{E}\{\mathbf{s}_n \mathbf{v}_n^H\}\,\mathbf{w} + \mathbf{w}^H \mathcal{E}\{\mathbf{v}_n \mathbf{s}_n^H\}\,\mathbf{C}^H \mathbf{w} + \mathbf{w}^H \mathbf{R}_{vv}^H \mathbf{w} - \\
&\quad \mathbf{w}^H \mathbf{C}\mathbf{R}_{ss}\mathbf{d}_d - \mathbf{w}^H \mathcal{E}\{\mathbf{v}_n \mathbf{s}_n^H\}\,\mathbf{d}_d - \mathbf{d}_d^H \mathbf{R}_{ss}\mathbf{C}^H \mathbf{w} - \mathbf{d}_d^H \mathcal{E}\{\mathbf{s}_n \mathbf{v}_n^H\}\,\mathbf{w} + \mathbf{d}_d^H \mathbf{R}_{ss}\mathbf{d}_d \\
&= \mathbf{w}^H \mathbf{C}\mathbf{R}_{ss}\mathbf{C}^H \mathbf{w} + \mathbf{w}^H \mathbf{R}_{vv}^H \mathbf{w} - \mathbf{w}^H \mathbf{C}\mathbf{R}_{ss}\mathbf{d}_d - \mathbf{d}_d^H \mathbf{R}_{ss}\mathbf{C}^H \mathbf{w} + \mathbf{d}_d^H \mathbf{R}_{ss}\mathbf{d}_d \quad . \quad (4.9)
\end{aligned}$$

The expression in (4.9) maps the equaliser coefficient vector space, onto the scalar quantity ξ_{MSE}. Evaluation of the cost function in (4.9) reveals that ξ_{MSE} is quadratic in the filter coefficients, which are elements of $\mathbf{w}$, and should therefore have a unique extremum. The minimum point of (4.9) is ξ_{MMSE}, or stated mathematically

$$\xi_{\text{MMSE}} \stackrel{!}{=} \min_{\mathbf{w}}\{\xi_{\text{MSE}}\} \quad ,$$

and it is obtained by equating the derivative of ξ_{MSE} to zero. This development requires the combined application of :

i. the product rule [106], which can be written as

$$\frac{\partial}{\partial \mathbf{w}^*}\mathcal{F}(\mathbf{w}^*)\mathcal{G}(\mathbf{w}^*) = \left(\frac{\partial}{\partial \mathbf{w}^*}\mathcal{F}(\mathbf{w}^*)\right)\mathcal{G}(\mathbf{w}^*) + \left(\frac{\partial}{\partial \mathbf{w}^*}\mathcal{G}(\mathbf{w}^*)^T\right)\mathcal{F}(\mathbf{w}^*)^T \quad ,$$

if $\mathcal{F}(\mathbf{w}^*)\mathcal{G}(\mathbf{w}^*)$ is a scalar quantity;

ii. the relationship [107]

$$(\mathbf{X}\mathbf{Y}\mathbf{Z})^T = \mathbf{Z}^T\mathbf{Y}^T\mathbf{X}^T \quad ; \quad \text{and}$$

iii. equations (4.6) and (4.7),

[3] A rule of thumb adopted in this work is to presume $d = \lfloor (L_w + L_c)/2 \rfloor$.

on (4.9) as follows

$$\begin{aligned}\frac{\partial \xi_{\text{MSE}}}{\partial \mathbf{w}^*} &= \left(\frac{\partial}{\partial \mathbf{w}^*}\mathbf{w}^H\right)\mathbf{C}\mathbf{R}_{ss}\mathbf{C}^H\mathbf{w} + \left(\frac{\partial}{\partial \mathbf{w}^*}\mathbf{w}^T\mathbf{C}^*\mathbf{R}_{ss}^T\mathbf{C}^T\right)\mathbf{w}^* \\ &\quad + \left(\frac{\partial}{\partial \mathbf{w}^*}\mathbf{w}^H\right)\mathbf{R}_{vv}^H\mathbf{w} + \left(\frac{\partial}{\partial \mathbf{w}^*}\mathbf{w}^T\mathbf{R}_{vv}^*\right)\mathbf{w}^* \\ &\quad - \frac{\partial}{\partial \mathbf{w}^*}\mathbf{w}^H\mathbf{C}\mathbf{R}_{ss}\mathbf{d}_d \\ &\quad - \left(\frac{\partial}{\partial \mathbf{w}^*}\mathbf{d}_d^H\mathbf{R}_{ss}\mathbf{C}^H\right)\mathbf{w} - \left(\frac{\partial}{\partial \mathbf{w}^*}\mathbf{w}^T\right)\mathbf{C}^*\mathbf{R}_{ss}^T\mathbf{d}_d^* \\ &\quad + \frac{\partial}{\partial \mathbf{w}^*}\mathbf{d}_d^H\mathbf{R}_{ss}\mathbf{d}_d \\ &= \mathbf{C}\mathbf{R}_{ss}\mathbf{C}^H\mathbf{w} + \mathbf{R}_{vv}^H\mathbf{w} - \mathbf{C}\mathbf{R}_{ss}\mathbf{d}_d = \mathbf{0} \quad . \end{aligned} \tag{4.10}$$

Hence, (4.10) infers that the theoretical MMSE equaliser coefficients, often referred to as the Wiener-Hopf solution [108, 109, 110], are given by

$$\mathbf{w}_{\text{opt}} \stackrel{!}{=} \min_d\{\ (\mathbf{C}\mathbf{R}_{ss}\mathbf{d}_d)(\mathbf{C}\mathbf{R}_{ss}\mathbf{C}^H + \mathbf{R}_{vv}^H)^{-1}\ \} \quad , \tag{4.11}$$

and in uncorrelated noise conditions this can be further simplified to

$$\mathbf{w}_{\text{opt}} \stackrel{!}{=} \min_d\{\ (\mathbf{C}\mathbf{R}_{ss}\mathbf{d}_d)(\mathbf{C}\mathbf{R}_{ss}\mathbf{C}^H + \sigma_v^2\mathbf{I}_{L_{\text{w}}})^{-1}\} \quad ,$$

where σ_v^2 is the variance of the noise and $\mathbf{I}_{L_{\text{w}}}$ is an $L_{\text{w}} \times L_{\text{w}}$ identity matrix. The result in (4.11) is relevant to this research because in Sec. 4.8 it is used as a benchmark with which to compare performance of equaliser algorithms discussed later on in this thesis.

4.4 Least Mean Square Algorithm

The least mean square (LMS) algorithm is well documented in various texts and technical papers, and notably in [111, 112, 104]. It is related to the theoretical minimum mean square error solution of Sec. 4.3 because the mean square error ξ_{MSE} in (4.9), is replaced by the instantaneous squared error $\hat{\xi}_{\text{MSE}}$. This implies that ideally, the LMS equaliser coefficients converge to the MMSE equaliser solution. However, unlike the purist approach of Sec. 4.3, the LMS algorithm represents a stochastic gradient method.

To accomplish this the LMS requires that a replica of the transmitted signal is available at the receiver. Fig. 4.1 illustrates such a scenario when the switch is at position 1. Nonetheless, there would be no need for a receiver if the transmitted signal was completely predictable, and so considerable ingenuity is required to select a training signal for

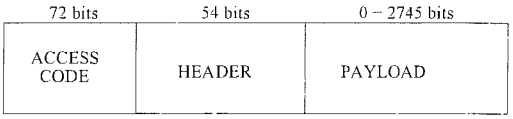

Figure 4.3: Standard Bluetooth packet format.

the equaliser update process. For example, the Bluetooth standard specifies 16 different packet types, the general format of which is portrayed by Fig. 4.3, and comprises of an access code, header, and payload [17]. The access code is known to all transceivers involved in a communication session, while the payload and header contain the information. Some researchers and practitioners exploit the 72 bit access code, by using a copy of it in the receiver as the training sequence for equaliser update. The adaptation process is stopped, and the equaliser coefficients "frozen" while the header and payload are being transmitted. Unfortunately, the access code computed by the receiver device makes assumptions about the transmitter carrier frequency and modulation index, and if these assumptions are not correct, then a price will be paid in terms of bit error ratio.

4.4.1 Stochastic Gradient Strategy

The stochastic gradient strategy[4] employed by LMS results in a relatively simple equaliser adaptation equation, and this has fueled its popularity. The LMS update procedure will be formulated in this section, but a more detailed development is available in [112, 104, 102]. We begin by denoting the samples of the received signal $r[n]$, which occupy the equaliser tap delay line with

$$\mathbf{r}[n] = \mathbf{r}_n = [\ \mathrm{r}_0[n], \mathrm{r}_1[n], \cdots, \mathrm{r}_{L_\mathrm{w}-1}[n]\ ]^T \quad .$$

Hence, if $\mathbf{w}_n$ is kept constant, and the subscript dropped, then the momentary estimate of the mean square error in (4.8) can be expressed as

$$\begin{aligned}
\hat{\xi}_{\mathrm{MSE}} &= |\epsilon[n]|^2 = |s[n-d] - \mathbf{w}^H \cdot \mathbf{r}_n|^2 \\
&= (s[n-d] - \mathbf{w}^H \cdot \mathbf{r}_n)(s^*[n-d] - \mathbf{r}_n^H \cdot \mathbf{w}) \\
&= |s[n-d]|^2 - \mathbf{w}^H \cdot s^*[n-d] \cdot \mathbf{r}_n - s[n-d] \cdot \mathbf{r}_n^H \cdot \mathbf{w} + \mathbf{w}^H \cdot \mathbf{r}_n \cdot \mathbf{r}_n^H \cdot \mathbf{w} \\
&= |s[n-d]|^2 - \mathbf{w}^H \cdot \hat{\mathbf{p}} - \hat{\mathbf{p}}^H \cdot \mathbf{w} + \mathbf{w}^H \cdot \hat{\mathbf{R}} \cdot \mathbf{w} \\
&= |s[n-d]|^2 - \mathbf{w}^H \cdot \hat{\mathbf{p}} - \mathbf{w}^T \cdot \hat{\mathbf{p}}^* + \mathbf{w}^H \cdot \hat{\mathbf{R}} \cdot \mathbf{w} \quad , \qquad (4.12)
\end{aligned}$$

[4] A novel algorithm for carrier frequency offset correction in Bluetooth systems, that is also based on a stochastic gradient strategy, is detailed in Sec. 5.1.

where the estimation of the auto-correlation matrix is based on the instantaneous values of the equaliser input $\hat{\mathbf{R}} = \mathbf{r}_n \cdot \mathbf{r}_n^H$, while the instantaneous estimate of the cross-correlation vector is given by $\hat{\mathbf{p}} = s^*[n-d] \cdot \mathbf{r}_n$. The plot of ξ_{MSE} against $\mathbf{w}$ in Fig. 4.4 for a simple case where ideal conditions exist and $L_{\text{w}} = 1$, confirms that ξ_{MSE} has a unique extremum because it is quadratic in filter coefficients $\mathbf{w}$.

The LMS algorithm employs a stochastic gradient step by step descent towards the minimum point [112], whereby the current equaliser filter coefficients $\mathbf{w}^*$ are adapted by the equation

$$\mathbf{w}_{n+1} = \mathbf{w}_n - \mu_{\text{w}} \frac{\partial \hat{\xi}_{\text{MSE}}}{\partial \mathbf{w}_n^*} \quad , \tag{4.13}$$

with μ_{w} symbolising a positive step size. The derivative of $\hat{\xi}_{\text{MSE}}$ with respect to the current equaliser filter coefficients $\mathbf{w}^*$ is derived from (4.12) as follows

$$\begin{aligned}
\frac{\partial \hat{\xi}_{\text{MSE}}}{\partial \mathbf{w}^*} &= \frac{\partial}{\partial \mathbf{w}^*}(|s[n-d]|^2 - \mathbf{w}^H \hat{\mathbf{p}} - \mathbf{w}^T \hat{\mathbf{p}}^*) + \left(\frac{\partial}{\partial \mathbf{w}^*}\mathbf{w}^H\right)\hat{\mathbf{R}}\mathbf{w} + \left(\frac{\partial}{\partial \mathbf{w}^*}\mathbf{w}^T \hat{\mathbf{R}}^T\right)\mathbf{w}^* \\
&= -\hat{\mathbf{p}} + \hat{\mathbf{R}}\mathbf{w} \\
&= -\mathbf{r}_n s^*[n-d] + \mathbf{r}_n \mathbf{r}_n^H \mathbf{w} \\
&= -\mathbf{r}_n (s^*[n-d] - \mathbf{r}_n^H \mathbf{w}) \\
&= -\mathbf{r}_n \epsilon^*[n] \quad ,
\end{aligned} \tag{4.14}$$

where $\epsilon[n]$ is the error of the equaliser output compared to a training signal defined in (4.8).

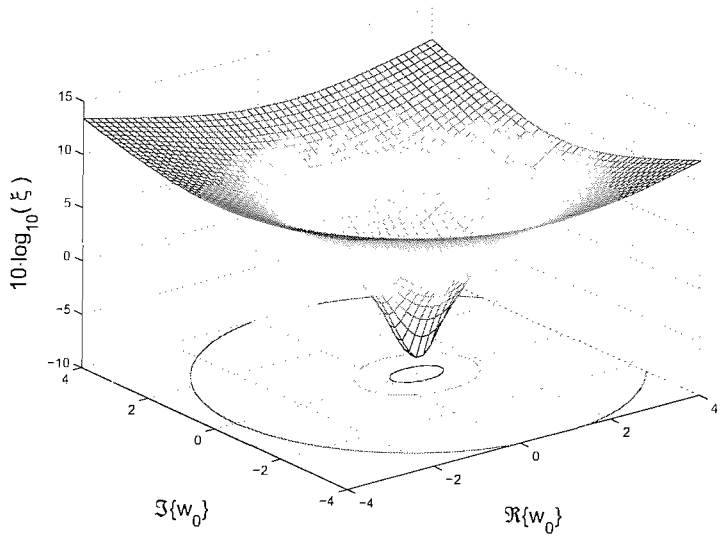

Figure 4.4: Mean square error cost function ξ_{MSE}, for an equaliser with a single complex coefficient.

Notice that all parameters of the right hand side of (4.14) are available at the receiver, and so by substituting (4.14) into (4.13) we obtain the LMS equaliser update equation

$$\mathbf{w}_{n+1} = \mathbf{w}_n + \mu_{\mathrm{w}}\mathbf{r}_n\epsilon^*[n] \quad , \tag{4.15}$$

with $\mu_{\mathrm{w}} \in [0, \frac{2}{\lambda_{\max}})$, where $\lambda_{\max}$ is the largest eigenvalue of $\mathbf{R}$ [112, 102]. However, in a common variant of the LMS algorithm introduced in Sec. 4.4.2, the step size is normalised such that $\hat{\mu}_{\mathrm{w}} \in [0, 1)$.

4.4.2 Normalised LMS Algorithm

The normalised LMS (NLMS) procedure selects an appropriate step size for each iteration based on the statistics of the received signal sequence in the equaliser tap-delay line, in other words, μ_{w} is based on the instantaneous estimate $\hat{\mathbf{R}}$ [113, 114, 115, 116]. It may be viewed as a solution to a constrained optimisation (minimisation) problem [117], whereby given $s[n]$, $\mathbf{r}_n$, and $\mathbf{w}_n$, at time instance n, the tap-weight vector $\mathbf{w}_{n+1}$ that will minimise

$$||\Delta\mathbf{w}_{n+1}|| = ||\mathbf{w}_{n+1} - \mathbf{w}_n|| \quad ,$$

subject to the constraint

$$\mathbf{w}_{n+1}^H\mathbf{r}_n = s[n-d],$$

is sought. Stated in another way, the NLMS algorithm updates the tap-weight vector in such a way that $\mathbf{w}_{n+1}$ exhibits minimum change — in the Euclidean norm sense — with respect to $\mathbf{w}_n$. This is a manifestation of the principle of minimal disturbance, which states that "in light of new input data, the parameters of an adaptive system should only be disturbed in a minimal fashion" [118]. These criteria are used in a complete analytic derivation of the NLMS for a normalised iteration step size of $\hat{\mu}_{\mathrm{w}}$=1 in [104], and are employed in a geometric interpretation of the NLMS in [104, 102]. Here we simply state that the equaliser update process for the NLMS algorithm is given by

$$\mathbf{w}_{n+1} = \mathbf{w}_n + \frac{\hat{\mu}_{\mathrm{w}}}{(||\mathbf{r}_n||^2+\lambda)} \cdot \mathbf{r}_n\epsilon^*[n] \quad ,$$

with $\hat{\mu}_{\mathrm{w}} \in [0, 1)$ [104] and λ is a small constant to prevent division by zero. This sort of normalisation is done so often that the use of the LMS algorithm often implicitly implies normalisation. Normalised LMS will be employed in this thesis, and to ease reference we shall drop the " ˆ ", thereby using μ_{w} to refer to the normalised iteration step size.

4.4.3 Convergence Speed

A detailed quantitative analysis of the convergence speed of the LMS algorithm can be found in the texts [112, 104, 119, 120, 102], here we summarise their results as follows:

- the overall convergence speed of the system is limited by the smallest eigenvalue $\lambda_{\min}$ of $\mathbf{R}$; while
- the step size is limited by the largest eigenvalue $\lambda_{\max}$ of $\mathbf{R}$.

Therefore if $\lambda_{\min}$ is much less than $\lambda_{\max}$, then the rate of convergence reduces significantly. The influence of the statistical properties of $\mathbf{R}$ on the convergence speed of the LMS algorithm is best quantified by its condition number (or eigenvalue spread), which is defined as [104]

$$\Psi = \frac{\lambda_{\max}}{\lambda_{\min}} \leq \frac{\max_\omega \ P_{rr}(e^{j\omega})}{\min_\omega \ P_{rr}(e^{j\omega})} \quad , \tag{4.16}$$

where $P_{rr}(e^{j\omega})$ is the power spectral density of $r[n]$.

It is apparent from the expression on the right of (4.16) that band-limited received signals will have a larger condition number, which entails a slower convergence speed than white signals. This phenomenon is true even for alternative equalisation procedures like the constant modulus algorithm, which is covered in Sec. 4.5, and is probably due to the lack of sufficient excitation of the equaliser in some spectral regions. However for LMS, techniques like tap length control [121, 122, 123, 124, 125], time varying step sizes [126, 127], and the use of affine projections [128, 129, 130] have been proposed to speed it up, but mostly assume that correlation between received signal samples is due to intersymbol interference (ISI) introduced by the equaliser, and that the transmitted signal itself is white, which is not the case in Bluetooth.

The LMS algorithm is a relatively simple and efficient equalisation method, and is a safe option whenever a reasonably accurate reference signal is available at the receiver. However, we shall see in Sec. 4.8 that the LMS algorithm may be rendered useless in the presence of a carrier frequency offset of the magnitude permitted in Bluetooth networks, and this is why in the next section we propose the application of the constant modulus algorithm as a promising alternative.

4.5 Constant Modulus Algorithm

Unlike the LMS algorithm, the constant modulus algorithm (CMA) does not require a template signal for equalisation; instead it utilises knowledge of the magnitude of the transmitted signal for this purpose [43]. This case is portrayed in Fig. 4.1 when the switches are in position 2. CMA employs a constant modulus optimisation criterion, implying that it seeks to compensate for the channel effects by restoring the received signal to the magnitude of the transmitted one. The justification for this lies in the fact that there are no dispersive channel effects that are able to produce phase errors that cannot be "seen" as a deviation from the ideal magnitude [131]. Since the CMA does not exploit phase information, it is insensitive to misleading errors in carrier frequency that are typical in low cost networks like Bluetooth [131]. There is a general understanding that the CMA is much slower than the LMS algorithm, however, experiments have shown that there is not a substantial difference in the convergence rates of the two methods in the case of constant envelope signals [132], of which Bluetooth forms a subset. Although CMA has been successfully used for signals with a multi-level modulus like 16-QAM [133], it performs best when the magnitude is constant [132].

4.5.1 Constant Modulus Cost Function

The CM equalisation criterion first appeared in [134], before being generalised into a family of blind equaliser structures called Godard equalisers in [131]. Godard equalisers employ a cost function of the form

$$\xi_{\mathrm{CM}} = \mathcal{E}\{(|\tilde{r}[n]|^p - |s[n]|^p)^q\} \quad ,$$

where p and q are positive integers. An alternative development and interpretation of the special case of a Godard equaliser with $p = q = 2$ and $\mathcal{E}\{|s[n]|^2\} = 1$ is presented in [135]. This form was coined the constant modulus algorithm, and shall be the case we limit our discussions to, hence we redefine

$$\xi_{\mathrm{CM}} = \mathcal{E}\{(|\tilde{r}[n]|^2 - 1)^2\} \quad . \tag{4.17}$$

If $\mathbf{w}_n$ is kept constant then (4.17) can be rewritten in vector notation as

$$\begin{aligned} \xi_{\mathrm{CM}} &= \mathcal{E}\{(|\mathbf{w}^H \cdot \mathbf{r}_n|^2 - 1)^2\} \\ &= \mathcal{E}\{(\mathbf{w}^H \cdot \mathbf{r}_n \cdot \mathbf{r}_n^H \cdot \mathbf{w} - 1)^2\} \\ &= \mathcal{E}\{\mathbf{w}^H \cdot \mathbf{r}_n \cdot \mathbf{r}_n^H \cdot \mathbf{w} \cdot \mathbf{w}^H \cdot \mathbf{r}_n \cdot \mathbf{r}_n^H \cdot \mathbf{w} - 2\mathbf{w}^H \cdot \mathbf{r}_n \cdot \mathbf{r}_n^H \cdot \mathbf{w} + 1\} \quad . \end{aligned} \tag{4.18}$$

The cost function in (4.18) maps the equaliser coefficient vector space onto a scalar quantity ξ_{CM}, and ξ_{CM} contains fourth and second order elements of $\mathbf{w}$. The cost function ξ_{CM} is plotted in Fig. 4.5 for the simple case where $L_{\mathrm{w}} = 1$. It is evident from Fig. 4.5 that there are a host of solutions for the equaliser coefficient, each with a magnitude of 1.

4.5.2 CM Algorithm

The CMA is a gradient search algorithm that seeks to minimise ξ_{CM}. In particular the equaliser coefficient vector $\mathbf{w}_n$ is updated according to

$$\mathbf{w}_{n+1} = \mathbf{w}_n - \mu_{\mathrm{w}} \frac{\partial \hat{\xi}_{\mathrm{CM}}}{\partial \mathbf{w}^*} \quad , \tag{4.19}$$

where $\hat{\xi}_{\mathrm{CM}}$ is the instantaneous estimate of ξ_{CM}, and μ_{w} is a small positive iteration step size. The gradient of ξ_{CM} is derived by applying the product rule and Wirtinger calculus to differentiate (4.18) as follows

$$\begin{aligned}
\frac{\partial \xi_{\mathrm{CM}}}{\partial \mathbf{w}^*} &= \frac{\partial}{\partial \mathbf{w}^*} \mathcal{E}\left\{ (|\tilde{r}[n]|^2 - 1)^2 \right\} \\
&= 2 \cdot \mathcal{E}\left\{ (|\tilde{r}[n]|^2 - 1) \left(\frac{\partial}{\partial \mathbf{w}^*} (\mathbf{w}^H \mathbf{r}_n \mathbf{r}_n^H \mathbf{w} - 1) \right) \right\} \\
&= 2 \cdot \mathcal{E}\left\{ \mathbf{r}_n \mathbf{r}_n^H \mathbf{w} \cdot (|\tilde{r}[n]|^2 - 1) \right\} \\
&= 2 \cdot \mathcal{E}\left\{ \mathbf{r}_n \cdot \tilde{r}^*[n] \cdot (|\tilde{r}[n]|^2 - 1) \right\} \quad ,
\end{aligned} \tag{4.20}$$

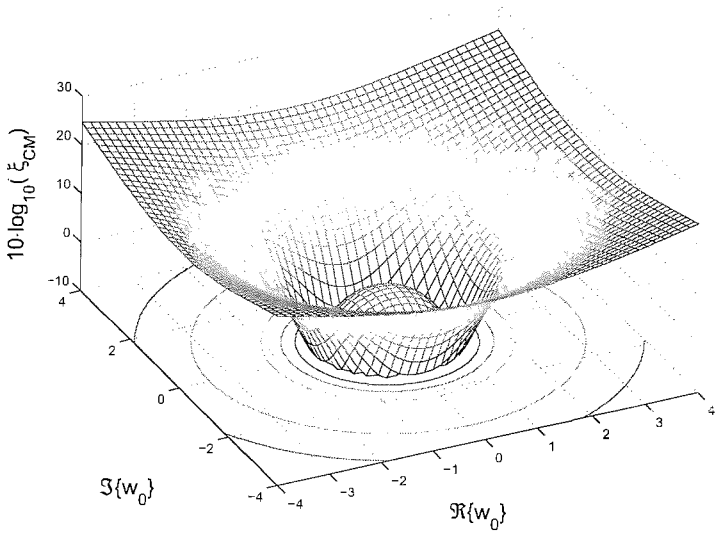

Figure 4.5: Constant modulus cost function ξ_{CM}, for an equaliser with a single complex coefficient.

and the instantaneous gradient is estimated by dropping expectations in (4.20) such that

$$\frac{\partial \hat{\xi}_{\mathrm{CM}}}{\partial \mathbf{w}^*} = 2(|\tilde{r}[n]|^2 - 1) \cdot \mathbf{r}_n \cdot \tilde{r}^*[n] \quad . \tag{4.21}$$

A fixed step size may not be efficient for a substantial portion of the input signal if the signal is non-stationary. This makes the normalised CMA (NCMA) attractive for use with Bluetooth signals because the iteration step size will be based on the statistics of the current equaliser input vector only, and is therefore not limited in size by the statistics of the whole received signal. However, there have been a couple of different derivations of the NCMA in the literature, and an added benefit of this research will be to compare them for equivalence, and to determine which is most suitable for Bluetooth. Hence, more detailed formulations of the suggestions made in [136] and [137, 138], are provided in Sec. 4.5.4 and Sec. 4.6 respectively. Note that in Sec. 4.6 the normalised CMA corresponds to having a window size of 1, and that the window size may be increased to speed up the algorithm.

4.5.3 Initialisation of CMA

It is well documented that the CM cost function possesses global and local minima [139, 43], the positions of which are influenced by the nature of the signal and channel. It is also noted that a correlated input signal like those used in Bluetooth are likely to generate additional local minima [139, 43]. Ill-convergence to a local minimum will guarantee an excess steady state error [43]. In this work we try to avoid local minima by initialising the equaliser centre tap with a non-zero constant and the rest to zero, which according to [131, 140] will ensure that the equaliser is initialised within the gravitational pull of the global solution.

4.5.4 Normalised CMA

This section will enrich the formulation of the NCMA equaliser update procedure that appears in [136]. Similar to the NLMS development highlighted in Sec. 4.4.2, the derivation presented here is based on the constrained optimisation principle, whereby the step size μ_{w} is adapted subject to the constraint that the updated filter coefficients should produce zero-error with the current data vector $\mathbf{r}_n$. This can be stated mathematically by expressing the desired result as

$$|\mathbf{w}_{n+1}^H \mathbf{r}_n|^2 = \mathbf{r}_n^H \mathbf{w}_{n+1} \mathbf{w}_{n+1}^H \mathbf{r}_n = 1 \quad . \tag{4.22}$$

Now by merging (4.19) and (4.21), the CMA equaliser update equation can be rewritten as

$$\begin{aligned}\mathbf{w}_{n+1} &= \mathbf{w}_n - \mu_{\mathrm{w}} \cdot \underbrace{2(|\tilde{r}[n]|^2 - 1)\tilde{r}^*[n]}_{\mathcal{K}} \mathbf{r}_n \\ &= \mathbf{w}_n - \mu_{\mathrm{w}} \mathcal{K} \mathbf{r}_n \quad , \end{aligned} \tag{4.23}$$

and by substituting (4.23) into (4.22) it emerges that

$$\begin{aligned} 1 &= \mathbf{r}_n^H (\mathbf{w}_n - \mu_{\mathrm{w}} \mathcal{K} \mathbf{r}_n)(\mathbf{w}_n^H - \mu_{\mathrm{w}} \mathcal{K}^* \mathbf{r}_n^H)\mathbf{r}_n \\ &= (\mathbf{r}_n^H \mathbf{w}_n - \mu_{\mathrm{w}} \mathcal{K} \mathbf{r}_n^H \mathbf{r}_n)(\mathbf{w}_n^H \mathbf{r}_n - \mu_{\mathrm{w}} \mathcal{K}^* \mathbf{r}_n^H \mathbf{r}_n) \\ &= (\tilde{r}^*[n] - \mu_{\mathrm{w}} \mathcal{K} \mathbf{r}_n^H \mathbf{r}_n)(\tilde{r}[n] - \mu_{\mathrm{w}} \mathcal{K}^* \mathbf{r}_n^H \mathbf{r}_n) \\ &= |\tilde{r}[n]|^2 - \mu_{\mathrm{w}} \mathcal{K} \tilde{r}[n] ||\mathbf{r}_n||^2 - \mu_{\mathrm{w}} \mathcal{K}^* \tilde{r}^*[n] ||\mathbf{r}_n||^2 + \mu_{\mathrm{w}}^2 |\mathcal{K}|^2 ||\mathbf{r}_n||^4 \\ &= |\tilde{r}[n]|^2 - 2\mu_{\mathrm{w}} \mathcal{K} \tilde{r}[n] ||\mathbf{r}_n||^2 + \mu_{\mathrm{w}}^2 |\mathcal{K}|^2 ||\mathbf{r}_n||^4 \quad . \end{aligned} \tag{4.24}$$

It is obvious that (4.24) is a quadratic equation in μ_{w} when it is written in the form

$$\mu_{\mathrm{w}}^2 (|\mathcal{K}|^2 ||\mathbf{r}_n||^4) - \mu_{\mathrm{w}} (2\mathcal{K}\tilde{r}[n] ||\mathbf{r}_n||^2) + (|\tilde{r}[n]|^2 - 1) = 0 \quad ,$$

and hence the well known formula for roots of a quadratic equation[5] provide the solutions

$$\mu_{\mathrm{w}} = \frac{\mathcal{K}\tilde{r}[n] \pm |\mathcal{K}|}{|\mathcal{K}|^2 ||\mathbf{r}_n||^2} \quad . \tag{4.25}$$

The derivations of (4.24) and (4.25) exploit the fact that $\mathcal{K}\tilde{r}[n] = \mathcal{K}^*\tilde{r}^*[n] = |\mathcal{K}||\tilde{r}[n]|$. Now by substituting $\mathcal{K} = 2(|\tilde{r}[n]|^2 - 1)\tilde{r}^*[n]$ in (4.25) we obtain

$$\begin{aligned} \mu_{\mathrm{w}} &= \frac{(|\tilde{r}[n]|^2 - 1) \cdot |\tilde{r}[n]|^2 \pm |\tilde{r}[n]|^2 - 1| \cdot |\tilde{r}^*[n]|}{2||\tilde{r}[n]|^2 - 1|^2 \cdot |\tilde{r}^*[n]|^2 \cdot ||\mathbf{r}_n||^2} \\ &= \frac{\mathrm{sign}\{|\tilde{r}[n]|^2 - 1\} \cdot ||\tilde{r}[n]|^2 - 1| \cdot |\tilde{r}[n]|^2 \pm ||\tilde{r}[n]|^2 - 1| \cdot |\tilde{r}^*[n]|}{2||\tilde{r}[n]|^2 - 1|^2 \cdot |\tilde{r}^*[n]|^2 \cdot ||\mathbf{r}_n||^2} \\ &= \frac{\mathrm{sign}\{|\tilde{r}[n]|^2 - 1\} \cdot |\tilde{r}[n]| \pm 1}{2||\tilde{r}[n]|^2 - 1| \cdot |\tilde{r}^*[n]| \cdot ||\mathbf{r}_n||^2} \quad , \end{aligned}$$

but we are interested only in the smallest non-negative solution given by

$$\mu_{\mathrm{w}} = \frac{\mathrm{sign}\{|\tilde{r}[n]|^2 - 1\} \cdot |\tilde{r}[n]| \pm 1}{2||\tilde{r}[n]|^2 - 1| \cdot |\tilde{r}^*[n]| \cdot ||\mathbf{r}_n||^2} \quad . \tag{4.26}$$

According to the development above, (4.26) defines the iteration step size that will facilitate the smallest jump to the desired equaliser solution in one iteration, in other words a normalised step size of $\hat{\mu}_{\mathrm{w}} = 1$. However, stochastic gradient techniques require that the solution is approached more gradually, and hence the definition

$$\mu_{\mathrm{w}} = \hat{\mu}_{\mathrm{w}} \frac{\mathrm{sign}\{|\tilde{r}[n]|^2 - 1\} \cdot |\tilde{r}[n]| \pm 1}{2||\tilde{r}[n]|^2 - 1| \cdot |\tilde{r}^*[n]| \cdot ||\mathbf{r}_n||^2} \qquad \text{with} \quad \hat{\mu}_{\mathrm{w}} \in [0, 1) \quad .$$

[5] If $ax^2 + bx + c = 0$, then $x = \frac{-b \pm \sqrt{b^2 - 4ac}}{2a}$ [81].

The parameter $\hat{\mu}_w$ shall be coined the normalised step size, but since it will be the parameter of reference in the rest of this thesis we drop the " ˆ " and denote it with μ_w only.

Unfortunately, the coloured nature of Bluetooth signals tends to flatten the CM cost surface of Fig. 4.5 in the radial direction, and thereby makes convergence to the minimum much slower [43]. This is particularly unfavourable in Bluetooth for reasons mentioned in the next section, and therefore in Sec. 4.6 we propose a method to speed up the CMA.

4.6 Normalised Sliding Window Constant Modulus Algorithm

The Bluetooth standard has a lax specification for parameters such as carrier frequency and modulation index [17]. Research has shown that significant system degradation can occur even when operating within the permitted limits [44, 95]. Hence, a reliable Bluetooth receiver will need to compensate for this mismatch. Where multipath propagation exists, it will undermine parameter synchronising algorithms unless equalisation is performed upstream. Taking into account the limited burst lengths of Bluetooth packets, it is essential that equalisation occurs fast enough so as to give algorithms downstream sufficient time to converge. Ideally, all compensation activity should be completed within the time it takes to receive the mutually known 72-bit access code, thereby preventing information loss. This problem is aggravated by the fact that a master node may receive alternate packets from different transmitters [17], each having a different carrier frequency and modulation index, and experiencing different channel conditions. Therefore fresh adaptive processing could begin with each arriving packet, and a slow converging equaliser will impede the progress of other parameter synchronising blocks, and increase the bit error ratio.

Unfortunately, correlation between signal samples introduced by GFSK modulation causes slow convergence. A number of suggestions to speed up the CMA have been made. These methods include the Quasi-Newton cross-correlation constant modulus algorithm [141, 142] that is faster than conventional CMA at the expense of an increase in complexity, and a transform domain CMA that has a faster convergence rate than the standard algorithm, while a genetic search based CMA has been applied with less impressive results in [143]. The use of a pre-whitening filter is suggested in [144], and an accelerated CMA based on the accelerating tuner [145] is proposed in [146]. Nonetheless, since many of these techniques assume that the transmit signal $s[n]$ is white and that ISI is only introduced by the channel, they are therefore not suitable for Bluetooth. The normalised

sliding window CMA (NSWCMA) however [137, 138], which is akin to the affine projection algorithm (APA) [128, 147, 148, 149, 150] but based on the CM criterion, imposes more constraints than the classical CMA, and as a result achieves faster convergence [137, 138]. It is this method that is proposed here, but regularisation shall be performed to cater for correlated transmit signal $s[n]$.

4.6.1 Formulation of the NSWCMA

To enable an elaborate yet simpler derivation of the NSWCMA than that provided in [137, 138], we first assume knowledge of the desired equaliser output sequence $s[n-d]$, or short s_{n-d}, and similar to the APA [102] we aim to solve the constrained optimisation (minimisation) problem [117], whereby

$$||\Delta\mathbf{w}_{n+1}||^2 = ||\mathbf{w}_{n+1} - \mathbf{w}_n||^2 \stackrel{!}{=} \min \quad , \tag{4.27}$$

is minimised, subject to the constraints

$$\begin{aligned} \mathbf{r}_n^H \mathbf{w}_{n+1} &= s_{n-d}^* \quad , & (4.28)\\ \mathbf{r}_{n-1}^H \mathbf{w}_{n+1} &= s_{n-d}^* \quad , & (4.29)\\ &\vdots \\ \mathbf{r}_{n-P+1}^H \mathbf{w}_{n+1} &= s_{n-d}^* \quad , & (4.30) \end{aligned}$$

where P is the window size, $||\mathbf{w}||^2 = \mathbf{w}^H\mathbf{w}$, and

$$\mathbf{r}[n] = \mathbf{r}_n = [\, \mathrm{r}_0[n], \mathrm{r}_1[n], \cdots, \mathrm{r}_{L_\mathrm{w}-1}[n] \,]^T \quad . \tag{4.31}$$

The system of equations (4.28)-(4.30) can conveniently be expressed in matrix notation as

$$\mathbf{R}_n^H \mathbf{w}_{n+1} = \mathbf{s}_{n-d}^* \quad ,$$

where

$$\mathbf{R}_n = [\, \mathbf{r}_n, \mathbf{r}_{n-1}, \cdots, \mathbf{r}_{n-P+1} \,] \in \mathbb{C}^{L_\mathrm{w} \times P} \quad , \tag{4.32}$$

and

$$\mathbf{s}_{n-d} = [\, s_{n-d}, s_{n-d}, \cdots, s_{n-d} \,]^T \in \mathbb{C}^{P \times 1} \quad , \tag{4.33}$$

such that the corresponding error vector is given by

$$\begin{aligned} \mathbf{e}_n^* &= \mathbf{s}_{n-d}^* - \mathbf{R}_n^H \mathbf{w}_n \quad , \\ &= \mathbf{R}_n^H \mathbf{w}_{n+1} - \mathbf{R}_n^H \mathbf{w}_n \quad , \\ &= \mathbf{R}_n^H \Delta\mathbf{w}_{n+1} \quad . & (4.34) \end{aligned}$$

Equation (4.34) can be rewritten as

$$\Delta \mathbf{w}_{n+1} = (\mathbf{R}_n^H)^\dagger \mathbf{e}_n^* \quad ,$$

where $\Delta \mathbf{w}_{n+1}$ is the minimum norm solution demanded by (4.27), and $(\mathbf{R}_n^H)^\dagger$ is the pseudoinverse of $\mathbf{R}_n^H$ [107, 151]. If $P < L_\mathrm{w}$ the system of equations is said to be underdetermined and the right pseudoinverse

$$(\mathbf{R}_n^H)^\dagger = \mathbf{R}_n(\mathbf{R}_n^H\mathbf{R}_n)^{-1} \quad , \tag{4.35}$$

is required, and if $P > L_\mathrm{w}$ the system is overdetermined and the left pseudo-inverse

$$(\mathbf{R}_n^H)^\dagger = (\mathbf{R}_n\mathbf{R}_n^H)^{-1}\mathbf{R}_n \quad , \tag{4.36}$$

is appropriate, while if $P = L_\mathrm{w}$ then

$$(\mathbf{R}_n^H)^\dagger = (\mathbf{R}_n^H)^{-1} \quad .$$

Hence the equaliser update equation is given by

$$\begin{aligned} \mathbf{w}_{n+1} &= \mathbf{w}_n + \mu_\mathrm{w}\Delta \mathbf{w}_{n+1} \quad , \\ &= \mathbf{w}_n + \mu_\mathrm{w}(\mathbf{R}_n^H)^\dagger \mathbf{e}_n^* \quad , \end{aligned} \tag{4.37}$$

where $\mu_\mathrm{w} \in [0, 1)$ is an iteration step size. Notice that (4.37) with P set to 1, defines an alternative normalised CMA which we shall compare with the form described in Sec. 4.5.4.

To overcome the assumption of the availability of a reference signal at the receiver, which was necessary for the derivation above, we now relax the constraints of (4.28)-(4.30) and only insist on a constant modulus, such that $|s_{n-d}| = 1$. Hence, we set $s_{n-d} = \frac{\tilde{r}_n}{|\tilde{r}_n|}$, where $\tilde{r}_n$ is the equaliser output at the nth time instance, such that the NSWCMA vector of desired signal elements in (4.33) is given by

$$\mathbf{s}_{n-d} = \left[\frac{\tilde{r}_n}{|\tilde{r}_n|}, \frac{\tilde{r}_n}{|\tilde{r}_n|}, \cdots, \frac{\tilde{r}_n}{|\tilde{r}_n|} \right]^T \in \mathbb{C}^{P\times 1} \quad ,$$

and this is what differentiates the NSWCMA from the APA.

4.6.2 Regularisation of the NSWCMA

It is obvious from (4.35), (4.36) and (4.37) that implementing the NSWCMA involves the inversion of the received signals instantaneous covariance matrix $\breve{\mathbf{R}}_n = \mathbf{R}_n^H\mathbf{R}_n \in \mathbb{C}^{P\times P}$ or $\breve{\mathbf{R}}_n = \mathbf{R}_n\mathbf{R}_n^H \in \mathbb{C}^{L_\mathrm{w}\times L_\mathrm{w}}$, once per iteration. However, the correlated nature of $r[n]$ means that this matrix is potentially ill-conditioned [104]. A solution is possible if regularisation is applied, which will be the focus of this section.

4.6.2.1 Diagonal Loading

The regularisation method discussed here will be referred to as "diagonal loading", and is similar to that employed for the affine projection algorithm in [152, 153]. In this case the matrix to be inverted is modified by adding to it a diagonal matrix with non-zero elements equal to ρ, in other words

$$\begin{aligned} \breve{\mathbf{R}}_n &= \mathbf{R}_n^H \mathbf{R}_n + \rho \mathbf{I}_P \quad , \quad \text{or} \\ \breve{\mathbf{R}}_n &= \mathbf{R}_n \mathbf{R}_n^H + \rho \mathbf{I}_{L_\text{w}} \quad , \end{aligned}$$

for the right and left pseudoinverse respectively, where ρ is a real valued constant referred to as the regularisation term.

Regularisation stabilises the solution of $\breve{\mathbf{R}}_n^{-1}$, but the choice of ρ will influence the accuracy of the result and the convergence speed [107]. Efforts to compute a pseudo-optimal regularisation factor for the APA are reported in [152], but these is mainly theoretical because they involve the complex task of estimating system mismatch, while a reduced-cost implementation in [153] maintains the assumption that $s[n]$ is white, which is not the case in Bluetooth. Therefore an appropriate range for ρ will be determined by experiments performed in Sec. 4.8.

4.6.2.2 High-pass Signal Covariance Matrix Loading

As an alternative to the diagonal loading technique, we propose the use of a high-pass signal covariance matrix. The results in Sec. 4.8 will demonstrate that convergence of the NSWCMA is faster when this new technique is applied compared to diagonal loading. Regularisation in this case requires that a covariance matrix derived from a high-pass signal is added to the potentially ill-conditioned matrix to be inverted, that is to say the matrix that is actually inverted is given by

$$\begin{aligned} \breve{\mathbf{R}}_n &= \mathbf{R}_n^H \mathbf{R}_n + \mathbf{H}_p \quad , \quad \text{or} \\ \breve{\mathbf{R}}_n &= \mathbf{R}_n \mathbf{R}_n^H + \mathbf{H}_{L_\text{w}} \quad , \end{aligned}$$

for the right or left pseudoinverse respectively, where $\mathbf{H}_p$ and $\mathbf{H}_{L_\text{w}}$ are defined analogously to $\mathbf{R}_n$ in (4.32), as the $p \times p$ and $L_\text{w} \times L_\text{w}$ covariance matrix of a complementary high-pass signal $h[n]$.

Motivation: Let $P_{ss}(e^{j\omega})$ and $\gamma_{ss}[n]$ be the power spectral density (PSD) and autocorrelation function of the transmitted low-pass Bluetooth signal $s[n]$, such that $P_{ss}(e^{j\omega}) \bullet\!\!-\!\!\circ\, \gamma_{ss}[n]$.

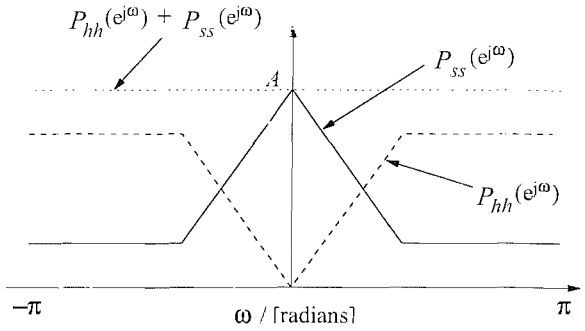

Figure 4.6: An idealised sketch of the power spectral density of a Bluetooth signal $P_{ss}(e^{j\omega})$ and that of the corresponding high-pass signal used for regularisation $P_{hh}(e^{j\omega})$.

Similarly, assume $P_{hh}(e^{j\omega})$ and $\gamma_{hh}[n]$ are the PSD and autocorrelation function of a high-pass signal $h[n]$, such that $P_{hh}(e^{j\omega}) \bullet\!\!-\!\!\circ\, \gamma_{hh}[n]$, and that $h[n]$ satisfies the condition

$$P_{ss}(e^{j\omega}) + P_{hh}(e^{j\omega}) = A \quad , \tag{4.38}$$

with

$$A = \max_{\omega} P_{ss}(e^{j\omega}) \quad . \tag{4.39}$$

As an illustration, the conditions in (4.38) and (4.39) are satisfied by the idealised sketch in Fig. 4.6. Hence, the summation of $s[n]$ and $h[n]$ has the desired flat frequency response, and by inverse Fourier transform of (4.38) we obtain

$$\gamma_{hh}[n] = A \cdot \delta[0] - \gamma_{ss}[n] \quad ,$$

and therefore

$$\mathbf{H}_p = A \cdot \mathbf{I}_p - \mathbf{S}_p \quad , \tag{4.40}$$

or

$$\mathbf{H}_{L_\mathrm{w}} = A \cdot \mathbf{I}_{L_\mathrm{w}} - \mathbf{S}_{L_\mathrm{w}} \quad , \tag{4.41}$$

where $\mathbf{S}_p$ and $\mathbf{S}_{L_\mathrm{w}}$ are the $p \times p$ and $L_\mathrm{w} \times L_\mathrm{w}$ covariance matrices of the transmitted signal $s[n]$. Since everything on the right hand side of (4.40) and (4.41) are known, $\mathbf{H}_p$ and $\mathbf{H}_{L_\mathrm{w}}$ can be computed off-line, thereby making the covariance matrix regularisation equal in complexity to the method of diagonal loading. However, during the presentation of results in Sec. 4.8, it will be demonstrated using a high-pass signal covariance matrix produces a faster convergence than employing diagonal loading.

4.7 General Comments on Constant Modulus Criterion

The CMA, NCMA, and NSWCMA are all based on the constant modulus criterion. Properties of the CM criterion are detailed in various publications [154, 155, 104, 43], and some are implied in the discussions above. However, features of the CM criterion that are relevant to further sections of this thesis will be highlighted here as follows:

- The CM cost function ξ_{CM} is minimised when the equaliser output $\tilde{r}[n]$ has a magnitude of 1, at this point $\frac{\partial \xi_{\mathrm{CM}}}{\partial \mathbf{w}^*} = 0$.
- Once convergence has been established, the impulse response of the cascade of the channel with equaliser $h_{\mathrm{cw}}[n] = c[n] * \mathrm{w}[n]$, ideally consists of only one nonzero coefficient $h_{\mathrm{cw}}[d] = e^{j\phi}$. Where ϕ and d are an ambiguous phase rotation and a signal delay respectively, and these may be resolved further along the signal processing chain.
- Equaliser update algorithms are generally much slower when the input signal is coloured, and this is particularly disadvantageous when the received signal consists of short bursts from multiple transmitters as in Bluetooth. The severity of this phenomenon will become clear in Sec. 4.8.

4.8 Simulation Results and Discussion

Having already highlighted considerations necessary when selecting an equalisation method for Bluetooth, in this section supporting experimental results are presented and discussed. The non-linear and coloured nature of Bluetooth signals, coupled with the absence of a widely accepted theoretical constant modulus solution, make a quantitative analysis difficult. However, comparative results in this section give insight into acceptable regularisation factors for the NSWCMA.

4.8.1 Default Parameters

The signal model was established as specified in Sec. 2.2 and portrayed in Fig. 2.1, with parameters set to Bluetooth specification of $K_{BT} = 0.5$ and $h = 0.35$ [17], while $N = 2$. Unless stated otherwise the channel used in the simulations was the Saleh-Valenzuela channel model derived Sec. 2.3.3, with a sample rate of 2 MHz and an approximate RMS of $\sigma_\tau = 300$ ns.

As a default, the index of the non-zero element in the equaliser initialisation vector was set to $i_\delta = \lfloor \frac{L_w-1}{2} \rfloor$, while the delay due to the channel-MMSE equaliser composite system was $d = \lfloor \frac{L_w+L_c-1}{2} \rfloor$. Noting that the Bluetooth specification permits a maximum of 75 kHz carrier frequency offset for a signal of 1 MHz bandwidth, in Sec. 2.2 it was shown that this translates to a normalised angular frequency offset of $\Delta\Omega = \frac{2\pi \cdot 75}{N \cdot 1000}$, which will be used as our initial carrier frequency offset when applicable.

Learning curves and frequency responses were obtained at 15 dB E_b/N_0 because this is the approximate signal quality required for the MFB receiver to attain a bit error ratio of 10^{-3} (with $K = 3$), which is the minimal performance requirement for Bluetooth [17]. The learning curves portray the square of the error in the magnitude of the equaliser output, or

$$e[n] = (|\tilde{r}[n]| - 1)^2 \quad .$$

The learning curves shown have been averaged over multiple runs of a simulation. By default diagonal loading matrix regularisation was applied with a regularisation term equal to the size of the NSWCMA window, or $\rho = P$, and the equaliser was allowed to converge before computing BER curves.

4.8.2 Results and Discussion

The learning curves in Fig. 4.7 illustrate that NLMS, NCMA and first order NSWCMA take a comparable amount of time to converge, with the NLMS being slightly faster. This

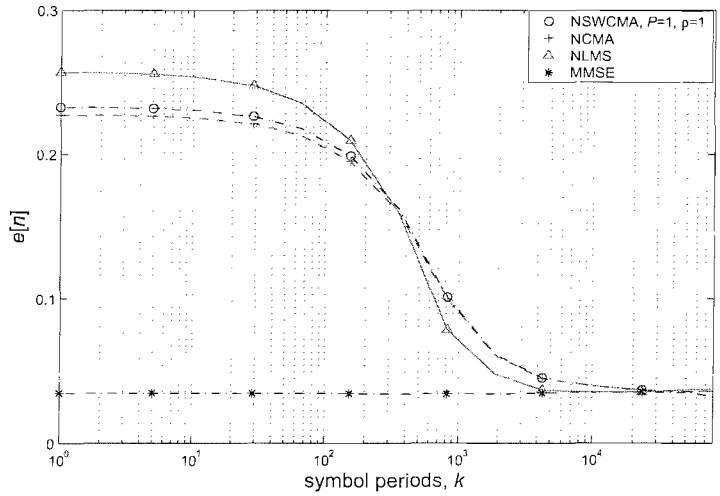

Figure 4.7: Learning curves for various equaliser algorithms, using $N = 2$, $K_{BT} = 0.5$, $h = 0.35$, $\Delta\Omega = 0$, $L_w = 64$, $\mu_w = 0.1$, $E_b/N_0 = 15$ dB and $\sigma_\tau = 300$ ns.

supports the argument that the NLMS is not significantly faster than CMA if the signal of interest has a constant modulus [132]. However, unlike the NCMA and NSWCMA, the NLMS can only be adapted for the small fraction of time during which the training sequence is transmitted, this implies that in practice NLMS will be relatively slower than illustrated in Fig. 4.7, so this is further justification for selecting a CM based criterion.

Additionally, it is evident from Fig. 4.7 that the NCMA and first order NSWCMA have similar convergence properties despite different formulations and tracking procedures. The similarity between the final solution of the NLMS algorithm and the MMSE is more obvious from the frequency response of the channel-equaliser composite systems depicted in Fig. 4.8. It is interesting to note that none of the equalisers is able to compensate for the channel in regions without a rich supply of spectral components, resulting in a low-pass filter

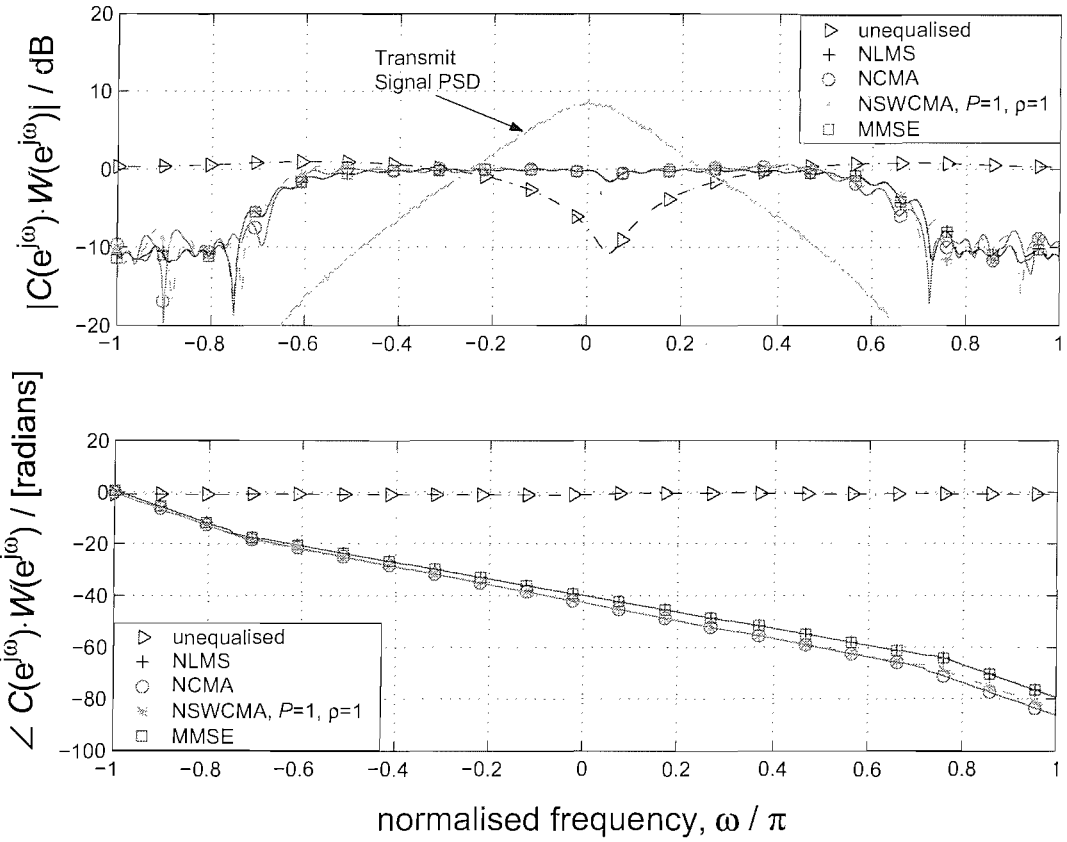

Figure 4.8: PSD of the transmit signal $s[n]$, and the frequency response of the unequalised channel, and that of the corresponding channel-equaliser composite system, after convergence of various equaliser algorithms, using $N = 2$, $K_{BT} = 0.5$, $h = 0.35$, $\Delta\Omega = 0$, $L_w = 64$, $\mu_w = 0.1$, $E_b/N_0 = 15$ dB and $\sigma_\tau = 300$ ns.

characteristic that is unlike the flat magnitude response we would expect after equalisation. This is consistent with the observation that the lack of a "persistently exciting" white signal is a source of mismatch between the steady-state equaliser coefficients and their ideal values [156].

Irrespective of convergence speed, the NLMS algorithm and derivatives of it like the affine projection algorithm, utilise phase information, and are therefore susceptible to carrier frequency offsets. For example, Fig. 4.9 portrays the learning curves for the NLMS, NCMA and first order NSWCMA when exposed to a carrier frequency offset of the magnitude permitted in Bluetooth, while Fig. 4.10 depicts the corresponding channel-equaliser frequency response after 10^5 iterations of the equaliser. It is clear from these illustrations that unlike the NCMA and NSWCMA, the NLMS will collapse under these conditions, and hence the CM criterion is a more reliable option for the equalisation of Bluetooth links.

While deriving the MMSE solution in Sec. 4.3, we assumed that the channel-MMSE equaliser delay constant d was selected to be optimum. A summary of experiments performed to determine d is presented in Fig. 4.11, and confirms the best BER performance is attained by assuming that the combined delay introduced by the channel and equaliser is half the summation of their lengths, or $d = \lfloor \frac{L_w + L_c - 1}{2} \rfloor$.

Fig. 4.12 demonstrates that speeding up the NSWCMA is easily attained by increasing its window size. The importance of the regularisation of matrix $\breve{\mathbf{R}}_n$ in the tracking procedure is apparent from Figs. 4.12 to 4.13. These figures indicate that regularisation is more critical

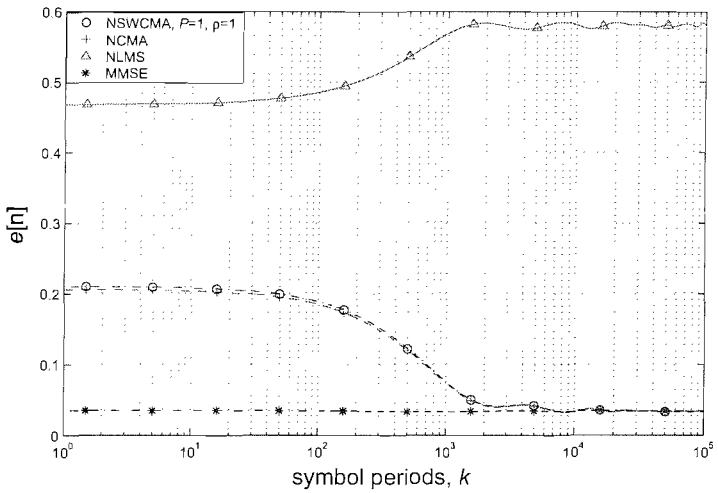

Figure 4.9: Learning curves for various equaliser algorithms, using $N = 2$, $K_{BT} = 0.5$, $h = 0.35$, $\Delta\Omega = 0.075\pi$, $L_w = 64$, $\mu_w = 0.1$, $E_b/N_0 = 15$ dB and $\sigma_\tau = 300$ ns.

for large P, in which case ill-convergence results if no regularisation is applied. In the top plot of Fig. 4.13 selecting $\rho \gg P$ actually slows down the algorithm, while the bottom plot of the same figure demonstrates that if $\rho \ll P$ instability will result. It is for this reason that we use $\rho = P$ in our experiments.

It is interesting to note from the learning curves shown in this section, that despite the fact that NSWCMA never out-performs the MMSE in terms of error in magnitude of the equaliser output $e[n]$, the BER performance of the NSWCMA, shown in Fig. 4.14, is better than that of the MMSE at high SNR. This is supportive of the idea of minimum bit error rate (MBER) filtering [157], which asserts that the MBER and not the MMSE solution will provide the best performance in terms of BER. Our findings suggest that the NSWCMA solution comes closer to the MBER solution than the MMSE.

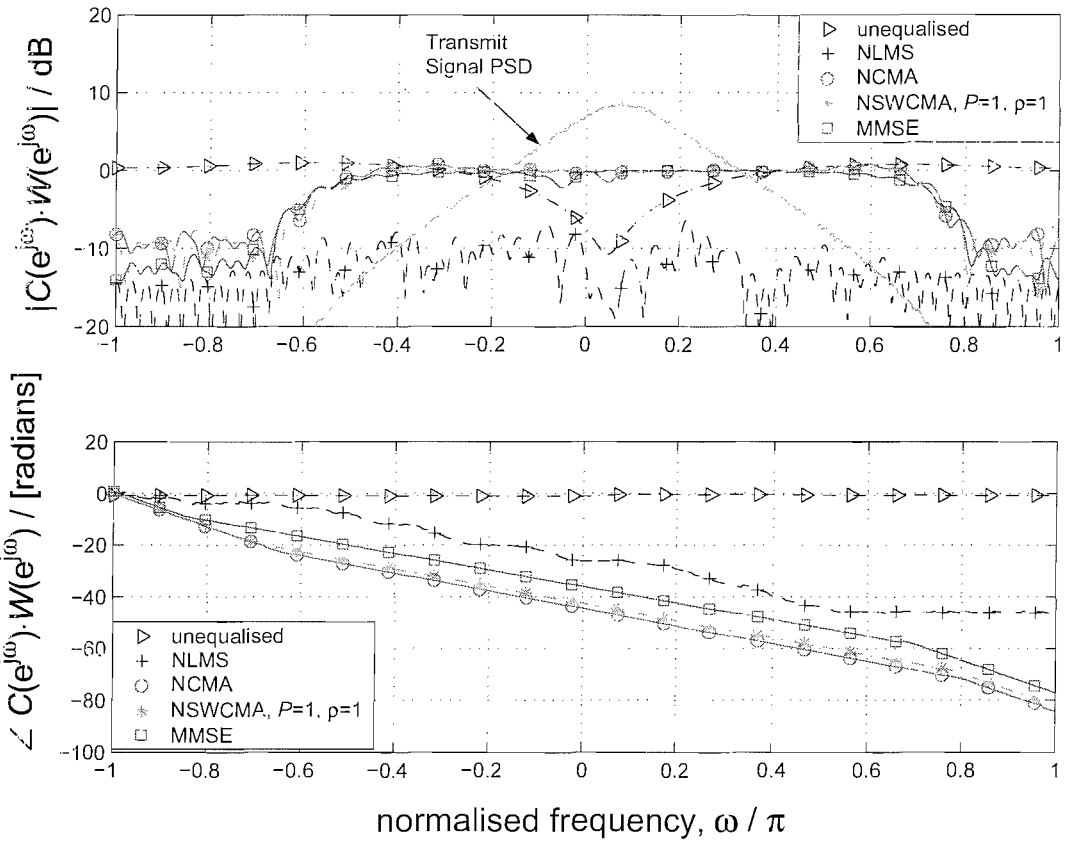

Figure 4.10: PSD of the transmit signal $s[n]$, and the frequency response of the unequalised channel, and that of the corresponding channel-equaliser composite system, after convergence of various equaliser algorithms, using $N = 2$, $K_{BT} = 0.5$, $h = 0.35$, $\Delta\Omega = 0.075\pi$, $L_w = 64$, $\mu_w = 0.1$, $E_b/N_0 = 15$ dB and $\sigma_\tau = 300$ ns.

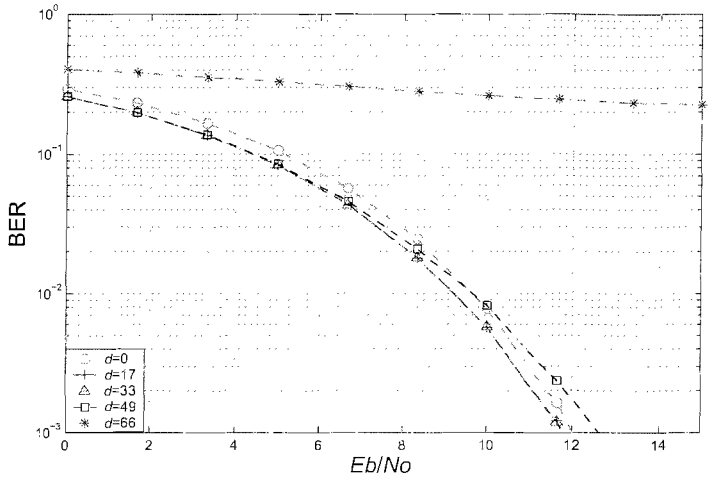

Figure 4.11: BER performance of the MMSE equaliser solution with different delay constants d, using $K = 3$, $N = 2$, $K_{BT} = 0.5$, $h = 0.35$, $\Delta\Omega = 0$, $L_w = 64$ and $\sigma_\tau = 300$ ns.

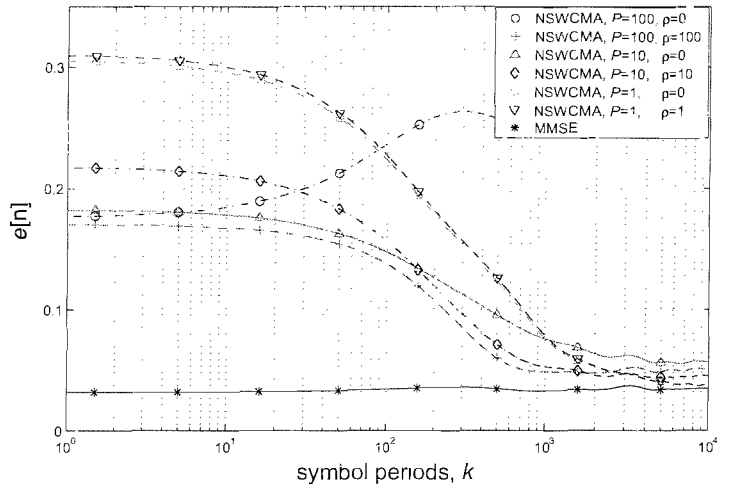

Figure 4.12: Learning curves for NSWCMA equaliser with and without regularisation, using $N = 2$, $K_{BT} = 0.5$, $h = 0.35$, $\Delta\Omega = 0$, $L_w = 64$, $\mu_w = 0.1$, $E_b/N_0 = 15$ dB and $\sigma_\tau = 300$ ns.

Finally, the two alternative regularisation techniques are compared in Fig. 4.15. The learning curve derived using the high-pass signal covariance matrix loading method leads that in which diagonal loading is employed, and demonstrates a significant improvement in the convergence speed.

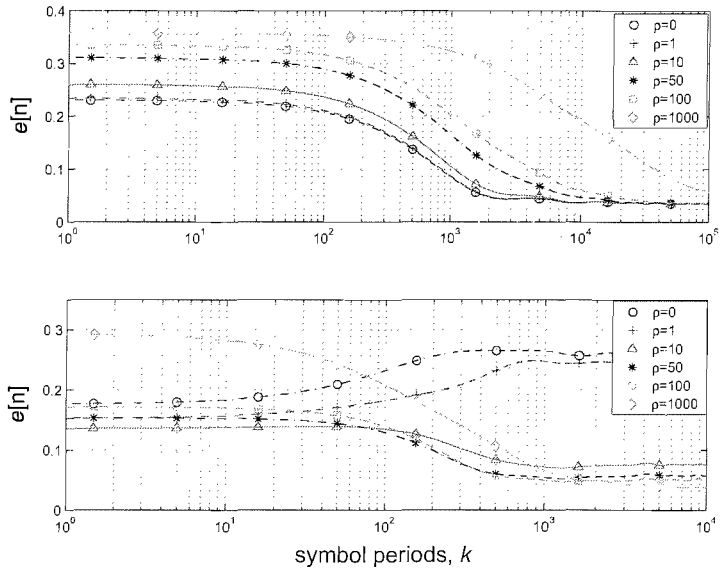

Figure 4.13: Learning curves for the NSWCMA equaliser with $P = 1$ (top) and $P = 100$ (bottom) and different regularisation factors, using $N = 2$, $K_{BT} = 0.5$, $h = 0.35$, $\Delta\Omega = 0$, $L_{\mathrm{w}} = 64$, $\mu_{\mathrm{w}} = 0.1$, $E_b/N_0 = 15$ dB and $\sigma_\tau = 300$ ns.

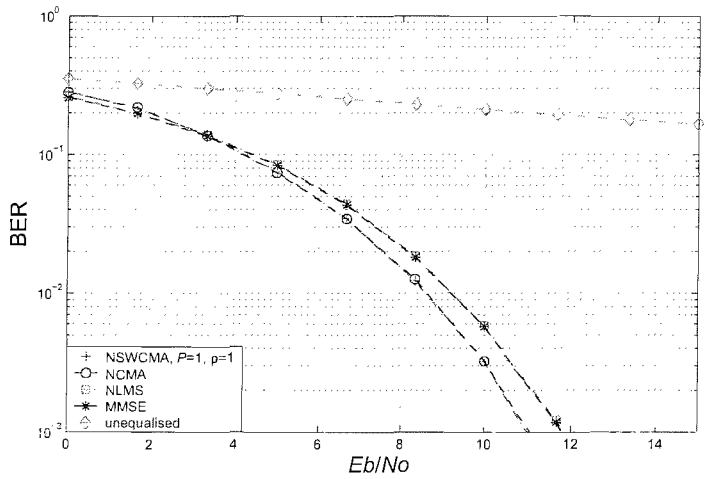

Figure 4.14: BER performance for various equaliser algorithms, using $K = 3$, $N = 2$, $K_{BT} = 0.5$, $h = 0.35$, $\Delta\Omega = 0$, $L_{\mathrm{w}} = 64$, $\mu_{\mathrm{w}} = 0.01$ and $\sigma_\tau = 300$ ns.

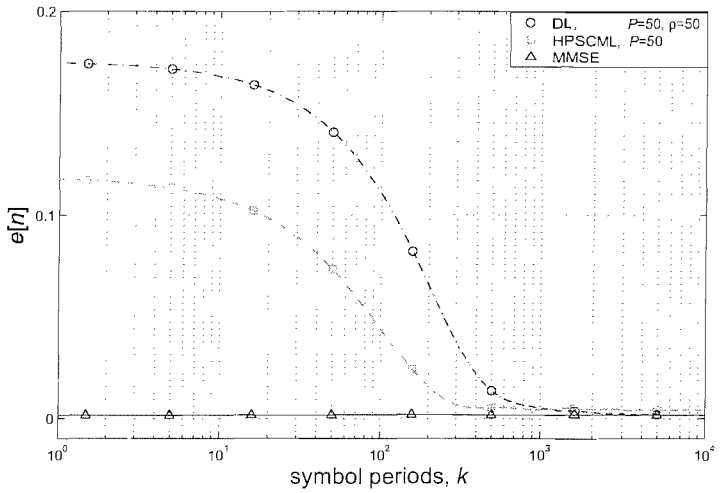

Figure 4.15: Learning curves for NSWCMA equaliser with regularisation by diagonal loading (DL) and high-pass signal covariance matrix loading (HPSCML), using $N = 2$, $K_{BT} = 0.5$, $h = 0.35$, $\Delta\Omega = 0$, $L_{\mathrm{w}} = 64$, $\mu_{\mathrm{w}} = 0.1$, and $\sigma_\tau = 300$ ns.

4.9 Summary and Concluding Remarks

A high integrity receiver for Bluetooth signals will require rapid equalisation to ensure that parameter synchronising algorithms downstream from the equaliser in the signal processing chain, are able to converge quickly and prevent information loss. The probability of a significantly large carrier frequency offset makes LMS and its derivatives unsuitable, while popular equalising procedures are too slow with correlated input signals like Bluetooth. The NSWCMA is advantageous because convergence can be hastened by increasing its window size appropriately.

However, for signals like Bluetooth with correlated signal samples, the adaptation procedure can be unstable if regularisation is not applied to the received signal covariance matrix. In this chapter we have derived a regularisation method in which a complementary high-pass signal covariance matrix is added to the received signal covariance matrix prior to inversion, and we have demonstrated that our method is more beneficial in terms of convergence speed when compared with the only alternative technique reported in the literature.

Chapter 5

Carrier Frequency and Modulation Index Offset Correction

Having addressed the dispersive channel problem, parameters such as the carrier frequency and modulation index may still be unsynchronised. This is prevalent in wireless standards like Bluetooth, in which significant parameter offsets are permitted in order to ensure that production of cheap transmitter and receiver devices is feasible. For example, in Bluetooth an initial carrier frequency offset of 75 kHz is allowed for a signal with $B = 1$ MHz, and the modulation index may lie in the range $h \in (0.28, 0.35)$ [17]. Research has shown that performance of simple receivers deteriorates significantly even when operating within this range of frequency error [44], and this will be a more acute problem for multi-symbol detectors where such offsets accumulate over a longer observation interval. For example, it has been demonstrated that the Viterbi receiver for CPM signals cannot function if the modulation index offset exceeds 0.01 [34].

There is limited literature on carrier frequency correction procedures for Bluetooth signals, nonetheless, a data aided scheme to solve this problem is described in [95]. The method in [95] determines mismatch in carrier frequency by employing the preamble of a Bluetooth packet to subtract the receiver's estimate of the instantaneous frequency from the time derivative of the phase of the received signal. However, this technique might be undermined if the training signal is compromised by multipath propagation or modulation index offsets. Alternative carrier frequency synchronisation schemes specified for CPM signals in [158, 159, 160] require a fixed modulation index $h = \frac{1}{2}$, which is out of the range permitted in Bluetooth. Similarly, even though modulation index offsets of the magnitude

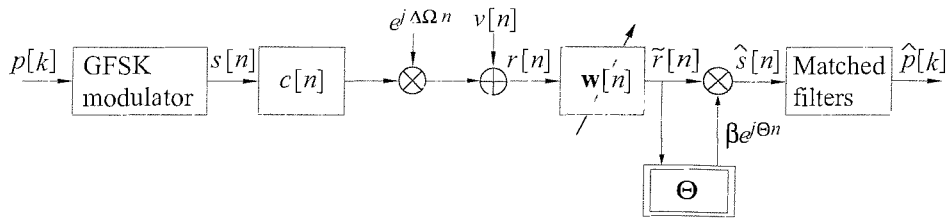

Figure 5.1: Signal flow graph with carrier frequency offset correction by the SG algorithm.

permitted in Bluetooth can cause significant performance loss, especially for multi-symbol receivers, we have not come across any literature on efforts to compensate for a mismatch in h.

Hence, in Sec. 5.1 we present a novel blind algorithm for carrier frequency offset correction based on stochastic gradient (SG) techniques, with a theoretical maximum offset correction capability of half the sampling rate. Alternatively, in Sec. 5.2 we introduce new algorithms for carrier frequency and modulation index offset correction, designed specifically for the lower complexity MFB receiver, which exploits the intermediate filter outputs (IFO) to determine the difference between the transmitter and receiver phase trajectories and thus detect these errors. The algorithms are derived analytically, and assessed via simulation in Sec. 5.3.

5.1 Stochastic Gradient Algorithm for Carrier Frequency Offset Correction

In this section we introduce a stochastic gradient carrier frequency offset correction algorithm that first appeared in our publications [46, 50, 48, 52]. Simply speaking, if we can estimate the gradient of a cost function $\xi_{\Omega,\mathrm{SG}}$ that is concave in Θ, then gradient descent methods entail that Θ is adapted via

$$\Theta[n+1] = \Theta[n] - \mu_\Theta \frac{\partial \xi_{\Omega,\mathrm{SG}}}{\partial \Theta} \quad , \tag{5.1}$$

where μ_Θ is a positive step-size [112, 104], such that under ideal conditions

$$\lim_{n\to\infty} \Theta[n] \to \Theta_{\mathrm{opt}} \quad . \tag{5.2}$$

Stochastic gradient algorithms differ from the purist view in (5.1) because only an instantaneous estimate of the gradient is employed [112, 104]. The benefit of such a solution

is a relatively simple adaptive algorithm[1], and it is for this reason that we shall pursue a stochastic gradient solution. However, the engineering challenge lies in defining a suitable cost function $\xi_{\Omega,\mathrm{SG}}$, whose instantaneous gradient can be estimated by the receiver. This section is focused on formulating such a cost function to track the transmitter carrier frequency.

5.1.1 Detection

From the discussions in Chapter 4, and assuming perfect equalisation, the signal emanating from the equaliser will be

$$\tilde{r}[n] = \alpha s[n] e^{j\Delta\Omega n} + \tilde{v}[n] \quad , \tag{5.3}$$

where

$$\tilde{v}[n] = \mathrm{w}[n] * v[n] \quad ,$$

is the AWGN filtered by the equaliser, and α is a complex gain. Therefore an estimation of the carrier frequency offset can be based on $\tilde{r}[n]$ by denoting

$$\begin{aligned}
\mathcal{E}\{\tilde{r}[n]\tilde{r}^*[n-M]\} &= \mathcal{E}\Big\{(\alpha s[n]e^{j\Delta\Omega n} + \tilde{v}[n])(\alpha^* s^*[n-M]e^{-j\Delta\Omega(n-M)} + \tilde{v}^*[n-M])\Big\} \\
&= |\alpha|^2 \mathcal{E}\{s[n]s^*[n-M]\}\, e^{j\Delta\Omega M} + \alpha\mathcal{E}\Big\{s[n]\tilde{v}^*[n-M]e^{j\Delta\Omega n}\Big\} + \\
&\quad \alpha^*\mathcal{E}\Big\{\tilde{v}[n]s^*[n-M]e^{-j\Delta\Omega(n-M)}\Big\} + \mathcal{E}\{\tilde{v}[n]\tilde{v}^*[n-M]\} \qquad (5.4) \\
&= |\alpha|^2 e^{j\Delta\Omega M} \quad . \qquad (5.5)
\end{aligned}$$

Due to the independence and zero mean of $s[n]$ and $\tilde{v}[n]$, the second and third term in (5.4) will be zero. Since the instantaneous frequency accumulated over M samples of the transmitted signal $s[n]$ will either rotate in a positive or negative direction but on average be zero, we have $\mathcal{E}\{s[n]\, s^*[n-M]\} = 1$. Later on in this chapter it will be elaborated that by selecting a sufficiently large delay constant M, the autocorrelation term of the noise in (5.4) vanishes[2]. Note that if the assumptions made here hold, then detection of the carrier frequency offset is independent of all other receiver functions.

[1] Note that the LMS is an example of a stochastic gradient adaptive algorithm [112, 104].

[2] No ambiguity should arise from denoting a delay constant with M in this chapter, and symbolising the number of symbol levels with the same in Chapter 3.

5.1.2 Cost Function

From the equaliser output $\tilde{r}[n]$, we create a received signal

$$\hat{s}[n] = \tilde{r}[n]\, \beta e^{j\Theta n} \quad , \tag{5.6}$$

i.e. modulating by Θ to match the carrier offset $\Delta\Omega$, and scaling by a gain parameter β, which is ideally selected such that $\beta^{-1} = |\tilde{r}[n]| = |\alpha|$. In order to determine Θ, we formulate the following constant modulus cost function,

$$\xi_{\Omega,\mathrm{SG}} = |\mathcal{E}\{\hat{s}[n]\hat{s}^*[n-M]\} - 1|^2 \quad . \tag{5.7}$$

Inserting (5.5) and (5.6) into (5.7) yields

$$\begin{aligned}
\xi_{\Omega,\mathrm{SG}} &= (\mathcal{E}\{\hat{s}[n]\hat{s}^*[n-M]\} - 1)(\mathcal{E}\{\hat{s}^*[n]\hat{s}[n-M]\} - 1) \\
&= (\mathcal{E}\{\beta\tilde{r}[n]e^{j\Theta n}\beta\tilde{r}^*[n-M]e^{-j\Theta(n-M)}\} - 1)(\mathcal{E}\{\beta\tilde{r}^*[n]e^{-j\Theta n}\beta\tilde{r}[n-M]e^{j\Theta(n-M)}\} - 1) \\
&= (\beta^2\mathcal{E}\{\tilde{r}[n]\tilde{r}^*[n-M]\}\, e^{j\Theta M} - 1)(\beta^2\mathcal{E}\{\tilde{r}^*[n]\tilde{r}[n-M]\}\, e^{-j\Theta M} - 1) \qquad (5.8) \\
&= (|\alpha\beta|^2 e^{j(\Delta\Omega+\Theta)M} - 1)(|\alpha\beta|^2 e^{-j(\Delta\Omega+\Theta)M} - 1) \\
&= 1 + |\alpha\beta|^4 - 2|\alpha\beta|^2 \cos((\Theta + \Delta\Omega)M) \quad , \qquad (5.9)
\end{aligned}$$

with

$$\xi_{\Omega,\mathrm{SG}} = 0 \longleftrightarrow \Theta = \frac{2\pi k}{M} - \Delta\Omega \quad \forall \quad |\alpha\beta| = 1 \quad .$$

The cost function given by (5.9) is plotted in Figs. 5.2 and 5.3, where the illustration in Fig. 5.2 is a 3 dimensional plot that shows the effect of Θ and β on the cost function, while the contour plot in Fig. 5.3 demonstrates the result of keeping the cosine term in (5.9) constant, and varying α and β, in which case the minimum point is achieved if $|\alpha\beta| = 1$.

We are however interested in the solution for $k = 0$ only, for which the cost function provides a unique minimum under the condition

$$-\pi < (\Theta + \Delta\Omega)M < \pi \quad , \tag{5.10}$$

making it possible to employ stochastic gradient tracking techniques. Hence, a trade-off exists for the selection of M between decorrelating the noise in the receiver and not exceeding the bounds in (5.10).

5.1.3 Stochastic Gradient Method

Within the bounds of (5.10), Θ can be iteratively adapted over time based on gradient descent techniques [112] according to

$$\Theta[n+1] = \Theta[n] - \mu_\Theta \frac{\partial \xi_{\Omega,\mathrm{SG}}[n]}{\partial \Theta} \quad , \tag{5.11}$$

with a suitable step size parameter μ_Θ. The gradient of the cost function in (5.7), $\frac{\partial \xi_{\Omega,\mathrm{SG}}}{\partial \Theta}$, can be approximated by an instantaneous estimate, hence dropping the expectations in (5.7). For small changes in Θ and β such that $\Theta[n] \approx \Theta[n-M]$ and $\beta[n] \approx \beta[n-M]$, this stochastic gradient is obtained by differentiating the instantaneous estimate of (5.8) as follows

$$\begin{aligned}
\frac{\partial \hat{\xi}_{\Omega,\mathrm{SG}}[n]}{\partial \Theta} &= \frac{\partial}{\partial \Theta}\{(\beta^2 \tilde{r}[n]\tilde{r}^*[n-M]e^{j\Theta M} - 1)(\beta^2 \tilde{r}^*[n]\tilde{r}[n-M]e^{-j\Theta M} - 1)\} \\
&= jM\beta^2 \tilde{r}[n]\tilde{r}^*[n-M]e^{j\Theta M}(\beta^2 \tilde{r}^*[n]\tilde{r}[n-M]e^{-j\Theta M} - 1) + \\
&\quad (\beta^2 \tilde{r}[n]\tilde{r}^*[n-M]e^{j\Theta M} - 1)(-jM)\beta^2 \tilde{r}^*[n]\tilde{r}[n-M]e^{-j\Theta M} \\
&= -2M\Im\{\beta^2 \tilde{r}[n]\tilde{r}^*[n-M]e^{j\Theta M}(\beta^2 \tilde{r}^*[n]\tilde{r}[n-M]e^{-j\Theta M} - 1)\} \\
&= -2M\Im\{\beta\tilde{r}[n]e^{j\Theta n}\beta\tilde{r}^*[n-M]e^{-j\Theta(n-M)}(\beta\tilde{r}^*[n]e^{-j\Theta n}\beta\tilde{r}[n-M]e^{j\Theta(n-M)} - 1)\} \\
&= -2M\Im\{\hat{s}[n]\hat{s}^*[n-M]\big(\hat{s}[n]\hat{s}^*[n-M] - 1\big)^*\} \quad .
\end{aligned} \tag{5.12}$$

Notice that all parameters on the right side of (5.12) are accessible by the receiver, which can therefore compute a result for (5.12) each sample period without recourse to a training sequence.

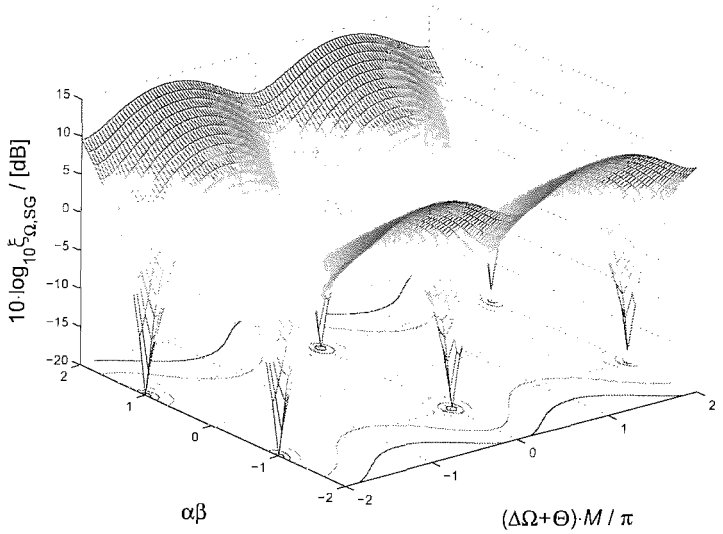

Figure 5.2: Cost function for the SG carrier frequency offset correction algorithm $\xi_{\Omega,\mathrm{SG}}$ in (5.9).

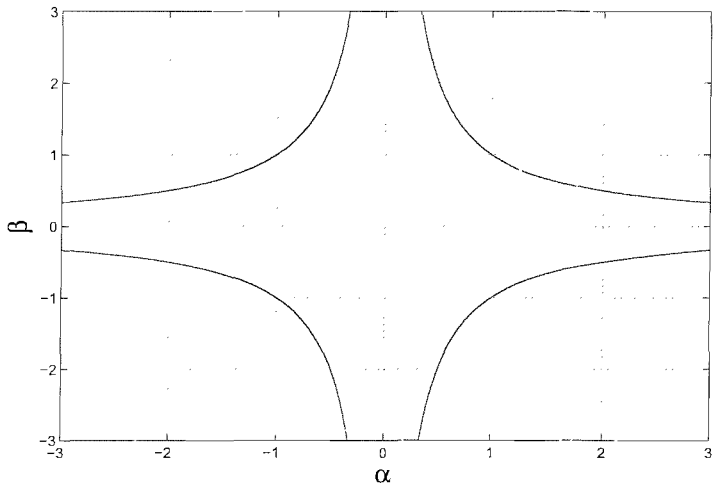

Figure 5.3: Contours of the solution to the cost function in (5.9), showing what the effect of the magnitude $|\alpha\beta|$ on the cost function when the cosine term is constant.

Additionally, the gain parameter β in (5.6) can be estimated by

$$\beta[n+1] = \beta[n] - \mu_\beta \frac{\partial \hat{\xi}_{\Omega,\mathrm{SG}}}{\partial \beta} \quad , \tag{5.13}$$

whereby analogous to the above formulation, the stochastic gradient is derived by assuming $\Theta[n] \approx \Theta[n-M]$ and $\beta[n] \approx \beta[n-M]$, and differentiating the instantaneous estimate of (5.8) as follows

$$\begin{aligned}
\frac{\partial \hat{\xi}_{\Omega,\mathrm{SG}}[n]}{\partial \beta} &= \frac{\partial}{\partial \beta}\{(\beta^2 \tilde{r}[n]\tilde{r}^*[n-M]e^{j\Theta M} - 1)(\beta^2 \tilde{r}^*[n]\tilde{r}[n-M]e^{-j\Theta M} - 1)\} \\
&= 2\beta \tilde{r}[n]\tilde{r}^*[n-M]e^{j\Theta M}(\beta^2 \tilde{r}^*[n]\tilde{r}[n-M]e^{-j\Theta M} - 1) + \\
&\quad (\beta^2 \tilde{r}[n]\tilde{r}^*[n-M]e^{j\Theta M} - 1)2\beta \tilde{r}^*[n]\tilde{r}[n-M]e^{-j\Theta M} \\
&= 4\beta \Re\{\tilde{r}[n]\tilde{r}^*[n-M]e^{j\Theta M}(\beta^2 \tilde{r}^*[n]\tilde{r}[n-M]e^{-j\Theta M} - 1)\} \\
&= \frac{4}{\beta}\Re\{\beta \tilde{r}[n]e^{j\Theta n}\beta \tilde{r}^*[n-M]e^{-j\Theta(n-M)}(\beta \tilde{r}^*[n]e^{-j\Theta n}\beta \tilde{r}[n-M]e^{j\Theta(n-M)} - 1)\} \\
&= \frac{4}{\beta}\Re\{\hat{s}[n]\hat{s}^*[n-M]\big(\hat{s}[n]\hat{s}^*[n-M] - 1\big)^*\} \quad .
\end{aligned} \tag{5.14}$$

The operand of the $\Re\{\cdot\}$ operator in (5.14) is equivalent to that of the $\Im\{\cdot\}$ operator in (5.12), and can be evaluated only once, and the result used in both (5.12) and (5.14). The modified received signal $\hat{s}[n]$ in (5.6) is passed to the MFB receiver instead of $\tilde{r}[n]$. Therefore the Θ block in Fig. 5.1 is mechanised by (5.6), (5.11), and (5.13), and would consume $3N$ MACs each symbol period to compensate for $\Delta\Omega$, and a similar computational cost to adjust for α.

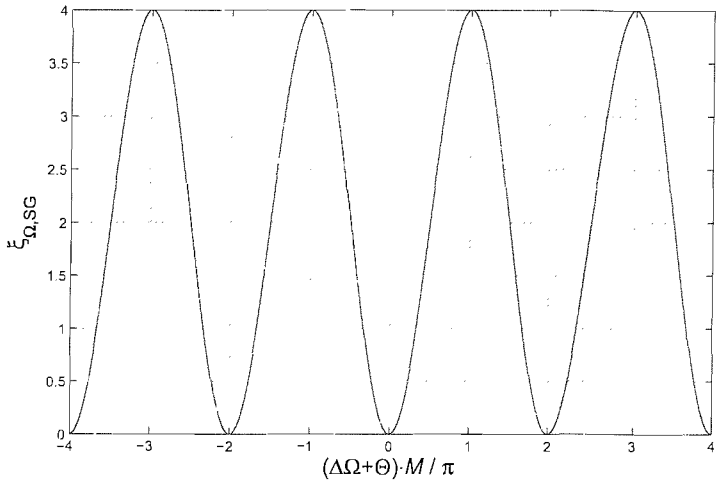

Figure 5.4: Cost function for the SG carrier frequency offset correction algorithm $\xi_{\Omega,\mathrm{SG}}$ in (5.17) .

On the other hand, if $|\tilde{r}[n]| = |\alpha| = 1$ is ensured by the use of CM equalisation earlier on in the signal processing chain, then (5.5) becomes

$$\mathcal{E}\{\tilde{r}[n]\tilde{r}^*[n-M]\} = e^{j\Delta\Omega M} \quad . \tag{5.15}$$

Thus the adaptive gain parameter β in (5.6) is set to 1, thereby simplifying (5.6) to

$$\hat{s}[n] = \tilde{r}[n]\, e^{j\Theta n} \quad , \tag{5.16}$$

and hence, (5.16), (5.15) and (5.7) allow us to modify (5.9) into

$$\begin{aligned} \xi_{\Omega,\mathrm{SG}} &= (e^{j(\Delta\Omega+\Theta)M} - 1)(e^{-j(\Delta\Omega+\Theta)M} - 1) \\ &= 2 - 2\cos((\Theta + \Delta\Omega)M) \quad , \end{aligned} \tag{5.17}$$

with

$$\xi_{\Omega,\mathrm{SG}} = 0 \longleftrightarrow \Theta = \frac{2\pi k}{M} - \Delta\Omega \quad .$$

The cost function in (5.17) is equivalent to that in (5.9) with $|\alpha\beta|$=1, and Fig. 5.4 illustrates that it has a unique minimum in the range specified by (5.10).

5.1.4 General Comments on the SG Carrier Frequency Offset Correction Algorithm

In the derivation of the cost function for the SG carrier frequency offset correction algorithm, ideal conditions were assumed, thus making the algorithm independent of processing blocks upstream. Here we elaborate on the effects of non-ideal conditions on the cost function $\xi_{\Omega,\mathrm{SG}}$.

5.1.4.1 Correlated Noise

In order for the assumption in (5.4) that $\mathcal{E}\{\tilde{v}[n]\tilde{v}^*[n-M]\} = 0$ to hold, we must select M sufficiently large so that $M \geq L_{\mathrm{w}}$ is fulfilled[3]. If this is not the case, then (5.5) must be rewritten as

$$\mathcal{E}\{\tilde{r}[n]\tilde{r}^*[n-M]\} = (e^{j\Delta\Omega M} + xe^{jy}) \quad ,$$

where $\mathcal{E}\{\tilde{v}[n]\tilde{v}^*[n-M]\} = xe^{jy}$ is the non-zero autocorrelation coefficient of the noise for lag M with $x, y \in \Re$ and $|\alpha\beta| = 1$. This necessitates the modification of the cost function in (5.17) to

$$\begin{aligned}
\xi_{\Omega,\mathrm{SG}} &= |\mathcal{E}\{\hat{s}[n]\hat{s}^*[n-M]\} - 1|^2 \\
&= |\mathcal{E}\Big\{\tilde{r}[n]\, e^{j\Theta n}\, \tilde{r}^*[n-M]\, e^{-j\Theta(n-M)}\Big\} - 1|^2 \\
&= |\mathcal{E}\{\tilde{r}[n]\, \tilde{r}^*[n-M]\}\, e^{j\Theta M} - 1|^2 \\
&= |(e^{j\Delta\Omega M} + xe^{jy})e^{j\Theta M} - 1|^2 \\
&= ((e^{j\Delta\Omega M} + xe^{jy})e^{j\Theta M} - 1)((e^{-j\Delta\Omega M} + xe^{-jy})e^{-j\Theta M} - 1) \\
&= (e^{j(\Delta\Omega+\Theta)M} + xe^{j(y+\Theta M)} - 1)(e^{-j(\Delta\Omega+\Theta)M} + xe^{-j(y+\Theta M)} - 1) \\
&= 1 + xe^{-j(\Delta\Omega M - y)} - e^{-j(\Delta\Omega+\Theta)M} + xe^{j(\Delta\Omega M - y)} + x^2 \\
&\quad - xe^{-j(\Theta M + y)} - e^{j(\Delta\Omega+\Theta)M} - xe^{j(\Theta M+y)} + 1 \\
&= 2 - 2\cos((\Delta\Omega + \Theta)M) + \underbrace{2x\cos(\Delta\Omega M - y) - 2x\cos(\Theta M + y) + x^2}_{\text{distortion}}, \qquad (5.18)
\end{aligned}$$

with the third, fourth and fifth term in (5.18) distorting the cost function in (5.17). Fig. 5.5 depicts the revised cost function for a sample case where $\mathcal{E}\{\tilde{v}[n]\tilde{v}^*[n-M]\} = 0$ and $\mathcal{E}\{\tilde{v}[n]\tilde{v}^*[n-M]\} = 0.5e^{j\pi}$. In the latter case the inverse proportionality between $\Delta\Omega$ and the value of Θ after convergence is undermined, and so the estimate for Θ will be biased. This phenomenon is more obvious from the sketch in Fig. 5.6.

5.1.4.2 Non-ideal Equalisation

Assuming a scenario where the SG carrier frequency offset correction algorithm is deployed in series with an equaliser that is adapted by the constant modulus algorithm or one of its derivatives. If equalisation is too slow, before convergence the impulse response of the channel-equaliser composite system will not comprise of a single non-zero element and the detection of the carrier frequency offset may not be as straight forward as in Sec. 5.1.1. As

[3]Consider that the autocorrelation of $\tilde{v}[n]$, $r_{\tilde{v}\tilde{v}}[n] = \mathrm{w}[n] * \mathrm{w}^*[-n] \cdot \sigma_v^2 = 0 \quad \forall \quad |n| \geq L_{\mathrm{w}}$.

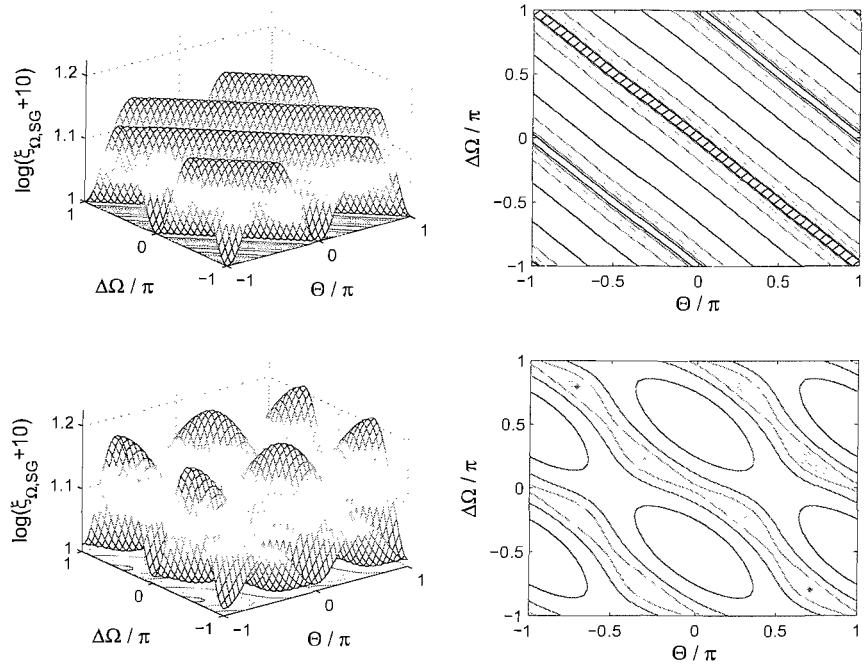

Figure 5.5: Cost function (left) and contour plot (right) for the SG carrier frequency offset correction algorithm $\xi_{\Omega,\mathrm{SG}}$ in (5.17), using $M = 2$, $\mathcal{E}\{\tilde{v}[n]\tilde{v}^*[n-M]\} = 0$ (top) and $\mathcal{E}\{\tilde{v}[n]\tilde{v}^*[n-M]\} = 0.5e^{j\pi}$ (bottom).

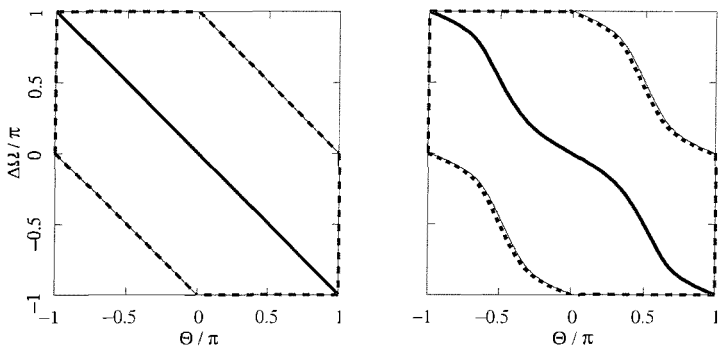

Figure 5.6: Sketch of the contour plot for the SG carrier frequency offset correction algorithm $\xi_{\Omega,\mathrm{SG}}$ in (5.17), using $M = 2$, $\mathcal{E}\{\tilde{v}[n]\tilde{v}^*[n-M]\} = 0$ (left) and $\mathcal{E}\{\tilde{v}[n]\tilde{v}^*[n-M]\} = 0.5e^{j\pi}$ (right), showing the region of convergence enclosed in a bold dashed line, and the minimum in a bold solid line.

an illustration of this phenomenon we consider a simplified case where noise is neglected, and the channel impulse response is $c[n] = \delta[n]$, while the impulse response of the channel-equaliser composite system is stationary and given by

$$c[n] * \mathrm{w}[n] = \delta[n] + xe^{jy}\delta[n-1] \quad ,$$

with a remaining dispersive coefficient characterised by $x, y \in \Re$. Then it follows from (5.3) and Fig. 5.1 that

$$\begin{aligned} \tilde{r}[n] &= s[n]e^{j\Delta\Omega n} * (c[n] * \mathrm{w}[n]) \\ &= s[n]e^{j\Delta\Omega n} + s[n-1]e^{j\Delta\Omega(n-1)}xe^{jy} \quad , \end{aligned}$$

and therefore the detection expression in (5.5) must be amended to

$$\begin{aligned} \mathcal{E}\{\tilde{r}[n]\tilde{r}^*[n-M]\} &= \mathcal{E}\{(s[n]e^{j\Delta\Omega n} + s[n-1]e^{j\Delta\Omega(n-1)}\cdot xe^{jy}) \cdot \\ &\quad (s^*[n-M]e^{-j\Delta\Omega(n-M)} + s^*[n-M-1]e^{-j\Delta\Omega(n-M-1)}\cdot xe^{-jy})\} \\ &= \mathcal{E}\{s[n]s^*[n-M]\}\, e^{j\Delta\Omega M} + x\mathcal{E}\{s[n]s^*[n-M-1]\}\, e^{j(\Delta\Omega M+\Delta\Omega-y)} + \\ &\quad x\mathcal{E}\{s[n-1]s^*[n-M]\}\, e^{j(\Delta\Omega M-\Delta\Omega+y)} + \\ &\quad x^2\mathcal{E}\{s[n-1]s^*[n-M-1]\}\, e^{j\Delta\Omega M} \qquad (5.19) \\ &= e^{j\Delta\Omega M} + xe^{j(\Delta\Omega M+\Delta\Omega-y)} + xe^{j(\Delta\Omega M-\Delta\Omega+y)} + x^2e^{j\Delta\Omega M} \\ &= e^{j\Delta\Omega M} + xe^{j\Delta\Omega M}(e^{j(\Delta\Omega-y)} + e^{-j(\Delta\Omega-y)}) + x^2e^{j\Delta\Omega M} \\ &= e^{j\Delta\Omega M}\underbrace{(1 + 2x\cos(\Delta\Omega - y) + x^2)}_{\text{amplitude term}} \quad , \qquad (5.20) \end{aligned}$$

whereby the autocorrelation terms in (5.19) will evaluate to 1, thus facilitating the simplification in (5.20). Notice that the amplitude term in (5.20) will always be real and positive definite, and would therefore not affect the phase term. This is supportive of results we obtain in practice whereby carrier frequency synchronisation occurs even though the channel-equaliser impulse response after convergence of the equaliser, comprises of more than one non-zero element. However, this is not the case if the equaliser is omitted from the signal processing chain because the channel output will not have a magnitude of 1 as required by the derivations in Sec. 5.1.

5.1.4.3 Size of M

Equation (5.10) sets the limits for the value of M, and results from the shrinking period of the cosine term in (5.9) with increase in M. In Fig. 5.7 $\xi_{\Omega,\mathrm{SG}}$ is plotted for $-\pi \leq (\Delta\Omega+\Theta) \leq \pi$, with $M \in \{2, 8, 16\}$, and it illustrates the reduced frequency range over which a unique extremum exists. It is also important to ensure that $M \leq LN$.

Hence, there are conflicting requirements for the selection of M. It is through simulations in Sec. 5.3 that we shall be able to determine the most important issues to consider for the case of Bluetooth signals.

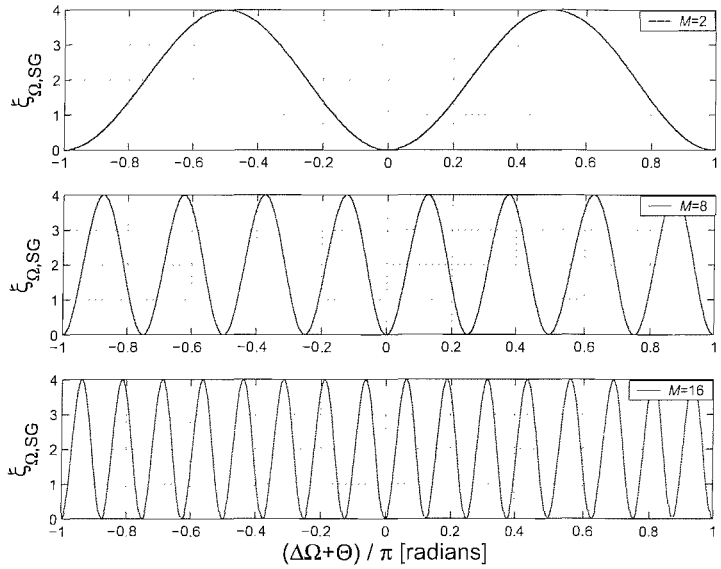

Figure 5.7: Cost function for the SG carrier frequency offset correction algorithm $\xi_{\Omega,\mathrm{SG}}$ in (5.17), using $M \in \{2, 8, 16\}$.

5.2 Intermediate Filter Output Carrier Offset and Modulation Index Offset Correction

In this section we explain a novel idea that we introduced in [53, 47, 52] to correct carrier frequency and modulation index offsets. It exploits the intermediate filter outputs (IFO) of the low-complexity MFB receiver to detect these errors, and compensation is realised by recomputing the coefficients of the relatively small intermediate filter bank $\mathbf{W}^{(1)}$. The low-complexity MFB receiver for GFSK signals is reproduced with slight modifications in Fig. 5.8 to aid the explanation, and it is assumed that the reader is familiar with the workings of the efficient MFB receiver described in Sec. 3.6.

5.2.1 Carrier Frequency

By excluding the noise term in (2.9) and assuming an ideal channel, such that

$$r[n] = s[n]e^{j\Delta\Omega n} \quad ,$$

it is apparent that $\mathcal{E}\{\angle(r[n]\cdot s^*[n])\} \propto \Delta\Omega$, and therefore $\Delta\Omega$ causes a difference in the phase trajectories of the signal computed by the transmitter and the prototype signal assumed by the receiver when computing its filter coefficients. If an initial phase difference of zero

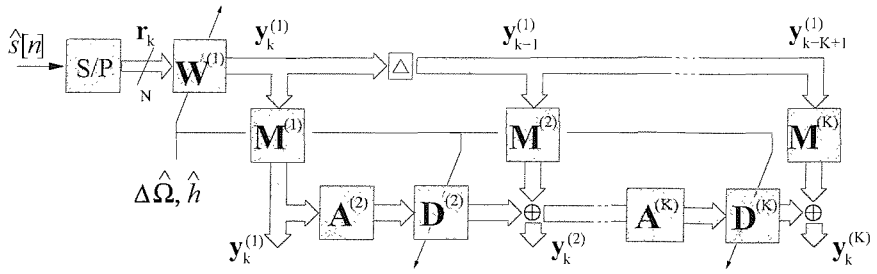

Figure 5.8: Low-complexity implementation of a matched filter bank high-performance GFSK receiver. The received GFSK signal $\hat{s}[n]$ is passed through a serial/parallel converter and a smaller intermediate filter bank $\mathbf{W}^{(1)}$ with a single symbol duration. Processed over K stages, the matched filter bank outputs are contained in $\mathbf{y}_k^{(K)}$.

is assumed, this anomaly amounts to $\pm\Delta\Omega{\cdot}N$ radians across a symbol period. This is illustrated in Fig. 5.9, which depicts the deviation in phase of the received signal relative to that of the matched filter coefficients. In Fig. 5.9 it is apparent that for the correctly matched filter, or row of $\mathbf{W}^{(1)}$, the phase of its tap outputs will grow in the positive or negative direction, from the first to the last column, for a positive or negative carrier frequency offset respectively.

Thus, in the low-complexity MFB receiver, an indication of the sign and magnitude of the carrier frequency offset $\Delta\Omega$ can be obtained via the phase term

$$\xi_{\Omega,\mathrm{IFO}} = \mathcal{E}\left\{\angle\left(y_k^{(K-(K-1)/2)} \cdot \left(y_k^{(K-(K+1)/2)}\right)^*\right)\right\} \propto \Delta\Omega \quad . \tag{5.21}$$

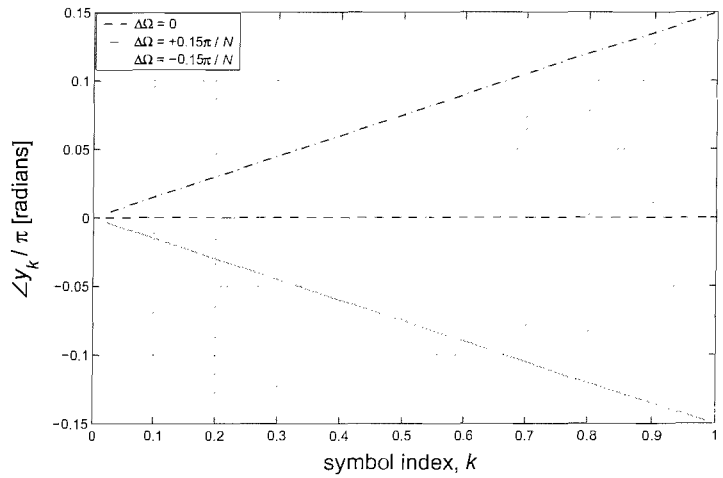

Figure 5.9: Relative increment in phase across a symbol period, between a received signal and the prototype signal assumed by the receiver, when carrier frequency offsets exist between transmitter and receiver.

Note that in (5.21), the quantities $y_k^{(a)}$ are the intermediate filter outputs after they have been appropriately rotated and accumulated by matrices $\mathbf{D}^{(a)}$, $\mathbf{A}^{(a)}$, and $\mathbf{M}^{(a)}$ to reflect the phase gained over the preceding $(a-1)$ symbol stages, in other words $y_k^{(a)}$ is the element of $\mathbf{y}_k^{(a)}$ in Fig. 5.8 with the largest magnitude. Hence, $\xi_{\Omega,\mathrm{IFO}}$ is a measure of the phase difference between the transmitted signal, and that assumed by the receiver to compute its filter coefficients, during the $(k-\frac{K-1}{2})$th symbol period. It is important to realise that during the kth symbol period, it is the symbol at the center of the current observation interval, or $p[k-\frac{K-1}{2}]$, that is estimated most accurately, and so fewer frequency tracking errors will be made if the relative phase increment of the received signal, and that of the receiver prototype signal are compared during this period.

The sketch in Fig. 5.10, in which $K=5$, is meant to support the above explanation. It portrays the phase trajectory of the outputs of filters matched to an arbitrary 5-symbol sequence. It is important to note that for this argument to hold we must consider only the filter that matches the received signal, because in that case, the phase gain in the received sequence due to the baseband signal is cancelled out by the matched filter coefficients, leaving only phase gain due to parameter offsets. In this case independent of k (5.21) can

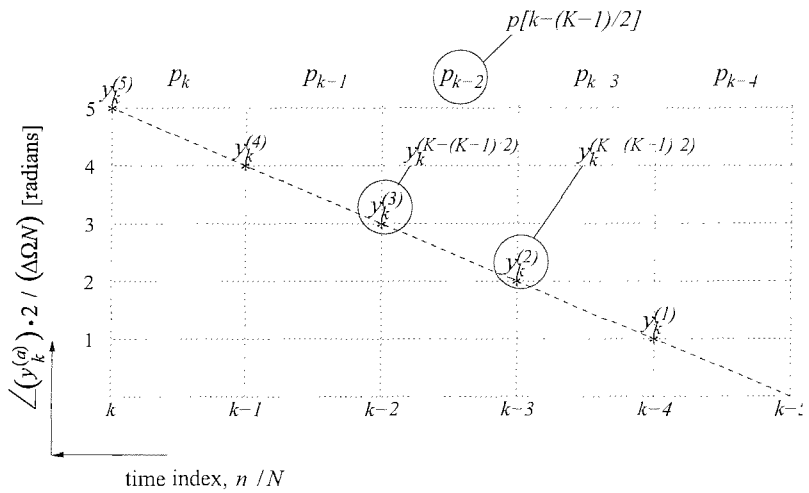

Figure 5.10: Sketch of a phase tree of the largest matched filter output $y_k^{(a)}$, for $a \in \{1,2,3,4,5\}$ and $K=5$, when a carrier frequency offset $\Delta\Omega$ exists.

be rewritten as

$$\begin{aligned}\xi_{\Omega,\mathrm{IFO}} &= \mathcal{E}\left\{\angle\left(\left(\sum_{n=(k-K)N+1}^{(k-(K-1)/2)N} e^{j(\Delta\Omega-\Delta\hat{\Omega})n}\right)\left(\sum_{n=(k-K)N+1}^{(k-(K+1)/2)N} e^{j(\Delta\Omega-\Delta\hat{\Omega})n}\right)^*\right)\right\} \\ &= \left\{\left((kN-KN+1)+\left[kN-\left(\frac{K-1}{2}\right)N\right]\right)-\right. \\ &\quad \left.\left((kN-KN+1)+\left[kN-\left(\frac{K+1}{2}\right)N\right]\right)\right\}\frac{(\Delta\Omega-\Delta\hat{\Omega})}{2} \qquad (5.22) \\ &= \frac{N}{2}(\Delta\Omega-\Delta\hat{\Omega}) \quad , \qquad (5.23)\end{aligned}$$

where $\Delta\hat{\Omega}$ is the receiver's estimate of the transmitter's carrier frequency offset. The development in (5.23) is possible because [55]

$$\angle\left\{\sum_{n=\alpha}^{\beta} e^{j\theta n}\right\} = \frac{1}{2}(\alpha+\beta)\theta \quad ,$$

as depicted in Fig. 5.11.

From the discussions above, and particularly from (5.23), it can be concluded that if $\Delta\Omega > \Delta\hat{\Omega}$ then $\xi_{\Omega,\mathrm{IFO}} > 0$, and vice-versa if $\Delta\Omega < \Delta\hat{\Omega}$. Hence, $\Delta\hat{\Omega}$ can be adjusted according to

$$\Delta\hat{\Omega}[k+1] = \Delta\hat{\Omega}[k] + \mu_{\Omega}\cdot\hat{\xi}_{\Omega,\mathrm{IFO}}[k] \quad ,$$

where $\hat{\xi}_{\Omega,\mathrm{IFO}}[k]$ is an instantaneous inference of the term in (5.21) based on a single symbol period, or simply

$$\hat{\xi}_{\Omega,\mathrm{IFO}}[k] = \angle\left\{y_k^{(K-(K-1)/2)}\cdot\left(y_k^{(K-(K+1)/2)}\right)^*\right\} \quad . \qquad (5.24)$$

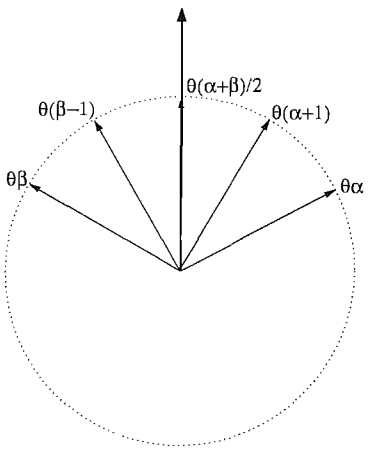

Figure 5.11: Illustration to show the resultant angle (in bold) of the sum of complex exponential terms $e^{j\theta n}$ with $n \in \{\alpha, \alpha+1, \ldots, \beta-1, \beta\}$.

Note that in (5.24), the element $y_k^{(a)}$ is based on the estimated symbol sequence rather than the true quantities assumed in (5.21). Since all terms on the right of (5.24) are available, per iteration, from the proposed low-cost MFB, the only additional complexity arises from the $2^L N$ MACs necessary to modify $\mathbf{W}^{(1)}$ and consequently $\mathbf{D}^{(a)}$.

5.2.2 Modulation Index

It follows from the development in Sec. 2.2, but mainly from (2.3) and (2.5), that $\angle\{s[n]\} \propto h \cdot p[k]$, and hence the phase tree for the transmitted signal $s[n]$, shown for the first symbol period in Fig. 5.12, would fan further out for a larger modulation index. Consequently, if the receiver adopts a modulation index $\hat{h}$, and $h > \hat{h}$, then phase trajectories of the transmitter will be positive with respect to those assumed by the receiver when $p[k] = 1$, and negative with respect to the phase trajectories assumed by the receiver when $p[k] = -1$. Accordingly, the deviation in phase increment between the transmit signal and the corresponding receiver specimen signal amounts to approximately $p[k](h - \hat{h})\pi$ across a symbol period. This discrepancy can be observed from the angle of the output of the correctly matched intermediate filter after it has been appropriately rotated and accumulated to reflect the phase gain over preceding symbol stages. This is exemplarily shown in Fig. 5.13 for a single symbol, whereby the dashed and solid lines imply trajectories due to a modulating pulse of +1 and -1 respectively. It is clear from Fig. 5.13 that a negative modulation index offset reflects the phase tree about the zero axis.

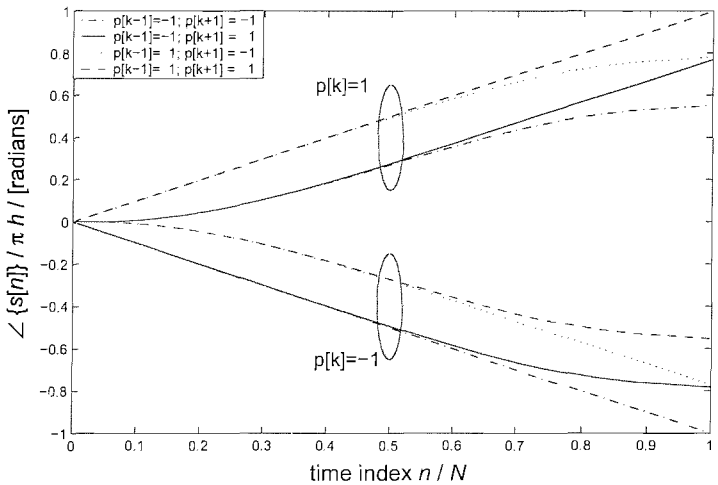

Figure 5.12: Legitimate phase increments in $s[n]$ during a single symbol period with modulating symbol $p[k] = 1$ and $p[k] = -1$, using $K_{BT} = 0.5$ ($L = 3$).

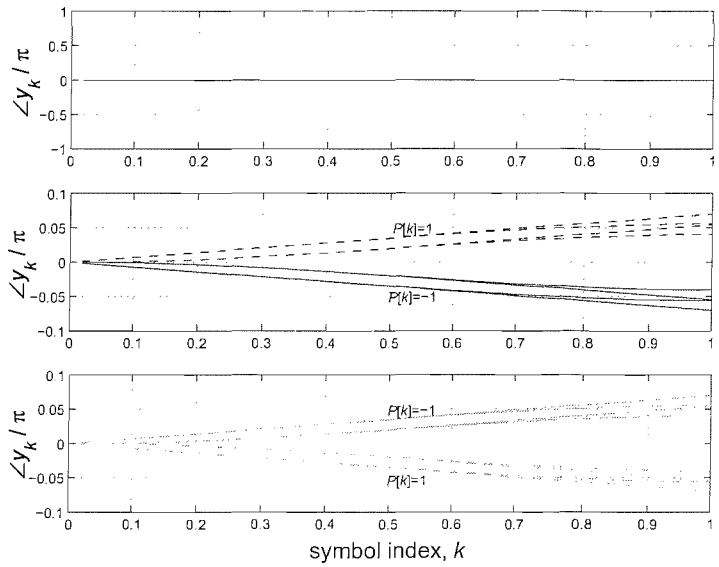

Figure 5.13: Relative increment in phase across a symbol period, between a received signal and the corresponding matched filter coefficients, when modulation index offsets of $\Delta h = 0$ (top), $\Delta h = 0.07$ (middle), and $\Delta h = -0.07$ (bottom) exist between transmitter and receiver.

Hence, in the low-cost MFB receiver, we employ the phase term

$$\xi_{h,\mathrm{IFO}} = \mathcal{E}\left\{\angle\left(y_k^{(K-(K-1)/2)} \cdot \left(y_k^{(K-(K+1)/2)}\right)^*\right) \cdot p\left[k - \frac{K-1}{2}\right]\right\} \propto h - \hat{h} \quad , \qquad (5.25)$$

to determine the amount by which the transmitter modulation index exceeds that of the receiver. Analogous to Sec. 5.2.1, in (5.25) the quantity $y_k^{(a)}$ refers to the maximum element of $\mathbf{y}_k^{(a)}$ in Fig. 3.9, associated with the correct symbol sequence, and leading to the detection of the symbol at the center of the observation interval, $p[k - \frac{K-1}{2}]$. The complex conjugate term in (5.25) ensures that the phase is measured relative to zero, while as implied in Fig. 5.13, $p[k - \frac{K-1}{2}]$ compensates for the sign change imposed by the modulating symbol during the interval over which signal phase is assessed. This is more obvious for the simple case where an all 1 symbol steam is transmitted, and if we assume $K_{BT} = \infty$ so that no ISI exists. Therefore from (2.2) we have

$$|g[n]| = \frac{1}{2N} \quad ,$$

leading to the evaluation of (2.3) as

$$\begin{aligned} |\omega[n]| &= 2\pi h \cdot |g[n]| \\ &= \frac{\pi h}{N} \quad , \end{aligned}$$

so that (5.25) can be derived as follows

$$\begin{aligned}
\xi_{h,\mathrm{IFO}} &\approx \mathcal{E}\left\{\angle\left(\left(\sum_{\kappa=k-K+1}^{k-(K-1)/2}\sum_{n=(\kappa-1)N+1}^{\kappa N} e^{jp[\kappa]\pi(h-\hat{h})n/N}\right)\cdot\right.\right. \\
&\quad \left.\left.\left(\sum_{\kappa=k-K+1}^{k-(K+1)/2}\sum_{n=(\kappa-1)N+1}^{\kappa N} e^{-jp[\kappa]\pi(h-\hat{h})n/N}\right)\right) p\left[k-\frac{(K-1)}{2}\right]\right\} \\
&\approx \mathcal{E}\left\{\angle\left(\left(\sum_{n=(k-K)N+1}^{(k-(K-1)/2)N} e^{j\pi(h-\hat{h})n/N}\right)\cdot\left(\sum_{n=(k-K)N+1}^{(k-(K+1)/2)N} e^{-j\pi(h-\hat{h})n/N}\right)\right)\right\} \\
&\approx \left\{\left((kN-KN+1)+\left[kN-\left(\frac{K-1}{2}\right)N\right]\right)-\right. \\
&\quad \left.\left((kN-KN+1)+\left[kN-\left(\frac{K+1}{2}\right)N\right]\right)\right\}\frac{\pi(h-\hat{h})}{2N}\cdot \\
&\approx \frac{\pi}{2}(h-\hat{h}) \quad . \qquad (5.26)
\end{aligned}$$

The proportionality of $\xi_{\Omega,\mathrm{IFO}}$ to the modulation index offset is confirmed for a random bit stream by the simulation results depicted in Fig. 5.14

From the above discussion, and mainly from (5.26), it follows that if $h > \hat{h}$ then $\xi_{h,\mathrm{IFO}} > 0$. and the converse is true when $h < \hat{h}$. Therefore to adapt the receiver's estimate of the modulation index $\hat{h}$, we employ an iterative technique

$$\hat{h}[k+1] = \hat{h}[k] + \mu_h \cdot \hat{\xi}_{h,\mathrm{IFO}}[k] \quad , \qquad (5.27)$$

where $\hat{\xi}_{h,\mathrm{IFO}}[k]$ is an instantaneous value of the term in (5.25) based on a single symbol period, and evaluated as

$$\hat{\xi}_{h,\mathrm{IFO}}[k] = \angle\left\{y_k^{(k-(K-1)/2}\cdot\left(y_k^{(k-(K+1)/2)}\right)^*\right\}\cdot\hat{p}[k] \qquad (5.28)$$

Bear in mind that the element $y_k^{(a)}$ in (5.28) is based on the estimated symbol sequence and the detected symbol $\hat{p}[k]$, rather than the true quantities assumed in (5.25), and that ideally $\hat{p}[k] = p[k-\frac{K-1}{2}]$.

The adoption of $\hat{h}[k+1]$ following (5.27) requires few extra computations because the coefficients in $\mathbf{W}^{(1)}$ and subsequently $\mathbf{D}^{(a)}$ can be recalculated at the same time as the carrier frequency offset.

5.2.3 General Comments on the IFO Algorithms

In practice the tracking functions $\xi_{\Omega,\mathrm{IFO}}$ and $\xi_{h,\mathrm{IFO}}$, will both depend on $\Delta\Omega$ and Δh. This is despite the fact that while determining $\xi_{\Omega,\mathrm{IFO}}$ in (5.23) only a carrier frequency offset

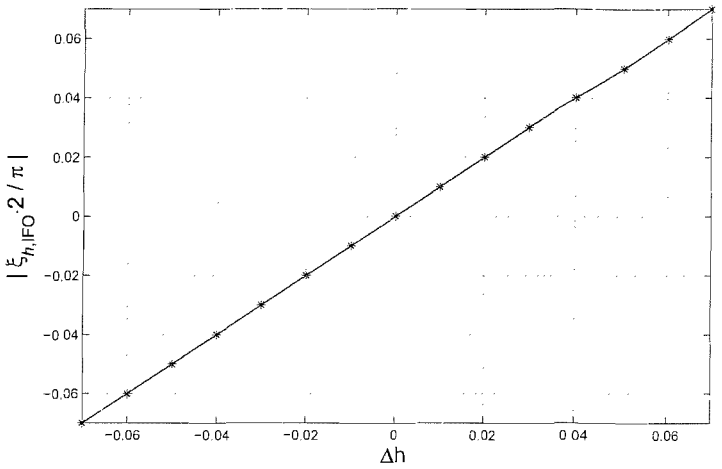

Figure 5.14: Relationship between $\xi_{h,\mathrm{IFO}}$ and the modulation index offset $\Delta h = h - \hat{h}$.

was considered, and to formulate $\xi_{h,\mathrm{IFO}}$ in (5.26) only a modulation index was catered for. Unfortunately, if both parameters are unsynchronised, then the situation is not so straightforward.

To illustrate, we determine from practical measurements and from the analysis in (5.23) and (5.26) that the actual cost computed by the operations (5.24) and (5.28) in the synchronisation blocks, if both parameters were unsynchronised can be written as

$$\hat{\xi}_{\Omega,\mathrm{IFO}} \approx \underbrace{\frac{\pi}{2}(h-\hat{h})\cdot\hat{p}[k]}_{\text{distortion}} + \frac{N}{2}(\Delta\Omega - \Delta\hat{\Omega}) \tag{5.29}$$

and

$$\hat{\xi}_{h,\mathrm{IFO}} \approx \frac{\pi}{2}(h-\hat{h}) + \underbrace{\frac{N}{2}(\Delta\Omega - \Delta\hat{\Omega})\cdot\hat{p}[k]}_{\text{distortion}} \tag{5.30}$$

respectively, whereby the terms due to $\Delta\Omega - \Delta\hat{\Omega}$ and $h - \hat{h}$ are easily distinguishable, and enable us to realise that:

- Irrespective of the magnitude of the carrier frequency and modulation index offset, the average value of the distortion terms in (5.29) and (5.30) will be zero as long as the symbol stream is random. However, for a transceiver pair abiding by the Bluetooth specifications, the distortion term due to the carrier frequency offset has a greater maximum magnitude than that caused by the modulation index offset, and these amount to 0.075π and $0.07\pi/2$ respectively. Carrier frequency errors also tend to accumulate faster over time because they are independent of $p[k]$. Hence, accuracy of

the modulation index offset compensation is relatively more limited by the presence of a carrier frequency offsets than vice versa. A practical way to deal with this problem that worked well for our simulations at low E_b/N_0, which are sampled in Sec. 5.3, is to ensure $\mu_\Omega \gg \mu_h$.

- A reasonably good estimate of the received symbol $\hat{p}[k]$, in (5.28), is required to ensure synchronisation. Errors in determining $\hat{p}[k]$ will be fed back into the tracking process. Where large carrier frequency and modulation index offsets exist between the transmitter and receiver, a smaller observation interval is more reliable. It is recommended that if such errors are expected, the low-cost MFB should be initialised with a small K, and synchronisation performed prior to increasing the observation interval for even better BER.

5.3 Simulation Results and Discussion

A simulation based appraisal of the carrier frequency and modulation index offset correction algorithms discussed in this chapter is carried out in the following. To ease the presentation, the stochastic gradient based carrier frequency offset correction algorithm is assessed in Sec. 5.3.2, while the intermediate filter output based carrier and modulation index offset correction algorithms are evaluated together in Sec. 5.3.3, but first the default settings for our simulation model are stipulated in Sec. 5.3.1.

5.3.1 Default Parameters

Similar to Sec. 4.8, the signal development in this section was as specified in Sec. 2.2, with parameters $K_{BT} = 0.5$ and $h = 0.35$ in order to typify a Bluetooth system [17], and $N = 2$. A Saleh-Valenzuela channel impulse response with an RMS of approximately 300 ns and sample rate of 2 MHz was used to model a multipath propagation, while the maximum carrier frequency and modulation index offsets permitted in Bluetooth networks, which are 75 kHz (or a normalised angular frequency of $\Delta\Omega = \frac{2\pi \cdot 75}{N \cdot 1000}$) and $\Delta h = 0.07$ respectively, were used in the experiments. This enables us to simulate the worst case scenario for a transceiver pair adhering to the Bluetooth standard.

Power efficiency was evaluated as the minimum E_b/N_0 necessary to reach the maximum acceptable bit error ratio specified for Bluetooth [17], which is 10^{-3}, and all algorithms

were given ample time to converge before computing BER. Unless specified otherwise, β, M, $\Delta\hat{\Omega}$, and $\hat{h}$ where initialised to 1, 1, 0, and 0.35 respectively, while the learning curves displayed in this section are an ensemble of a simulation result.

5.3.2 SG Carrier Frequency Offset Correction Algorithm

Firstly, in Fig. 5.15 we present a demonstration of the stochastic gradient carrier frequency offset correction algorithm. This illustration depicts ideal convergence of the gain parameter β, and the frequency compensation factor Θ, when simultaneously driven by the tracking procedures derived in Sec. 5.1. However, in practice the assumption that $\Theta[n] \approx \Theta[n-M]$ and $\beta[n] \approx \beta[n-M]$, that was made while differentiating the cost function in Sec. 5.1.3, was found to be very important, and a conflicting requirement in our desire for speedy convergence. So in order to cater for this we utilise block processing, whereby each iteration a subsequent block of $M+1$ samples are considered. In other words, the same modulating phasor $\beta e^{j\Theta}$, from (5.6), is employed to derive the sequence $\hat{s}[n], \ldots, \hat{s}[n-M]$, before reevaluating Θ and β, and moving on to the next block of samples. This alteration enabled the use of bigger step sizes without undermining convergence.

Further evidence of the ability of the SG algorithm for carrier frequency offset compensation is provided in Fig. 5.16, which demonstrates that convergence is possible even in the presence of the largest modulation index offset permitted in Bluetooth systems. This is a

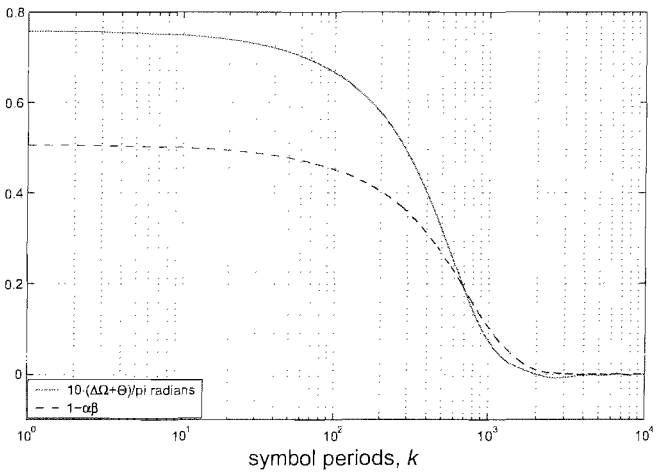

Figure 5.15: Learning curves for the SG carrier frequency offset correction algorithm, using $N = 2$, $K_{BT} = 0.5$, $h = 0.35$, $\Delta\Omega = 0.075\pi$, $\mu_\Theta = 0.005$, $M = 1$, $\alpha = 0.5$, and $\mu_\beta = 0.005$.

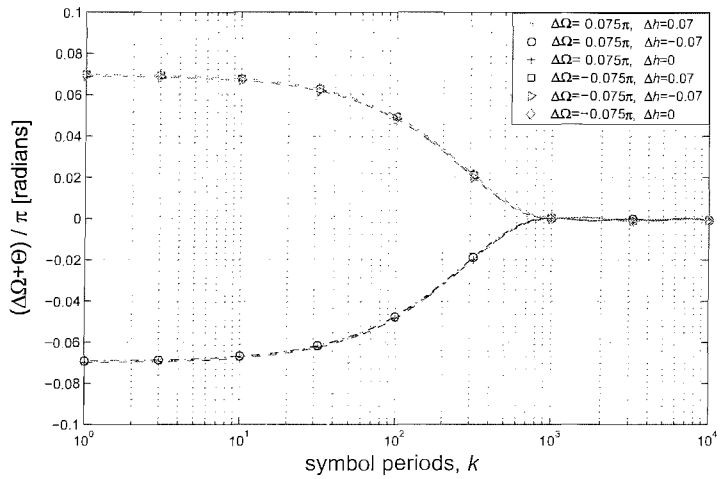

Figure 5.16: Learning curves for the SG carrier frequency offset correction algorithm in presence of modulation index offsets, using $N = 2$, $K_{BT} = 0.5$, $h = 0.35$, $M = 1$, and $\mu_\Theta = 0.005$.

desirable property, because errors in modulation index will not have been corrected prior to frequency synchronisation.

Another important aspect to consider when selecting a carrier frequency offset compensation algorithm is that its range of operation is sufficiently large. In Bluetooth networks we expect frequency offsets of up to 75 kHz, and in Sec. 2.2 it was ascertained that this amounted to a normalised angular frequency of $\Delta\Omega = \frac{2\pi 75}{N \cdot 1000}$ radians. Therefore, from (5.10), it can be concluded that

$$\left| \frac{2\pi 75 \cdot M}{N \cdot 1000} \right| < \pi \quad ,$$

is a necessary condition for carrier frequency synchronisation. Hence, the largest acceptable value for M is

$$M \leq \left\lfloor \frac{N \cdot 1000}{150} \right\rfloor \quad ,$$

which evaluates to 13 if $N = 2$. This assertion is confirmed by the learning curves in Fig. 5.17, where only the simulation in which $M > 13$, fails to conform.

The potential of the SG carrier frequency offset correction algorithm to restore ideal BER in AWGN appears high, and this is underpinned by simulations in Fig. 5.18, in which a Bluetooth MFB receiver is employed with observation intervals of $K = 3$ and $K = 9$. When $K = 3$, frequency synchronisation saves 11 dB that would otherwise have been lost. However, greater benefit is derived when $K = 9$, because in this case detection would not have been possible without frequency correction, but with it, only about 10 dB E_b/N_0 is

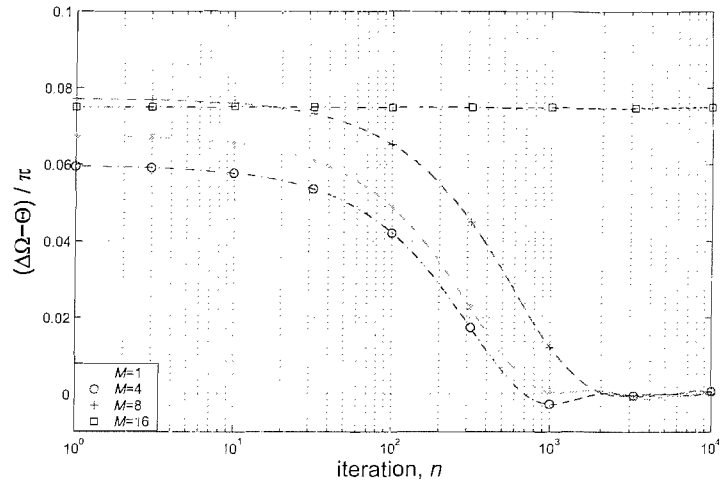

Figure 5.17: Learning curves for SG carrier frequency offset correction, with different values for M, using $N = 2$, $K_{BT} = 0.5$, $h = 0.35$, $\Delta\Omega = 0.075\pi$, and $\mu_\Theta = 0.005$.

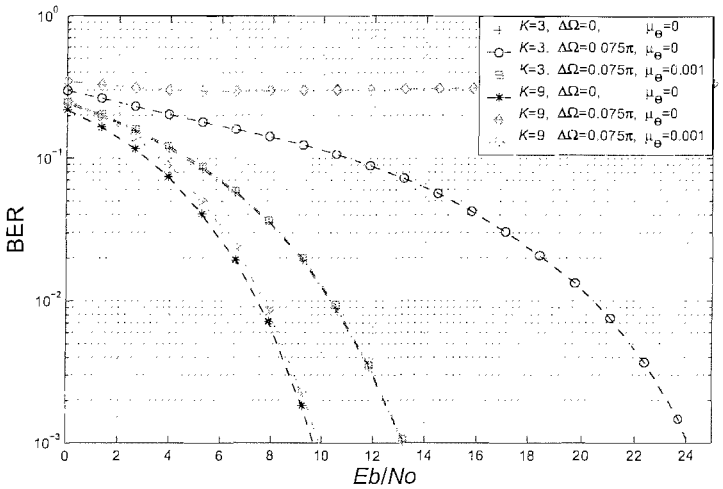

Figure 5.18: BER performance in with a carrier frequency offset and correction by the SG tracking algorithm, using $N = 2$, $K_{BT} = 0.5$, $h = 0.35$, and $M = 1$.

required to attain BER=10^{-3}, and this represents only a small degradation compared to the ideal case.

Synchronised transmitter and receiver carrier frequency is more critical for long observation intervals because carrier frequency offsets accumulate across a longer period and cause more degradation. Thus a trade-off exists between selecting a large observation interval, in which case frequency errors could cripple the system, but a better BER is attainable if synchronisation is assured, or selecting a small K, with more immunity to carrier frequency offsets, but modest optimum BER performance. Use of the SG algorithm for frequency

correction provides confidence, and alleviates this dilemma.

The results in Fig. 5.19 give an indication of what kind of performance would be expected in a moderately dispersive channel. For this experiment a relative noise level of 15 dB E_b/N_0 was applied because this is typically the power efficiency at which we would expect to be above minimum Bluetooth performance requirements with the MFB receiver when $K = 3$. A channel with $\sigma_\tau = 300$ ns was selected for reasons already elaborated. Fig. 5.19 demonstrates that under these conditions equalisation is essential for synchronisation to occur. This is consistent with the requirement in Sec. 5.1 of $|\tilde{r}[n]| = 1$ for frequency synchronisation to occur.

A more comprehensive indication of the improvement facilitated by deploying the SG carrier frequency synchronisation algorithm in series with a CM equaliser is presented in Fig. 5.20. For this simulation an observation interval of $K = 3$ is utilised, a channel with $\sigma_\tau = 300$ was applied, and the worst case carrier frequency and modulation index offsets between a pair of legitimate Bluetooth transceivers was set. The worst BER occurs when no compensation whatsoever is applied. After equalisation however, but prior to any parameter synchronisation, roughly 21 dB E_b/N_0 is required for a BER of 10^{-3}, while carrier frequency correction ensures further gain of 11 dB E_b/N_0. In this case, if the IFO modulation index correction algorithm is deployed, the improvement amounts to a fraction of a dB. However, we shall see in Fig. 5.24 that the potential gain from correcting the modulation index offset will be greater for larger K.

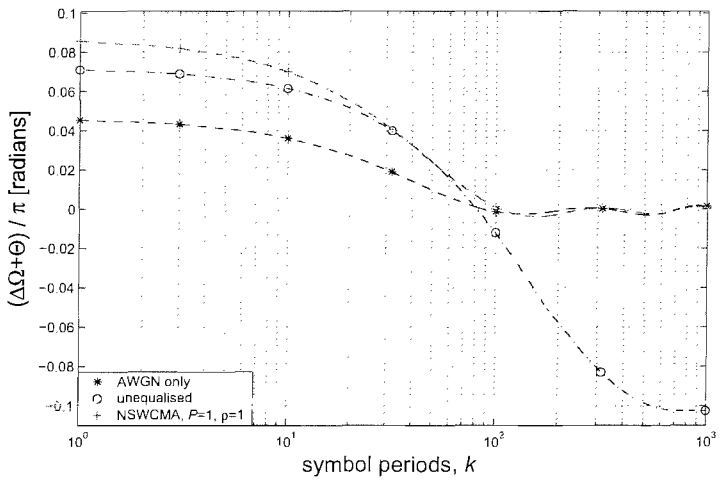

Figure 5.19: Learning curves for SG carrier frequency offset correction in dispersive channel conditions, using $K = 3$, $N = 2$, $K_{BT} = 0.5$, $h = 0.35$, $\Delta\Omega = 0.075\pi$, $\mu_\Theta = 0.05$, $E_b/N_0 = 15$ dB, and σ_τ=300 ns.

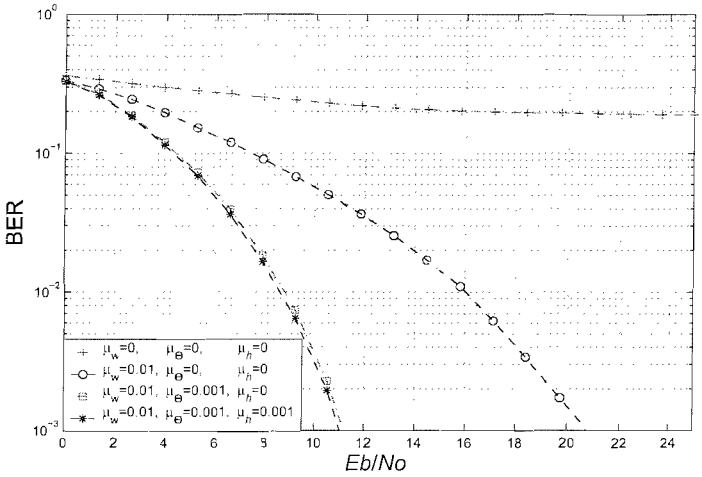

Figure 5.20: BER performance in a dispersive channel, with a carrier frequency and modulation index offsets, and equalisation by the NSWCMA, and carrier frequency and modulation index synchronisation with SG and IFO tracking algorithms respectively, using $K = 3$, $N = 2$, $K_{BT} = 0.5$, $h = 0.35$, initial $\Delta h = 0.07$, $\Delta\Omega = 0.075\pi$, $M = 1$, $L_w = 64$, $P = 1$, $\rho = 1$, and $\sigma_\tau = 300$ ns.

5.3.3 IFO Modulation Index and Carrier Frequency Offset Correction Algorithms

The comments in Sec. 5.2.3 have established a clear relationship between the ability of the IFO algorithms to synchronise either the carrier frequency, or the modulation index, when the other is unsynchronised. This is important because Bluetooth systems will potentially have offsets in both parameters. For this reason, in Fig. 5.21 we test that the maximum expected mismatch in carrier frequency can be corrected when the largest permitted modulation index offset exists between transmitter and receiver. The simulation results in Fig. 5.21 confirm that IFO carrier frequency synchronisation is possible even when $|h - \hat{h}| \leq 0.07$.

Similarly, in Fig. 5.22 we test the proficiency of IFO modulation index compensation while the maximum permitted carrier frequency offset prevails. In this case ill-convergence occurs because of the contribution due to the carrier frequency offset. This implies that we must correct the mismatch in carrier frequency first, before we can expect synchronisation of the modulation index to occur. This is achievable if both the correction of $\Delta\Omega$ and Δh is performed simultaneously, also, through experimentation, it was determined that at very low E_b/N_0, setting $\mu_\Omega \gg \mu h$ benefits convergence.

The performance of the IFO carrier frequency and modulation index synchronisation

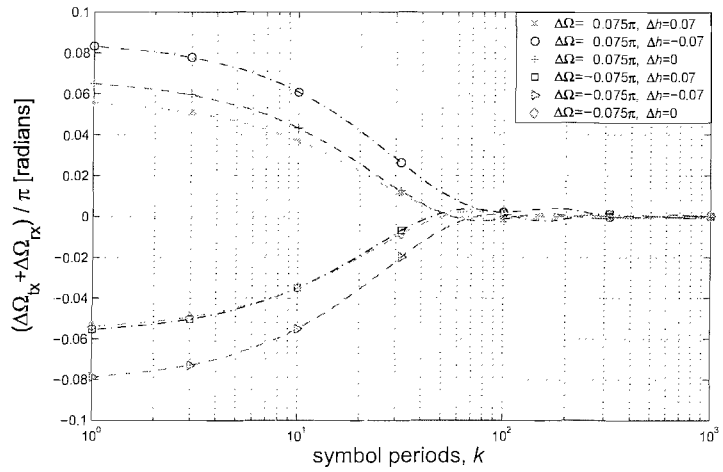

Figure 5.21: Learning curves for the IFO carrier frequency offset correction algorithm in presence of modulation index offsets, using $K = 3$, $N = 2$, $K_{BT} = 0.5$, $h = 0.35$, and $\mu_\Omega = 0.05$.

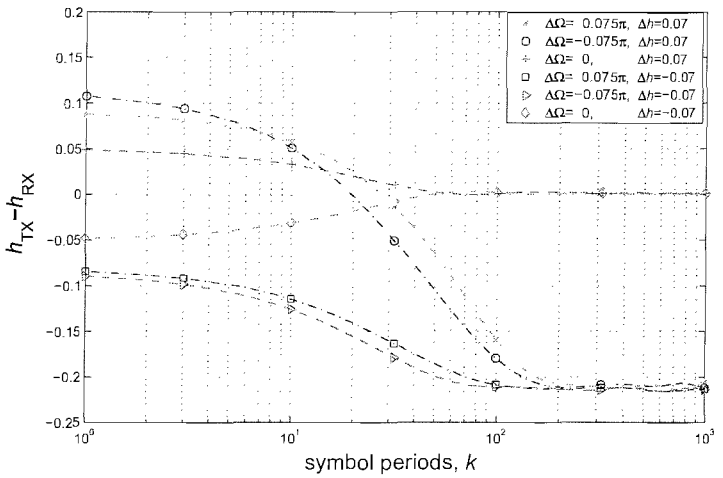

Figure 5.22: Learning curves for the IFO modulation index offset correction algorithm in presence of carrier frequency offsets, using $K = 3$, $N = 2$, $K_{BT} = 0.5$, $h = 0.35$, and $\mu_h = 0.05$.

algorithms in AWGN is exemplified by the BER plots in Figs. 5.23 and 5.24 respectively. Here the algorithms are engaged to synchronise the maximum Bluetooth carrier frequency and modulation index offsets respectively. In Figs. 5.23 and 5.24 after synchronisation the BER curves are indistinguishable from the ideal performance in an AWGN channel, except at very low E_b/N_0, where errors in determining $\hat{p}[k]$ are fed back into the parameter tracking procedures.

Hence, the power efficiency gained by deploying the IFO carrier frequency synchronisation procedure in AWGN is slightly better than that achieved with the SG algorithm.

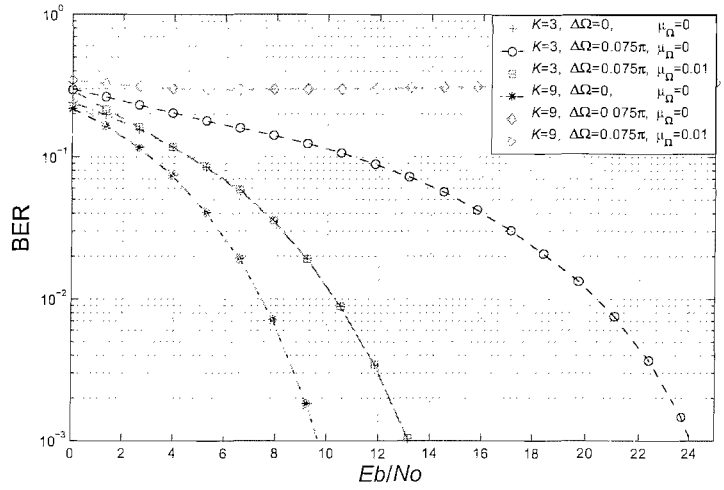

Figure 5.23: BER performance in with a carrier frequency offset and correction by the IFO tracking algorithm, using $N = 2$, $K_{BT} = 0.5$, and $h = 0.35$.

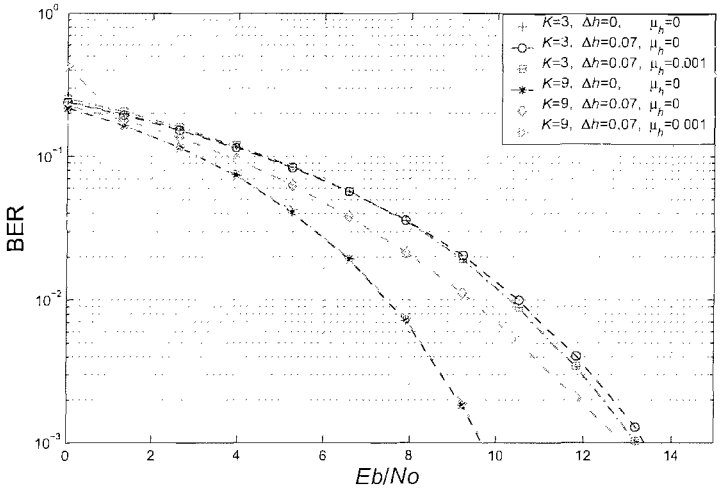

Figure 5.24: BER performance in with a modulation index offset and correction by the IFO tracking algorithm, using $N = 2$, $K_{BT} = 0.5$, and $h = 0.35$.

While a further 0.5 and 3.5 dB can be saved if IFO modulation index correction is also applied, for $K = 3$ and $K = 9$ respectively.

The BER improvement due to the IFO carrier frequency and modulation index offset correction in a multipath propagation environment is portrayed in Fig. 5.25. This result shows total system collapse when $K = 3$ in a dispersive channel, with the frequency and modulation index offset set to the maximum possible values for a Bluetooth system, and no compensation for any of these anomalies. Under the stipulated conditions, the inclusion of a CM equaliser improves the performance such that a BER of 10^{-3} is attained at ap-

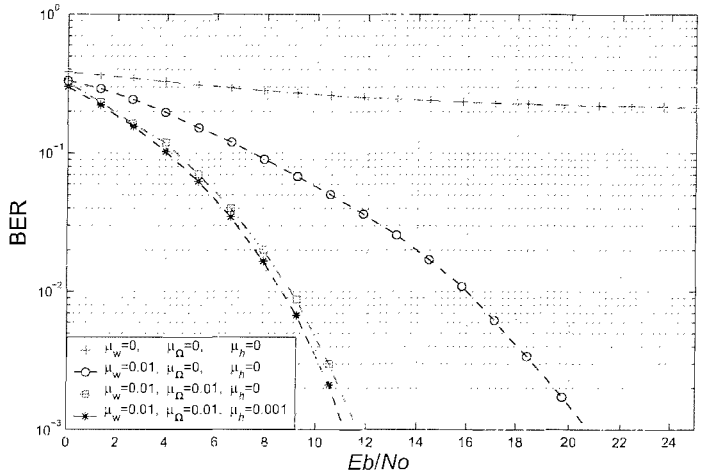

Figure 5.25: BER performance in a dispersive channel, with a carrier frequency and modulation index offset, and equalisation by the NSWCMA, and parameter synchronisation with the IFO tracking algorithms, using $K = 3$, $N = 2$, $K_{BT} = 0.5$, $h = 0.35$, $\Delta h = 0.07$, initial $(\Delta\Omega - \Delta\hat{\Omega}) = 0.075\pi$, $L_w = 64$, $P = 1$, $\rho = 1$, and $\sigma_\tau = 300$ ns.

proximately 21 dB E_b/N_0, and a further 9 dB is saved when the carrier frequency offset is corrected using the IFO algorithm. Since in this simulation a small observation interval of $K = 3$ was chosen, the benefit of modulation index correction is only half a dB. It is more advantageous to correct the modulation index if K is larger. However, it might be desirable to perform synchronisation when K is small, before increasing K. This is because, as noted in Sec. 5.2.2, synchronisation using the IFO algorithms is more difficult when K is large, because long observation intervals are more susceptible to unharmonised parameters, and the resulting errors in determining $\hat{p}[k]$ are fed back into the tracking procedure.

5.4 Summary and Concluding Remarks

The Bluetooth standard permits sizeable offsets in carrier frequency and modulation index, whose values at most are 75 kHz and 0.07 respectively. Mismatch between the transmitter and receivers parameters, of the order accepted by the specification, will degrade the performance of the low-complexity high-performance Bluetooth receiver, especially when the observation interval is large. In order to ensure that the efficient MFB receiver is reliable in the face of possibly unharmonised parameters, we have developed techniques to compensate for these anomalies.

A cost function for carrier frequency offset correction was developed, and a stochastic gradient approach was employed to attain the optimum value. Use of this algorithm can prevent total system collapse when a carrier frequency offset is 75 kHz and the observation interval is large. For example if $K = 9$ a signal quality of 10 dB E_b/N_0 is sufficient to attain BER=10^{-3}, while 11 dB will be saved if $K = 3$. Despite this potential gain, only $3N$ real valued multiply accumulates (MACs) are required per symbol period to implement this algorithm. In order to converge in a dispersive channel, this method requires an equaliser to compensate for distortion introduced by the channel, but is independent of parameters of the receiver.

Alternatively, we have shown that advantage can be taken of the intermediate filter outputs (IFO), which are readily available in the low-complexity MFB receiver, to detect carrier frequency and modulation index offsets. Then periodically, the receivers parameters can be adjusted slightly, and the coefficients of the relatively small intermediate filter bank $\mathbf{W}^{(1)}$ recomputed Simulations indicate that employing this method can prevent total system failure due to a frequency offset of 75 kHz, and restore ideal performance in AWGN, thereby allowing BER=10^{-3} to be attained at 9.8 dB E_b/N_0 for $K = 9$, while 11 dB improvement is achieved if $K = 3$. The improvement resulting from correcting the maximum possible modulation index offset between two transceivers adhering to the Bluetooth standard amounts to 0.5 dB or 3.5 dB for $K = 3$ or $K = 9$ respectively. Hence, the potential gain of these algorithms is worth the $2^L N$ MACs necessary for their realisation.

Hence, the synchronisation procedures developed in this chapter are quite inexpensive in complexity, yet very useful add-ons to the efficient MFB receiver for Bluetooth signals, because they ensure reliability of the system when faced with potentially performance-degrading parameter mismatches.

Chapter 6

Conclusion

To conclude this thesis, we first recount the background to this research in Sec. 6.1, which puts the final remarks on the achievements of this work in Sec. 6.2 into context. Lastly, potential areas for improvements are listed in Sec. 6.3.

6.1 Background

A plethora of standards for wireless communications exist today [31], and they differ greatly in terms of, for example, modulation scheme, multiple access technique, data rate, or application. Manufacturers of radio transceivers are therefore faced with a dilemma of which standards to support, and determining how best to accommodate their choices in a single product.

In the recent past, Bluetooth and Wi-Fi have come to the fore [27], and established themselves as widely accepted independent systems in their own right, but also as useful additions to transceivers with an all-together different basic technology or primary purpose. A useful example of this is with a GSM (Global System for Mobile Communications) handset, or a portable data assistant (PDA), both of which favour the setting up of add-hoc networks with devices produced by a different manufacturer, owned by a different individual, or used for a different task. For example:

1. Use of a GSM handset or a PDA to access large video and audio files from a computer network or the Internet, via a network access point;

2. Connecting a GSM handset or PDA to a wireless microphone/headphone for hands-

free convenience during a telephone conversation, or while listening to an integrated MP3 player.

The first example above favours the use of Wi-Fi, while Bluetooth is more suitable in the second scenario. Reasons for this distinction have much to do with the data rates of the prospective links, but also with the technology that will be resident on the communicating partner, which in the examples above, is a network access point, and a wireless microphone/headphone respectively. This was elaborated in Chapter 1. Hence, bearing in mind the enormous worldwide popularity of Bluetooth and Wi-Fi, where possible, it would be advantageous to manufactures of mobile handsets or PDAs if they could integrate these complementary systems onto their products.

Once a decision has been made to provide Bluetooth and Wi-Fi capabilities in a radio transceiver, the next hurdle is to determine how best to accomplish this. The more obvious, and most popular technique today is sometimes referred to as the "Velcro" method, whereby a number of independent radios are enclosed, in parallel, in a common case. This scheme offers simplicity of understanding, but most of all, it benefits from the high data rates inherent in the fixed hardware that is utilised.

However, as the computational power of state of the art general purpose processors grow in accordance with Moore's law, it is widely believed that software defined radio (SDR) will play a major role in integrating multiple wireless standards in a radio transceiver [161]. The potential gains of an SDR implementation include, but are not limited to, reduced cost and size, more power efficiency, and seamless reconfigurability [2].

Hence, assuming a likely scenario where Bluetooth and Wi-Fi are integrated by downloading standard specific software on a common hardware platform when required, the general purpose processor employed for this task, must have the computational capacity to handle the more complex standard, which is Wi-Fi. Our aim has therefore been to make suggestions on how to use the extra resource that is available when Bluetooth is in operation, to improve its performance. This mission is shared by other researchers [6, 7, 8].

6.2 Concluding Remarks

Consequently, this work has focused on defining a Bluetooth receiver that is suitable for integration in an SDR, with a more complex system like Wi-Fi, but which is high-performance,

yet as efficient as possible, and is reliable when faced with a slack in the modulation parameters that exist in Bluetooth networks.

6.2.1 High-Performance

The demodulation method employed in our receiver is of paramount importance because we cannot expect to exceed its ideal performance in an AWGN channel. So Bluetooth demodulation algorithms were categorised as being low or high performing in Chapter 3. Low-performing demodulation algorithms incorporated, for example, FM and Phase-shift discrimination, and these were immediately discarded due to their poor BER capability. High-performing demodulation techniques included the use of a matched filter bank (MFB), or a Viterbi receiver, however, the Viterbi receiver was eliminated because of its susceptibility to a common Bluetooth problem of mismatch between transmitter and receiver parameters. This left the MFB receiver for adoption.

6.2.2 Efficient

Despite relative resilience to parameter offsets, a large observation interval of K symbol periods is required to ensure best performance of the MFB receiver. Thus, the filter bank involved can be prohibitively complex. As part of this work, in Chapter 3, we have formulated an iterative technique that eliminates the redundancy of providing the matched filter outputs once per symbol period [45, 46, 47, 48, 49]. This is via the use of a smaller set of intermediate filters, whose outputs are stored for K symbol stages, and processed appropriately to obtain the desired outputs of a larger filter bank. This algorithm reduces system complexity by approximately 80% when the filter lengths are $K = 9$ symbol periods and the oversampling factor is $N = 2$, and it is applicable to multi-level GFSK signals as well.

6.2.3 Reliable

While the optimum performance of our receiver is important, it is also desirable that it should maintain minimum error ratio when the operating conditions are not ideal. This requires consideration of difficulties that may arise with reception, such as multipath propagation and carrier frequency and modulation index offsets.

6.2.3.1 Equalisation

Multipath propagation is likely to occur in the kind of environments in which Bluetooth transceivers are expected to operate. Since this will cause substantial signal dispersion, provision of an equaliser can improve the BER performance significantly. The potential for carrier frequency offsets make the LMS algorithm and its derivatives unworkable, so we select a constant modulus equalisation criterion [131, 135]. However, the bursty nature of Bluetooth transmissions requires speedy convergence if information loss is to be minimised [162], and this is not helped by the correlation between samples of the Bluetooth signal [43].

Therefore to speed up equalisation we employ the normalised sliding window constant modulus algorithm [137, 138], which is akin to the affine projection algorithm [128, 147, 148, 149, 150], but based on a constant modulus (CM) criterion. However, the NSWCMA update requires inversion of the received signal covariance matrix, which could be singular for coloured signals like Bluetooth. Thus in Chapter 4, in order to retain the desirable convergence speed of the NSWCMA, while maintaining its stability during the equalisation of Bluetooth signals, we develop a novel regularisation technique using a complementary high-pass signal covariance matrix, and demonstrate that it enables quicker convergence than the existing regularisation method of employing a diagonal matrix. The resulting implementation is much faster than classical CMA but more stable than the conventional NSWCMA, and prevents the receiver from total failure in a dispersive channel with an RMS delay spread of 300 ns, when $K = 9$ [51, 50].

6.2.3.2 Parameter Synchronisation

The Bluetooth specification tolerates frequency offsets of 75 kHz, while the modulation index may lie anywhere within the range (0.28,0.35) [17]. Research has shown that relatively simple receivers suffer considerably from offsets within the permitted range [44], while the Viterbi receiver is much more susceptible [34]. In Chapter 5 the loss in efficacy of the MFB receiver, caused by carrier frequency offsets of the magnitude accepted in Bluetooth systems, was quantified as 11 dB for a filter length of $K = 3$, while an error ratio of almost 0.5 occurs if $K = 9$. On the other hand, the loss due to modulation index offsets could be 0.5 and 3.5 dB for $K = 3$ and $K = 9$ respectively. If our receiver is to be reliable, these losses must be avoided.

Hence, in Chapter 5 we developed a method to compensate for carrier frequency offsets by multiplying the incoming signal by a derotating phasor, which is adapted to the optimum via stochastic gradient techniques [46, 50, 48]. We also showed that the outputs of the intermediate filters of the low-complexity MFB could be employed to detect carrier frequency and modulation index offsets, and these could be corrected for by recomputing the coefficients of the relatively small intermediate filter bank [53, 48]. These algorithms have been shown to eliminate the loss in BER performance that would otherwise have resulted due to the carrier frequency and modulation index offsets.

> *Through the use of the new efficient realisation of the matched filter bank receiver for Bluetooth signals that has been proposed in this thesis, the blind constant modulus equalisation procedure that was suggested, and the novel blind algorithms for carrier frequency and modulation index offset correction that were developed, it is possible to achieve the maximum bit error ratio specified for Bluetooth at a much lower signal to noise ratio than is typical, in harsh conditions, and at a much lower associated cost in complexity than would otherwise be expected. It would therefore make it possible to increase the range of a Bluetooth link, and reduce the number of requests for packets to be retransmitted, thereby increasing throughput.*

6.3 Suggestions for Future Work

Based on the findings presented in this thesis, further research in the areas of low-cost receivers, equalisation, carrier and modulation index offset compensation is proposed.

6.3.1 Low-Complexity Receiver

Further computational saving could be achieved by truncating the Gaussian filter support length to $L = 2$ symbol periods, rather than $L = 3$. Simulations could quantify the loss in BER performance that would result from this change.

All arithmetic operations in the low-complexity MFB are complex valued. Since certain filter coefficients are complex conjugates pairs, computational cost can be reduced even further if complex valued operations are decomposed, and considered as real valued calculations.

The MFB receiver effectively assesses the correlation between a received signal K symbol periods in length and its prototype signals, and uses the result to estimate the central symbol only. However, since when K is large, the central symbol and those adjacent to it have equivalent error probability, more complexity reduction is possible if more than one received symbol is detected per iteration.

There is a need to establish the computational requirements of the demodulator in a Wi-Fi system, to facilitate a comparison with our Bluetooth receiver.

There is a potential trade-off between numerical operations, and memory storage because the efficient implementation of the MFB receiver may require more memory than its standard counterpart. In our research we have assumed that memory is a much cheaper resource, however, if this is not the case, then more investigation is necessary.

More research could determine the impact that fixed point arithmetic would have if this efficient implementation of the MFB receiver is ported onto a digital signal processor.

6.3.2 Equalisation

The assumption that a good regularisation factor ρ for the NSWCMA is equivalent to the size of its window P, is a simple and practical relationship supported by experiments. Nonetheless, it is likely that a more complex relationship exists between an optimum ρ and parameters that might include P, SNR, and the length of the equaliser L_{w}. This could be confirmed by more exhaustive simulations, and a statistical analysis of the results.

Research is required to gain insight into why the CM criterion appears to perform better in terms of BER with respect to the MMSE criterion.

6.3.3 Carrier Frequency and Modulation Index Offset Correction

Apart from the initial carrier frequency offset which has been addressed in this thesis, the Bluetooth specification allows for a substantial rate in frequency drift. It would be useful to investigate how these parameter synchronisation procedures would cope with such scenarios.

Some sort of practical or analytical evaluation should be done to establish the legitimate range in step size for each synchronisation procedure, and how it relates to SNR. After this, the speed of the algorithms can be properly assessed.

Appendix A

Describing the Noise Level of an AWGN Channel

There are several quantisations for the relationship between the signal and noise powers in a communications channel, and these include:

- Signal to noise ratio (SNR);
- Symbol energy to noise power spectral density ratio (E_s/N_0); and
- Bit energy to noise power spectral density ratio (E_b/N_0).

A.1 Signal to Noise Ratio

This is the ratio of the signal power to that of the noise per sample, and it is evaluated as

$$\text{SNR} = \frac{\sigma_s^2}{\sigma_v^2} \quad ,$$

where σ_s^2 and σ_v^2 is the variance of the signal and noise respectively.

A.2 Symbol Energy to Noise Power Spectral Density Ratio

This measure refers to the ratio of energy invested in each symbol, to the noise power spectral density. If N denotes the number samples per symbol (spreading factor), then

E_s/N_0 is related to the SNR by the expression

$$E_s/N_0 = \text{SNR}\cdot N \quad , \tag{A.1}$$

for complex signals, and

$$E_s/N_0 = \text{SNR}\cdot 2N \quad ,$$

for real signals.

The distinction between complex and real signals emanates from the difference in the noise power spectral densities of a complex baseband signal and its real bandpass equivalent portrayed in Fig. A.1. In other words, if the power spectral density for complex signal is expressed as

$$\sigma_s^2 = N_0 \quad , \tag{A.2}$$

then that of its real bandpass equivalent signal is given by

$$\sigma_s^2 = \frac{N_0}{2} \quad , \tag{A.3}$$

where the factor of 2 is included to indicate a 2-sided power spectral density.

A derivation for the expression in (A.1), available in [84] is as follows

$$\begin{aligned} E_s/N_0 &= (P_s\cdot T_{\text{symb}})/(P_v/B_v) \\ &= (T_{\text{symb}}\cdot F_{\text{samp}})\cdot(P_s/P_v) \\ &= (T_{\text{symb}}/T_{\text{samp}})\cdot\text{SNR} \\ &= N\cdot\text{SNR} \quad , \end{aligned} \tag{A.4}$$

where P_s and P_v are the signal and noise powers in watts, T_{symb} and T_{samp} are the symbol and sample periods in seconds, while B_v is the noise bandwidth, which is also equal to the sampling frequency F_{samp}.

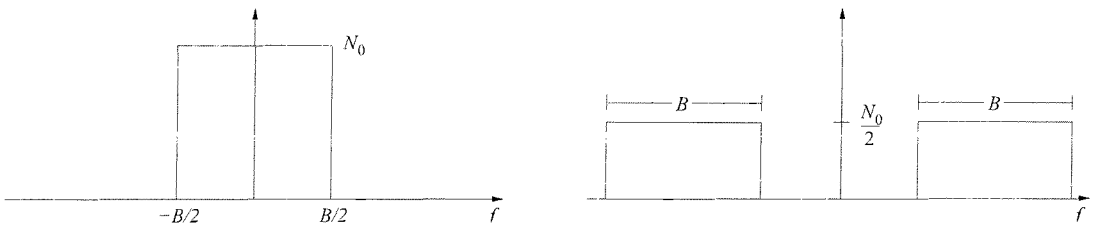

Figure A.1: Power spectral density of a complex baseband signal (left), and that of its real bandpass equivalent signal (right).

A.3 Bit Energy to Noise Power Spectral Density Ratio

This quantity is also referred to as the power efficiency, it is the ratio of the energy per information bit, to that of the noise power spectral density, and is related to E_s/N_0 by the formula

$$E_b/N_0 = (E_s/N_0)/q \tag{A.5}$$

where q is a factor that could be influenced by the number of bits per symbol N_b, or the coding rate. For example, if modulation is via 8-PSK, and a $\frac{1}{2}$ rate coder is used, then $q = \frac{3}{2}$. However, without considering redundant bits, it is obvious from (A.4) and (A.5) that

$$E_b/N_0 = \mathrm{SNR} \cdot \frac{N}{N_b} \quad .$$

List of Figures

List of Tables

List of Symbols

General Notations

h	scalar quantity
$\mathbf{h}$	vector quantity
$\mathbf{H}$	matrix quantity
$h(t)$	function of a continuous variable t
$h[n]$	function of a discrete variable n
h_n	short hand form for $h[n]$ for dense notation
$H(e^{j\omega})$	periodic Fourier spectrum of a discrete function $h[n]$
$H(z)$	z-transform of a discrete function $h[n]$
$P_{hh}(e^{j\omega})$	power spectral density of a discrete function $h[n]$

Relations and Operators

$\stackrel{!}{=}$	must equal
$\circ\!\!-\!\!\bullet$	transform pair, e.g. $h[n] \circ\!\!-\!\!\bullet H(e^{j\omega})$, $h[n] \circ\!\!-\!\!\bullet P_{hh}(e^{j\omega})$, or $h[n] \circ\!\!-\!\!\bullet H(z)$
$(\cdot)^*$	complex conjugate
$(\cdot)^H$	Hermitian (conjugate transpose)
$(\cdot)^T$	transpose
$(\cdot)^\dagger$	pseudoinverse
$*$	convolution
$\arg(\cdot)$	argument operator
blockdiag$\{\cdot\}$	block diagonal of a matrix
diag$\{\cdot\}$	diagonal of a matrix
$\mathcal{E}\{\cdot\}$	expectation operator

$\max(\cdot)$	maximum value operator
$\Re(\cdot)$	real value operator
∇	gradient operator (vector valued)
$\otimes$	Kronecker product
$a \mathrm{mod}_b$	modulo operator: remainder of a/b
$\mathcal{P}(\cdot)$	probability of
$\angle(\cdot)$	angle operator
$\lceil \cdot \rceil$	ceiling operator (round up)
$\lfloor \cdot \rfloor$	floor operator (round off)
$a : c : b$	row vector from a to b, in steps of c
(a, b)	greater than or equal to a, but less than or equal to b
$[a, b)$	greater than a, but less than or equal to b
$(a, b]$	greater than or equal to a, but less than b
$\lvert \cdot \rvert$	magnitude operator
$\lVert \cdot \rVert$	matrix or vector norm
$\mathrm{tr}(\mathbf{A})$	trace of $\mathbf{A}$
$\mathrm{erf}(\cdot)$	error function
$\delta(\cdot)$	delta function

Sets and Spaces

$\mathbb{C}$	set of complex numbers
$\mathbb{C}^{M \times N}$	set of $M \times N$ matrices with complex entries
$\mathbb{C}_{(z)}^{M \times N}$	set of $M \times N$ matrices with complex polynomial entries in z
$l^2(\mathbb{Z})$	space of square integrable (i.e. finite energy) discrete time signals
$\mathbb{N}$	set of integer numbers ≥ 0
$\mathbb{R}$	set of real numbers
$\mathbb{R}^{M \times N}$	set of $M \times N$ matrices with real entries
$\mathbb{R}_{(z)}^{M \times N}$	set of $M \times N$ matrices with real polynomial entries in z
$\mathbb{Z}$	set of integer numbers
$\mathbb{Z}$	set of integer numbers

Symbols and Variables

α	complex attenuation constant
α_ν	amplitude of the νth ray (multipath component)
α_{kl}	amplitude of the kth ray in the lth cluster
β	adaptive gain parameter
β_ν	phase of the νth ray (multipath component)
β_{kl}	phase of the kth ray in the lth cluster
γ	ray power decay constant
Γ	cluster power decay constant
$\Delta\Omega$	normalised (angular) carrier frequency offset
$\Delta\hat{\Omega}$	IFO algorithm carrier frequency offset compensation factor
Δf_c	carrier frequency offset
Δh	modulation index offset
$\epsilon[n]$	equaliser error signal
$\theta[k]$	phase of transmitted signal (symbol rate)
$\theta[n]$	phase of transmitted signal (sample rate)
$\theta_c[n]$	phase of carrier wave
$\hat{\theta}[n]$	phase of received signal after equalisation and synchronisation
Θ	SG algorithm carrier frequency offset compensation factor
λ	average number of rays arriving per second
$\lambda_{\max}$	largest eigenvalue of $\mathbf{R}$
$\lambda_{\min}$	smallest eigenvalue of $\mathbf{R}$
Λ	average number of clusters arriving per second
μ_Θ	step size for SG carrier frequency offset correction algorithm
μ_Ω	step size for IFO carrier frequency offset correction algorithm
μ_h	step size for IFO modulation index offset correction algorithm
μ_{w}	normalised equaliser step size
$\xi_{\Omega,\mathrm{IFO}}$	IFO carrier frequency offset tracking function
$\xi_{\Omega,\mathrm{SG}}$	SG carrier frequency offset correction cost function
ξ_{CM}	constant modulus cost function
$\xi_{h,\mathrm{IFO}}$	IFO modulation index offset tracking function
ξ_{MMSE}	minimum mean square error
ξ_{MSE}	mean square error cost function
$\hat{\xi}_{\Omega,\mathrm{IFO}}$	receivers instantaneous estimate of $\xi_{\Omega,\mathrm{IFO}}$
$\hat{\xi}_{\Omega,\mathrm{SG}}$	receivers instantaneous estimate of $\xi_{\Omega,\mathrm{SG}}$

$\hat{\xi}_{\text{CM}}$	receivers instantaneous estimate of ξ_{CM}
$\hat{\xi}_{h,\text{IFO}}$	receivers instantaneous estimate of $\xi_{h,\text{IFO}}$
$\hat{\xi}_{\text{MSE}}$	receivers instantaneous estimate of ξ_{MSE}
ρ	NSWCMA regularisation factor
σ_τ	root mean square delay spread
σ_s	standard deviation of $s[n]$
σ_v	standard deviation of $v[n]$
τ_ν	excess delay of the νth ray
τ_{kl}	excess delay of the kth ray in the lth cluster
$\bar{\tau}$	mean excess delay
$\phi[k]$	phase state sequence of the viterbi trellis
Ψ	condition number of $\mathbf{R}$
$\omega[n]$	information signals normalised (angular) frequency
$\mathbf{A}$	permutation matrix
$\hat{b}[k]$	received bit sequence ($M = 2$)
$\hat{\mathbf{b}}[k]$	received bit vector sequence ($M > 2$)
B	bandwidth of transmit signal
B_c	coherent bandwidth
$c[n]$	channel impulse response
$\mathbf{c}$	channel coefficient vector
$C_{\text{efficient}}$	efficient MFB receiver complexity in real valued multiply-accumulates
C_{standard}	standard MFB receiver complexity in real valued multiply-accumulates
$\mathbf{C}$	convolution matrix of channel
d	integral delay constant
$\mathbf{d}_d$	pinning vector
$\mathbf{D}$	permutation and phase correction matrix
$e[n]$	square of the error in magnitude of the equaliser output
E_b	bit energy
f_c	transmitter carrier frequency
$\hat{f}_c$	receiver carrier frequency
$g[n]$	gaussian filter impulse response
h	modulation index
$\hat{h}$	receivers estimate of h
i_δ	index of the non-zero element in the equaliser initialisation vector

$\mathbf{I}_x$	$x \times x$ identity matrix
k	symbol index
K	matched filter observation interval in symbol periods
K_{BT}	bandwidth-time product of gaussian filter
l	number of phase states in viterbi trellis
L	optimum support length of gaussian filter in symbol periods
L_c	length of channel impulse response
L_w	length of equaliser
n	chip index
M	number of modulation levels
$\mathbf{M}^{(K)}$	permutation matrix
N	number of chips (samples) per symbol
N_0	power spectral density of AWGN
N_b	number of bits per symbol
$p[k]$	transmit symbol stream at symbol rate
$p[n]$	upsampled transmit symbol stream (at chip rate)
$\hat{p}[k]$	received symbol stream at symbol rate
$\mathbf{p}$	cross-correlation vector of $s[n]$ and $\mathbf{r}_n$
$\hat{\mathbf{p}}$	instantaneous estimate of $\mathbf{p}$
$\grave{\mathbf{p}}$	ensemble average of $\grave{\mathbf{r}}_n$
P	NSWCMA order (window size)
$q[n]$	cumulative sum of the gaussian filter impulse response
$r[n]$	received signal
$\tilde{r}[n]$	equaliser output signal
$\mathbf{r}_n$	equaliser input vector
$\grave{\mathbf{r}}$	kronecker product of $\mathbf{r}_n$ and $\mathbf{r}_n^*$
R	data rate
$\mathbf{R}$	auto-correlation matrix of $\mathbf{r}_n$
$\mathbf{R}_n$	matrix of P equaliser input vectors
$\mathbf{R}_{ss}$	auto-correlation matrix of $\mathbf{s}_n$
$\mathbf{R}_{vv}$	auto-correlation matrix of $\mathbf{v}_n$
$\hat{\mathbf{R}}$	instantaneous estimate of $\mathbf{R}$
$\grave{\mathbf{R}}$	auto-correlation matrix of $\grave{\mathbf{r}}_n$
$s[n]$	transmit signal

$s_i[n]$	ith legitimate transmit signal
$s_{i,j}[n]$	legitimate transmit signal K-symbols long, with central modulating symbol i, and the jth combination of remaining $K+L-2$ modulating symbols
$\hat{s}[n]$	receiver input after equalisation and synchronisation
$\mathbf{s}_n$	composite channel-equaliser input signal vector
T_l	excess delay of the lth cluster
T_s	sampling period
$v[n]$	additive white gaussian noise sequence
$\mathbf{v}_n$	equaliser input noise vector
$\mathrm{w}_i[n]$	ith equaliser coefficient
$\mathbf{w}$	first column of $\mathbf{W}^{(1)}$, or constant equaliser coefficient vector
$\mathbf{w}_n$	equaliser coefficient vector
$\mathbf{w}_{\mathrm{CM,opt}}$	constant modulus algorithm optimum equaliser coefficients
$\mathbf{w}_{\mathrm{opt}}$	wiener-hopf equaliser coefficients
$\mathbf{W}^{(1)}$	intermediate filter bank, 1-symbol period in length
$y_k^{(a)}$	element of $\mathbf{y}_k^{(a)}$ with the largest magnitude
$\mathbf{y}_k^{(a)}$	vector of M^{a+L-1} equivalent matched filter outputs for received signal during the interval $(k-(K-a))N \geq n \geq (k-K)N+1$
$z_i[k]$	Viterbi ith incremental metric sequence
$Z_i[k]$	Viterbi ith path metric sequence

Glossary

ADC	analogue to digital converter
AM	amplitude modulation
APA	affine projection algorithm
AWGN	additive white gaussian noise
BER	bit error ratio
CCK	complementary code keying
CIR	channel impulse response
CM	constant modulus
CMA	constant modulus algorithm
CPFSK	continuous phase frequency shift keying
CPM	continuous phase modulation
DAC	digital to analogue converter
DBPSK	differential binary phase shift keying
DQPSK	differential quadrature phase shift keying
DSP	digital signal processor
FIR	finite impulse response
FM	frequency modulation
GFSK	gaussian frequency shift keying
GSM	global system for mobile communications
IEEE	institute of electrical and electronic engineers
IF	intermediate frequency
IFO	intermediate filter output
IIR	infinite impulse response
ISI	intersymbol interference
ISM	industrial, scientific and medical
LMS	least mean square

MAC	(real valued) multiply-accumulates
MBER	minimum bit error rate
MFB	matched filter bank
MMSE	minimum mean square error
MSE	mean square error
NCMA	normalised constant modulus algorithm
NLMS	normalised least mean square
NSWCMA	normalised sliding window constant modulus algorithm
PDA	portable data assistant
PDF	probability density function
RF	radio frequency
RMS	root mean square
SPIB	signal processing information base
SDR	software defined radio
SGD	stochastic gradient descent
SNR	signal to noise ratio
S-V	saleh-valenzuela
TDL	tap delay line
WI-FI	wireless fidelity
WLAN	wireless local area network
WMAN	wireless metropolitan area network
WPAN	wireless personal area network

Bibliography

[1] J. Mitola, "The Software Radio Architecture," *IEEE Communications Magazine*, vol. 33, pp. 26–38, May 1995.

[2] W. Tuttlebee, ed., *Software Defined Radio: Enabling Technologies*. West Sussex: John Wiley & Sons, July 2002.

[3] E. Buracchini, "The Software Radio Concept," *IEEE Communications Magazine*, vol. 38, pp. 138–143, September 2000.

[4] A. Wiesler and F. Jondral, "Software Radio Structure for Second Generation Mobile Communication Systems," in *48th Proc. IEEE Vehicular Technology Conference*, vol. 3, pp. 2363–2367, May 1998.

[5] A. Wiesler and F. K. Jondral, "A Software Radio for Second- and Third-Generation Mobile Systems," *IEEE Transactions on Vehicular Technology*, vol. 51, pp. 738–748, July 2002.

[6] R. Schiphorst, F. W. Hoeksema, and C. Slump, "A (Simplified) Bluetooth Maximum A Posteriori Probability (MAP) Receiver," in *Proc. IEEE Workshop on Signal Processing Advances in Wireless Communications,*, (Rome, Italy), June 2003.

[7] R. Schiphorst, F. W. Hoeksema, and C. H. Slump, "A Bluetooth-Enabled Hiper-LAN/2 Receiver," in *Proc. IEEE Vehicular Technology Conference*, vol. 5, (Orlando, Florida, USA), pp. 3443–3447, October 2003.

[8] R. Schiphorst, F W. Hoeksema, and K. Slump, "A Flexible WLAN Receiver," in *Proc. Program for Research on Integrated Systems and Circuits Workshop*, (Veldhoven, Netherlands), pp. 555–562, November 2003.

[9] IEEE, New Jersey, *Air Interface for Fixed Broadband Wireless Access Systems*, December 2001. Std 802.16.

[10] IEEE, New Jersey, *Air Interface for Fixed Broadband Wireless Access Systems-Amendment 2: Medium Access Control Modifications and Additional Physical Layer Specifications*, January 2003. Std 802.16a.

[11] ETSI, Sophia-Antipolis Cedex, France, *Broadband Radio Access Networks (BRAN); HIPERMAN Physical (PHY) Layer*, January 2005. ETSI TS 102 177.

[12] IEEE, New Jersey, *Wireless LAN Medium Access Control (MAC) and Physical Layer (PHY) Specifications*, 1999 ed., March 1999. Std. 802.11.

[13] IEEE, New Jersey, *Wireless LAN Medium Access Control (MAC) and Physical Layer (PHY) Specifications*, 1999 ed., September 1999. Std. 802.11a.

[14] IEEE, New Jersey, *Wireless LAN Medium Access Control (MAC) and Physical Layer (PHY) Specifications: Higher-Speed Physical Layer Extension in the 2.4 GHz Band*, 1999 ed., September 1999. Std. 802.11b.

[15] IEEE, New Jersey, *Wireless LAN Medium Access Control (MAC) and Physical Layer (PHY) Specifications. Amendment 4: Further Higher Data Rate Extension in the 2.4 GHz Band*, 2003 ed., June 2003. Std. 802.11g.

[16] ETSI, Sophia-Antipolis Cedex, France, *Broadband Radio Access Networks (BRAN); HIPERLAN Type 2; Physical (PHY) Layer*, February 2000. ETSI 101 475.

[17] Bluetooth Special Interest Group, *Specification of the Bluetooth System*, February 2002. Core.

[18] IEEE, New Jersey, *Wireless Medium Access Control (MAC) and Physical Layer (PHY) Specifications for Personal Area Networks (WPANs)Standard 802.15.1*, June 2002. Std. 802.15.1.

[19] IEEE, New Jersey, *Wireless Medium Access Control (MAC) and Physical (PHY) Specifications for High Rate Wireless Personal Area Networks (WPANs)*, June 2003. Std 802.15.3.

[20] IEEE, New Jersey, *Wireless Medium Access Control (MAC) and Physical (PHY) Specifications for Low-Rate Wireless Personal Area Networks (LR-WPANs)*, 2003. Std 802.15.4.

[21] H. Darabi, J. Chiu, S. Khorram, H. Kim, Z. Zhou, E. Lin, S. Jiang, K. Evans, E. Chien, B. Ibrahim, E. Geronaga, L. Tran, and R. Rofougaran, "A dual mode

802.11b/Bluetooth radio in 0.35/spl mu/m CMOS," in *d*, vol. 1, (San Fransico, California, USA), February 2003.

[22] Y.-J. Jung, H. Jeong, E. Song, J. Lee, S.-W. Lee, D. Seo, I. Song, S. Jung, J. Park, D.-K. Jeong, and W. Kim, "A Dual-Mode Direct-Conversion CMOS Transceiver for Bluetooth and 802.11b," in *Proc. European Conference on Solid-State Circuits*, (Estoril, Portugal), pp. 225–228, September 2003.

[23] A. A. Emira, A. Valdes-Garcia, B. Xia, A. N. Mohieldin, A. Valero-Lopez, S. T. Moon, C. Xin, and E. Sanchez-Sinencio, "A Dual-mode 802.11b/Bluetooth Receiver in 0.25/spl mu/m BiCMOS," in *Proc. IEEE International Conference on Solid-State Circuits*, vol. 1, (San Francisco, California, USA), February 2004.

[24] A. A. Emira, A. Valdes-Garcia, B. Xia, A. N. Mohieldin, A. Valero-Lopez, S. T. Moon, C. Xin, and E. Sanchez-Sinencio, "A BiCMOS Bluetooth/Wi-Fi Receiver," in *Proc. IEEE Radio Frequency Integrated Circuits Symposium*, (Fort Worth, Texas, USA), pp. 519–522, June 2004.

[25] E. Sanchez-Sinencio, "Chameleon: A Dual-Mode Bluetooth/802.11b Receiver," in *Midwest Symposium on Circuits and Systems*, vol. 2, (Hiroshima, Japan), pp. xv–xv, July 2004.

[26] T. B. Cho, D. Kang, C.-H. Heng, and B. S. Song, "A 2.4-GHz Dual-Mode 0.18-/spl mu/m CMOS Transceiver for Bluetooth and 802.11bd," *IEEE Journal of Solid-State Circuits*, vol. 39, pp. 1916 – 1926, November 2004.

[27] N. Hunn, "Bluetooth and Wi-Fi — The market status," white paper, TDK Systems, London, UK, March 2002.

[28] R. Ludwig and P. Bretchko, *RF Circuit Design: Theory and Applications.* Upper Saddle River, New Jersey, USA: Prentice Hall, 2000.

[29] M. Man, "Bluetooth and wi-fi," tech. rep., Socket Communications Inc, Newark, California, USA, March 2002.

[30] Z. Weissman, "Bluetooth vs. 802.11b: The access network perspective," white paper, Tadlys Last Yard Solutions Ltd, Rishon LeZiyyon, Israel, January 2002.

[31] C. Tibenderana and S. Weiss, "SDR enablers and obstacles: Technology study on waveforms," Report for the UK Office of Communications (OFCOM), School of Elec-

tronics and Computer Science, University of Southampton, Southampton, UK, March 2005.

[32] R. Schiphorst, F. Hoeksema, and K. Slump, "Bluetooth Demodulation Algorithms and their Performance," in *Proc. 2nd Karlsruhe Workshop on Software Radios*, (Karlsruhe), pp. 99–105, March 2002.

[33] T. Aulin, N. Rydbeck, and C.-E. W. Sundberg, "Continous Phase Modulation-Part II: Partial Response Signaling," *IEEE Transactions on Communications*, vol. COM-29, pp. 210–225, March 1981.

[34] A. Soltanian and R. E. Van Dyck, "Performance of the Bluetooth System in Fading Dispersive Channels and Interference," in *Proc. Global Telecommunications Conference*, vol. 6, (San Antonio, Texas), pp. 3499–3503, November 2001.

[35] J. B. Anderson, T. Aulin, and C.-E. Sundberg, *Digital Phase Modulation*. New York and London: Plenum Press, 1986.

[36] W. P. Osborne and M. B. Luntz, "Coherent and Noncoherent Detection of CPFSK," in *IEEE Transactions on Communications*, vol. COM-22, pp. 1023–1036, August 1974.

[37] T. A. Schonhoff, "Symbol Error Probabilities for M-ary CPFSK: Coherent and Noncoherent Detection," in *IEEE Transactions on Communications*, vol. COM-24, pp. 644–652, June 1976.

[38] W. Hirt and S. Pasupathy, "Suboptimal Reception of Binary CPSK Signals," in *Proc. IEE Communications, Radar and Signal Processing*, vol. 128, (United Kingdom), pp. 125–134, June 1981.

[39] G. E. Moore, "Cramming More Components onto Integrated Circuits," *Proceedings of the IEEE*, vol. 86, pp. 82–85, January 1998.

[40] T. S. Rappaport, S. Y. Seidel, and K. Takamizawa, "Statistical Channel Impulse Response Models for Factory and Open Plan Building Radio Communication System Design," *IEEE Transactions on Communications*, vol. 39, pp. 794–807, May 1991.

[41] H. Hashemi, "The Indoor Radio Propagation Channel," *Proceedings of the IEEE*, vol. 81, pp. 943–968, July 1993.

[42] M. Nafie, A. G. Dabak, T. M. Schmidl, and A. Gatherer, "Enhancements to the Bluetooth Specification," in *Proc. Asilomar Conference on Signals, Systems, and Computers*, vol. 2, (Pacific Grove, Califonia), pp. 1591–1595, November 2001.

[43] R. C. Johnson, P. Schniter, T. J. Endres, J. D. Behm, D. R. Brown, and R. A. Casas, "Blind Equalization Using the Constant Modulus Criterion: A Review," *Proceedings of the IEEE*, vol. 86, pp. 1927–1950, October 1998.

[44] C. Robinson, A. Purvis, A. Lechner, and M. Hoy, "Characterisation of Bluetooth Carrier Frequency Errors," in *Proc. IEEE Mixed Signal Testing Workshop* (June, ed.), (Seville, Spain), pp. 119–124, June 2003.

[45] C. Tibenderana and S. Weiss, "A Low-Complexity High-Performance Bluetooth Receiver," in *Proc. IEE Colloquium on DSP Enabled Radio* (R. W. Stewart and D. Garcia-Alis, eds.), (Livingston, Scotland, UK), pp. 426–435, September 2003.

[46] C. Tibenderana and S. Weiss, "Low-Complexity High-Performance GFSK Receiver With Carrier Frequency Offset Correction," in *Proc. IEEE International Conference on Acoustics, Speech, and Signal Processing*, vol. IV, (Montreal, Canada), pp. 933–936, May 2004.

[47] C. Tibenderana and S. Weiss, "Fast Multi-level GFSK Matched Filter Receiver," in *Proc. Institute of Mathematics and its Applications Conference on Mathematics in Signal Processing*, (Cirencester, Essex, UK), pp. 191–194, December 2004.

[48] C. Tibenderana and S. Weiss, "Efficient and Robust Detection of GFSK Signals Under Dispersive Channel, Modulation Index and Carrier Frequency Offset Conditions," *Special Issue on DSP Enabled Radio, EURASIP Journal on Applied Signal Processing*, January 2005. Accepted for Publication.

[49] C. Tibenderana and S. Weiss, "Simplified Matched Filter Bank Receiver for Multilevel GFSK," *IEEE Transactions on Circuits & Systems I.* Submitted.

[50] C. Tibenderana and S. Weiss, "Blind Equalisation and Carrier Offset Compensation for Bluetooth Signals," in *Proc. European Signal Processing Conference*, (Vienna, Austria), pp. 909–912, September 2004.

[51] C. Tibenderana and S. Weiss, "Rapid Equalisation for a High Integrity Bluetooth Receiver," in *Proc. IEEE Workshop on Statistical Signal Processing*, (Bordeaux, France), July 2005. Submitted to.

[52] C. Tibenderana and S. Weiss, "Investigation of Offset Recovery Algorithms for High Performance Bluetooth Receivers," in *Proc. IEE Colloquium on DSP Enabled Radio*, (Southampton, UK), September 2005. Accepted for Publication.

[53] C. Tibenderana and S. Weiss, "A Low-Cost Scalable Matched Filter Bank Receiver for GFSK Signals with Carrier Frequency and Modulation Index Offset Compensation," in *Proc. Asilomar Conference on Signals, Systems, and Computers*, (Pacific Groove, California, USA), pp. 682–686, November 2004.

[54] J. H. McClellan, R. W. Schafer, and M. A. Yoder, *DSP First: A Multimedia Approach*. Upper Sadle River, New Jersey, USA: Prentice Hall, 1st ed., June 1999.

[55] J. G. Proakis and D. G. Manolakis, *Digital Signal Processing*. Upper Saddle River, New Jersey: Prentice Hall, 3rd ed., 1996.

[56] H. Nyquist, "Certain Topics in Telegraph Transmission Theory." *Proceedings of the IEEE*, vol. 90, pp. 280–305, February 2002.

[57] L. R. Rabiner and B. Gold, *Theory and Application of Digital Signal Processing*. Englewood Cliffs, New Jersey: Prentice Hall, 1975.

[58] R. Steele and L. Hanzo, *Mobile Communications*. West Sussex: John Wiley & Sons, 2nd ed., 1999.

[59] L. Hanzo, W. Webb, and T. Keller, *Single- and Multi-carrier Quadrature Amplitude Modulation: Principles and Applications for Personal Communications, WLANs and Broadcasting*. Chichester, England: John Wiley & Sons, 1st ed., 2000.

[60] T. S. Rappaport, *Wireless Communications: Principles and Practice* New Jersey: Prentice Hall, July 1999.

[61] B. Glance and L. J. Greenstein, "Frequency-Selective Fading Effects in Digital Mobile Radio with Diversity Combining," *IEEE Transactions on Communications*, vol. COM-31, pp. 1085–1094, September 1983.

[62] S. Y. Seidel, T. Rappaport, M. J. Feuerstein, and K. L. Blackard, "The Impact of Surrounding Buildings on Propagation for Wireless In-Building Personal Communications System Design," in *Proc. IEEE Vehicular Technology Conference*, vol. 2, (Denver), pp. 814–818, May 1992.

[63] Y. P. Zhang and Y. Hwang, "Time Delay Characteristics of 2.4 GHz Band Radio Propagation Channels in Room Environments," in *Proc. IEEE International Symposium Personal, Indoor and Mobile Radio Communications*, vol. 1, (The Hague, Netherlands), pp. 28–32, September 1994.

[64] T. A. Wilkinson, "Channel Modelling and Link Simulation Studies for the DECT Test Bed Program," in *Proc. International Conference on Mobile Radio and Personal Communications*, (Warwick, UK), pp. 293–299, December 1991.

[65] W. C. Y. Lee, *Mobile Cellular Telecommunications : Analog and Digital Systems.* New York: McGraw-Hill, 2nd ed., 1995.

[66] J. G. Proakis, *Digital Communications.* New York: McGraw-Hill, 3rd ed., 1995.

[67] M. Schartz, W. R. Bennet, and S. Stein, *Communication Systems and Techniques.* New York: McGraw-Hill, 1966.

[68] R. Kennedy, *Fading Dispersive Communication Channels.* New York: Wiley-Interscience, 1969.

[69] G. L. Turin, F. D. Clapp, T. L. Johnston, S. B. Fine, and D. Lavry, "A Statistical Model of Urban Multipath Propagation," *IEEE Transactions on Vehicular Technology*, vol. VT-21, pp. 1–9, February 1972.

[70] H. Suzuki, "A Statistical Model for Urban Radio Propagation," *IEEE Transactions on Vehicular Technology*, vol. COM-25, pp. 673–680, July 1977.

[71] H. Hashemi, "Simulation of the Urban Radio Propagation Channel," *IEEE Transactions on Vehicular Technology*, vol. VT-28, pp. 213–224, August 1979.

[72] W. Shi, *Frequency Division Multiple Access using Spectrally Overlapping Signals.* PhD thesis, Churchill College, University of Cambridge, 2003.

[73] H. Mohamad, *Subband Adaptive Equalisation for Communication Transceivers.* PhD thesis, School of Electronics and Computer Science, University of Southampton, 2003.

[74] R. Gooch and B. Daellenbach, "Wideband PCM channel characterization study: Final report (revision)," technical report, Applied Signal Technology, (http://www.appsig.com), Sunnyvale, California, May 1988.

[75] SPIB, "Rice university signal processing information base." http://spib.rice.edu/spib.html.

[76] A. F. Molisch and J. R. Foerster, "Impulse Response Modeling of Indoor Radio Propagation Channels," *IEEE Journal on Selected Areas in Communications*, vol. 11, pp. 967–978, September 1993.

[77] R. H. Clark, "A Statistical Theory of Mobile-Radio Reception," *Bell Systems Technical Journal*, vol. 47, p. 1968, 1968.

[78] W. C. Jakes, *Microwave Mobile Communications.* New York, USA: Wiley-Interscience, 1974.

[79] A. A. M. Saleh and R. A. Valenzuela, "A Statistical Model for Indoor Multipath Propagation," *IEEE Journal on Selected Areas in Communications*, vol. SAC-5, pp. 128–137, February 1987.

[80] A. F. Molisch and J. R. Foerster, "Channel Models for Ultrawideband Personal Area Networks," *IEEE Wireless Communications*, vol. 10, pp. 14–21, December 2003.

[81] E. Kreyszig, *Advanced Engineering Mathematics.* New York: John Wiley & Sons, 6th ed., 1988.

[82] W. H. Press, S. A. Teukolsky, W. T. Vetterling, and B. P. Flannery, *Numerical Recipes in C: The Art of Scientific Computing.* Cambridge, UK: Cambridge University Press, 2nd ed., 1992.

[83] S. Weiss, R. W. Stewart, and D. M. Davis, *Handbook on Noise Reduction for Speech Applications.* Boca Raton: CRC Press, April 2002.

[84] Mathworks, Natick, MA, USA, www.mathworks.com, *Communications Toobox Documentation*, September 2000.

[85] K. Feher, *Wireless Digital Communications: Modulation and Spread Spectrum Applications.* Upper Sadle River, New Jersey, USA: Prentice Hall, 1995.

[86] B. A. Carlson, *Communication Systems.* Singapore: McGraw-Hill, 3rd ed., 1986.

[87] L. W. Couch, *Digital and Analog Communication Systems.* New York, USA: Macmillan Publishing Co., Inc., 1983.

[88] K. Feher, ed., *Advenced Digital Communications Systems and Signal Processing Techniques*. Englewood Cliffs, New Jersey, USA: Prentice Hall, 1987.

[89] M. H. L. Kouwenhoven, *High-Performance Frequency-Demodulation Systems*. Delft, Netherlands: Delft University Press, March 1998.

[90] H. L. Van Trees, *Detection, Estimation, and Modulation Theory*, vol. 1. New York: John Wiley & Sons, 1968.

[91] A. Viterbi, "Error Bounds for Convolutional Codes and an Asymptotically Optimum Decoding Algorithm," *IEEE Transactions on Information Theory*, vol. 13, pp. 260–269, April 1967.

[92] A. Viterbi and J. Omura, *Principles of Digital Communications and Coding*. New York, USA: McGraw-Hill, 1979.

[93] B. Sklar, *Digital Communications Fundamentals and Applications*. Upper Saddle River, New Jersey, USA: Prentice Hall, 1988.

[94] M. Speth, M. Madden, M. Hammes, and A. Neubauer, "MLSE Based Detection for GFSK Signals With Arbitrary Modulation Index," in *Proc. International Zurich Seminar on Communications*, (Zurich, Germany), pp. 228–231, February 2004.

[95] C. Robinson and A. Purvis, "Demodulation of Bluetooth GFSK Signals Under Carrier Frequency Error Conditions," in *Proc. IEE Colloquium on DSP Enabled Radio*, (Livingston, Scotland, UK), September 2003.

[96] Ericsson, *Ericsson Bluetooth Development Kit documentation*, October 1999.

[97] M. Nafie, A. Gatherer, and A. Dabak, "Decision Feedback Equalization for Bluetooth Systems," in *Proc. IEEE International Conference on Acoustics, Speech, and Signal Processing*, vol. 2, (Salt Lake City), pp. 909–912, May 2001.

[98] C.-H. Park, J.-H. Paik, Y.-H. You, and M.-C. J. J.-W. Cho, "Techniques for channel estimation, DC-offset compensation, and link quality control in Bluetooth system," *IEEE Transactions on Consumer Electronics*, vol. 46, pp. 682–687, August 2000.

[99] C.-H. Park, Y.-H. You, J.-H. Paik, and M.-C. J. J.-W. Cho, "Channel estimation and DC-offset compensation schemes for frequency-hopped Bluetooth networks," *IEEE Communications Letters*, vol. 5, pp. 4–6, January 2001.

[100] R. F. Fischer, *Precoding and Signal Shaping for Digital Transmission.* New York, USA: John Wiley & Sons, 2002.

[101] W. Fischer and I. Lieb, *Funktionentheorie.* Braunschweig, Germany: Vieweg Verlag, 1983.

[102] S. Weiss and R. W. Stewart, *On Adaptive Filtering in Oversampled Subbands.* Germany: Shaker Verlag, 1998.

[103] T. K. Moon and W. C. Stirling, *Mathematical Methods and Algorithms.* Upper Saddle River, NJ: Prentice Hall, 1999.

[104] S. Haykin, *Adaptive Filter Theory.* Englewood Cliffs, New Jersey: Prentice Hall, 2nd ed., 1991.

[105] V. Bale and S. Weiss, "A Low Complexity Subband Adaptive Equaliser for Broadband MIMO Channels," in *Proc. International Workshop on Spectral Methods and Multirate Signal Processing,* (Vienna, Austria), pp. 61–68, September 2004.

[106] V. K. Balakrishnan, *Schaum's Outline of Combinatorics.* Schaum's Outlines Series, McGraw-Hill, November 1994.

[107] G. H. Golub and C. F. V. Loan, *Matrix Computations.* Baltimore, Maryland, USA: John Hopkins University Press, 1983.

[108] N. Wiener, *Extrapolation, Interpolation, and Smoothing of Stationary Time Series, with Engineering Applications.* New York: John Wiley & Sons, 1949.

[109] H. W. Bode and C. E. Shannon, "A Simplified Derivation of Linear Least Square Smoothing and Prediction Theory," *Proceedings of the IEEE*, vol. 38, pp. 417–425, April 1950.

[110] T. Kailath, "A View of Three Decades of Linear Filtering Theory," *IEEE Transactions on Information Theory*, vol. 20, pp. 146–181, March 1974.

[111] B. Widrow and M. E. Hoff, " Adaptive Switching Circuits," *IRE Western Electric Show and Convention Record*, vol. 4, pp. 96–104, August 1960.

[112] B. Widrow and S. D. Stearns, *Adaptive Signal Processing.* New Jersey: Prentice Hall, Inc, 1985.

[113] N. J. Bershad, "Analysis of the Normalized LMS Algorithm with Gaussian Inputs," *IEEE Transactions on Acoustics, Speech, and Signal Processing*, vol. 34, pp. 793–806, August 1986.

[114] M. Rupp, "The Behavior of LMS and NLMS Algorithms in the Presence of Spherically Invariant Processes," *IEEE Transactions on Signal Processing*, vol. 41, pp. 1149–1160, March 1993.

[115] D. T. M. Slock, "On the Convergence Behavior of the LMS and the Normalized LMS Algorithms," *IEEE Transactions on Signal Processing*, vol. 41, pp. 2811–2825, September 1993.

[116] P. E. An, M. Brown, and C. J. Harris, "On the Convergence Rate Performance of the Normalized Least-Mean-Square Adaptation," *IEEE Transactions on Neural Networks*, vol. 8, pp. 1211–1214, September 1997.

[117] G. G. Goodwin and K. S. Sin, *Adaptive Filtering, Prediction and Control*. Englewood Cliffs, New Jersey: Prentice Hall, 1984.

[118] B. Widrow and M. A. Lehr, "30 Years of Adaptive Neural Networks Perceptron, Madaline, and Backpropagation," *Proceedings of the IEEE*, vol. 78, pp. 1415–1442, September 1990.

[119] V. Solo and X. Kong, *Adaptive Signals Processing Algorithms — Stability and Performance*. Englewood Cliffs, New Jersey, USA: Prentice Hall, 1995.

[120] O. M. Macchi, *Adaptive Processing: The LMS Approach with Applications in Transmission*. New York, USA: John Wiley & Sons, 1995.

[121] K. Wesolowski, C. M. Zhao, and W. Rupprecht, "Adaptive LMS Transversal Filters With Controlled Length," *IEE Proceedings: F, Radar and Signal Processing*, vol. 139, pp. 233–238, June 1992.

[122] V. H. Nascimento, "Improving the Initial Convergence of Adaptive Filters: Variable-Length LMS Algorithms," in *Proc. International Conference on Digital Signal Processing*, vol. 2, (Aegean Island of Santorini, Greece), pp. 667–670, July 2002.

[123] R. C. Bilcu, P. Kuosmanen, and K. Egiazarian, "A New Variable Length LMS Algorithm: Theoretical Analysis and Implementation," in *Proc. IEEE International Con-*

ference on Electronics, Circuits and Systems, vol. 3, (Dubrovnik, Croatia), pp. 1031–1034, September 2002.

[124] Y. Gu, K. Tang, and H. Cui, "Sufficient Condition for Tap-Length Gradient Adaptation of LMS Algorithm," in *Proc. IEEE International Conference on Acoustics, Speech, and Signal Processing*, vol. II, (Montreal, Canada), pp. 461–464, May 2004.

[125] Y. Gong and C. F. Cowan, "A Novel Variable Tap-Length Algorithm for Linear Adaptive Filters," in *Proc. IEEE International Conference on Acoustics, Speech, and Signal Processing*, vol. II, (Montreal, Canada), pp. 825–828. May 2004.

[126] J.-I. Nagumo and A. Noda, "A Learning Method for System Identification," *IEEE Transactions on Automatic Control*, vol. 12, pp. 282–287, June 1967.

[127] R. R. Bitmead and B. D. O. Anderson, "Performance of Adaptive Estimation Algorithms in Dependent Random Environments," *IEEE Transactions on Automatic Control*, vol. 25, pp. 788–794, August 1980.

[128] K. Ozeki and T. Umeda, "An Adaptive Filtering Algorithm using Orthogonal Projection to an Affine Subspace and its Properties," *Electronics and Communications in Japan*, vol. 67-A, no. 5, pp. 19–27, 1984.

[129] M. Rupp, "A Family of Adaptive Filter Algorithms with Decorrelating Properties," *IEEE Transactions on Signal Processing*, vol. 46, pp. 771–775, March 1998.

[130] S. G. Sankaran and A. A. L. Beex, "Convergence Behaviour of Affine Projection Algorithms," *IEEE Transactions on Signal Processing*, vol. 48, pp. 1086–1096, April 2000.

[131] D. N. Godard, "Self Equalization and Carrier Tracking in Two-Dimensional Data Communication Systems," *IEEE Transactions on Communications*, vol. COM-28, pp. 1867–1875, November 1980.

[132] S. L. Wood, M. G. Larimore, and J. Treichler, "CMA Convergence for Constant Envelope, Non-Zero Bandwidth Signals," in *Proc. IEEE International Conference on Acoustics, Speech, and Signal Processing*, vol. 3, (Munich, Germany), pp. 2525–2528, April 1997.

[133] N. Kikuma, K. Takai, K. Nishimori, and F. Saito, "Consideration on Performance of the CMA Adaptive Array Antenna for 16QAM Signals," in *Proc. IEEE International*

Symposium Personal, Indoor and Mobile Radio Communications, vol. 2, (Toronto, Canada), pp. 677–681, September 1995.

[134] Y. Sato, "A Method of Self-Recovering Equalization for Multilevel Amplitude-Modulation Systems," *IEEE Transactions on Communications*, vol. 23, pp. 679–682, July 1975.

[135] J. R. Treichler and B. G. Agee, "A New Approach to Multipath Correction of Constant Modulus Signals," *IEEE Transactions on Acoustics, Speech, and Signal Processing*, vol. ASSP-31, pp. 459–472, April 1983.

[136] D. L. Jones, "A Normalized Constant-Modulus Algorithm," in *Proc. Asilomar Conference on Signals, Systems, and Computers*, vol. 1, (Pacific Grove, Califonia), pp. 694–697, October 1995.

[137] C. B. Papadias and D. T. M. Slock, "New Adaptive Blind Equalization Algorithms for Constant Modulus Constellations," in *Proc. IEEE International Conference on Acoustics, Speech, and Signal Processing*, vol. 3, (Adelaide, Australia), pp. 321–324, April 1994.

[138] C. B. Papadias and D. T. M. Slock, "Normalized Sliding Window Constant Modulus and Decision-Directed Algorithms: a Link Between Blind Equalization and Classical Adaptive Filtering," *IEEE Transactions on Signal Processing*, vol. 45, pp. 231 – 235, January 1997.

[139] Z. Ding, R. A. Kennedy, B. D. O. Anderson, and R. C. Johnson, "Ill-Convergence of Godard Blind Equalizers in Data Communication Systems," *IEEE Transactions on Communications*, vol. 39, pp. 1313–1327, September 1991.

[140] B.-J. J. Kim, *Blind Equalization for Short Burst Wireless Communications*. PhD thesis, Stanford University, 1998.

[141] Y. Luo and J. A. Chambers, "Quasi-Newton Cross-Correlation and Constant Modulus Adaptive Algorithm for Space-Time Equalisation," in *Proc. Institute of Mathematics and its Applications Conference on Mathematics in Signal Processing*, (Warwick, UK), December 2000.

[142] Y. Luo and J. A. Chambers, "Quasi-Newton Constant Modulus Adaptive Algorithm for Use in Multi-user Communication Systems," *IEE Electronics Letters*, vol. 37, pp. 264–265, February 2001.

[143] T. Schirtzinger, X. Li, and W. K. Jenkins, "A Comparison of Three Algorithms for Blind Equalisation Based on the Constant Modulus Error Criterion," in *Proc. IEEE International Conference on Acoustics, Speech, and Signal Processing*, vol. 2, (Detroit, Michigan, USA), pp. 1049–1052, May 1995.

[144] J. P. LeBlanc and I. Fijalkow, "Blind Adapted, Pre-whitened Constant Modulus Algorithm," in *Proc. International Conference on Communications*, vol. 8, (Helsinki, Finland), pp. 2438 – 2442, June 2001.

[145] M. Gerken, F. M. Pait, and P. E. Jojoa, "An Adaptive Filtering Algorithm with Parameter Acceleration," in *Proc. IEEE International Conference on Acoustics, Speech, and Signal Processing*, vol. 1, (Istambul, Turkey), pp. 17–20, June 2000.

[146] M. T. M. Silva, M. Gerken, and M. D. Miranda, "An Accelerated Constant Modulus Algorithm for Space-Time Blind Equalisation," in *Proc. European Signal Processing Conference*, (Vienna, Austria), pp. 1853–1856, September 2004.

[147] D. T. M. Slock, "Underdetermining Growing and Sliding Window Covariance Fast Transversal Filter RLS Algorithms," in *Proc. European Signal Processing Conference*, (Brussels, Belgium), pp. 1169–1172, August 1992.

[148] D. T. M. Slock, "The Block Underdetermined Covariance (BUC) Fast Transversal Filter (FTF) Algorithm for Adaptive Filtering," in *Proc. Asilomar Conference on Signals, Systems, and Computers*, vol. 1, (Pacific Groove, California, USA), pp. 550 – 554, October 1992.

[149] M. Montazeri and P. Duhamel, "A Set of Algorithms Linking NLMS and Block RLS Algorithms," in *Proc. IEEE International Conference on Acoustics, Speech, and Signal Processing*, vol. 3, (Minneapolis, Minnesota, USA), pp. 412 – 415, April 1993.

[150] M. Montazeri and P. Duhamel, "A Set of Algorithms Linking NLMS and Block RLS Algorithms," *IEEE Transactions on Signal Processing*, vol. 43, pp. 444 – 453, February 1995.

[151] A. Cichocki and R. Unbehauen, *Neural Networks for Optimization and Signal Processing*. Chichester, UK: John Wiley & Sons, September 1993.

[152] V. Myllyla and G. Schmidt, "Pseudo-optimal Regularization for Affine Projection Algorithms," in *Proc. IEEE International Conference on Acoustics, Speech, and Signal Processing*, vol. 2, (Orlando, Florida, USA), pp. 1917–1920, May 2002.

[153] E. Chau, H. Sheikhzadeh, and R. L. Brennan, "Complexity Reduction and Regularization of a Fast Affine Projection Algorithm for Oversampled Subband Adaptive Filters," in *Proc. IEEE International Conference on Acoustics, Speech, and Signal Processing*, vol. 5. (Montreal, Canada), pp. 109–112, May 2004.

[154] J. R. Treichler and M. G. Larimore, "The Tone Capture Properties of CMA-Based Interference Suppressors," *IEEE Transactions on Acoustics, Speech, and Signal Processing*, vol. 33, pp. 946–958, August 1985.

[155] H. Jamali and S. L. Wood, "Error Surface Analysis for the Complex Constant Modulus Adaptive Algorithm," in *Proc. Asilomar Conference on Signals, Systems, and Computers*, vol. 1, (Pacific Grove, California), pp. 248–252, November 1990.

[156] B. Widrow and E. Walach, *Adaptive Inverse Control*. Upper Saddle River, New jersey, USA: Prentice Hall, 1996.

[157] S. Chen, "Adaptive Minimum Bit Error Rate Filtering," *IEE Proceedings — Vision, Image, and Signal Processing*, vol. 151, pp. 76–85, February 2004.

[158] A. N. D. Andrea, A. Ginesi, and U. Mengali, "Frequency Detector For CPM," *IEEE Transactions on Communications*, vol. 43, pp. 1828–1837, February 1995.

[159] A. Aziz, P. Spasojevic, and C. N. Georghiades, "A DSP-based Receiver for Large Frequency offset Compensations," in *Proc. International Conference on Signal Processing and Applications*, (Toronto, Canada), September 1998.

[160] P. Spasojevic and C. N. Georghiades, "Blind Frequency Compensation For Binary CPM with h=1/2 and A Positive Frequency Pulse." in *Proc. Global Telecommunications Conference*, (Sidney), November 1998.

[161] W. Tuttlebee, ed., *Software Defined Radio: Origins, Drivers and International Perspectives*. West Sussex: John Wiley & Sons, March 2002.

[162] G. D. Forney, S. U. H. Qureshi, and C. K. Miller, "Multipoint networks: Advances in modem design and control," in *National Telecommunications Conference*, (Dallas, TX), November 1976.